# OPTICAL PERFORMANCE MONITORING IN HIGH-SPEED OPTICAL COMMUNICATION SYSTEMS

**YU YI**

(*M. Sci., National University of Singapore, Singapore*)

(*B. Eng ., Commanding Communications Academy of Chinese People's Liberation Army, China*)

A THESIS SUBMITTED

FOR THE DEGREE OF DOCTOR OF PHILOSOPHY

DEPARTMENT OF ELECTRICAL AND COMPUTER ENGINEERING

NATIONAL UNIVERSITY OF SINGAPORE

2014

# DECLARATION

I hereby declare that this thesis is my original work and it has been written by me in its entirety.

I have duly acknowledged all the sources of information which have been used in the thesis.

This thesis has also not been submitted for any degree in any university previously.

_____

YU YI

December 18, 2014

# DEDICATION

*To my parents and Fei,*

*for their everlasting love and support.*

# Acknowledgement

I would like to thank my supervisor, Dr. Yu Changyuan, for his zealous support, professional guidance, and gracious mentorship during my graduate studies. From Dr. Yu, I learnt not only knowledge and research experience, but also hard-working altitude to work and life.

I would also like to deliver my sincere appreciation to the members of my thesis committee and qualifying examination committee for their precious time and invaluable suggestions. They are Prof. Kam Pooi-Yuen, Prof. Mohan Gurusamy and Dr. Kim Hoon.

I would like to express my hearty thanks to my colleagues for their beneficial suggestion and helpful support. They are Dr. Yang Jing, Dr. Zhang Banghong, Dr. Chen Jian, Dr. Hu Junhao, Dr. Zhang Hongyu, Dr. Cao Shengjiao, Dr. Dong Bo, Xu Zhuoran, Li Xiang, Zhou Jingjing, and Hu Qikai. I would also like to show my great appreciation to Dr. Kim Hoon for sharing several experimental facilities. Additionally, I want to thank my laboratory mates and friends for their kindly help and useful discussions. They are Dr. Xu Jie, Wu Tong, Luo Shixin, Song Tianyu, Liu Liang, Wang Yu, Wu Gaofeng, Dr. Zaineb Al-Qazwini, and Dr. Bi Shuzhi.

I would like to pay my heartfelt thanks to my family for their everlasting love and support.

Finally, I would like to convey my gratitude to the people, who provided me kindly help and support all the time.

# Contents

# Summary

As the rapid growth of internet data traffic, especially the wide application of multimedia technology, optical fiber transmission system becomes the best candidate for the backbone transmission in telecommunication networks. Current optical networks are operating in the static mode, which will face serious challenge of future high-speed reconfigurable systems, where dynamic routing and environment variation will cause unpredicted degradation effect to the transmission systems. The channel condition and component performance are the two major factors that determine the performance of optical transmission systems. In the optical transmission channel, additive spontaneous emission noise (ASE) generated by optical amplifier and chromatic dispersion (CD) of optical fiber are the major optical effects that degrade received signal quality and limit transmission distance. Additionally, the transceiver working performance is another vital factor that influences the system performance.

Optical performance monitoring (OPM) is a potential mechanism that diagnoses the optical impairments in the physical layer of optical networks, which can provide great assistance for the system management of future optical networks. It enables the capabilities of automatic system performance diagnosis, intelligent network reconfiguration and accurate optical impairment compensation. In this thesis, several topics of OPM are investigated, including monitoring optical impairments in fiber link and transmitter.

Firstly, the optical signal to noise ratio (OSNR) monitoring method using uncor-

related signal power is investigated, which relies on optical filtering effect. In this method, a single optical band-pass filter (OBPF) is used to shrink the bandwidth of the monitored signal. The bandwidth-shrunk signal and the monitored signal have a part of overlapped frequency components, which are correlated. The correlated part is removed by a balanced receiver, which leaves the uncorrelated signal that is sensitive to signal OSNR variation. Moreover, low bandwidth receivers are used in this scheme, which reject the high-frequency radio frequency (RF) power variation induced by dispersion effect. Thus, the uncorrelated signal power is insensitive to dispersion effect, which leads to a dispersion insensitive OSNR monitoring method. This method is demonstrated in both single polarization and polarization division multiplexed (PDM) systems in the experiment. Furthermore, the optical interference between the correlated signals is another way to generate uncorrelated signal, which is also investigated and demonstrated in the simulation work. In this scheme, an optical coupler replaces the balanced receiver to generate uncorrelated signal, whose destructive output exhibits a novel band-stop filtering effect. The OSNR monitoring based on the novel band-stop filtering effect shows a better monitoring dynamic range than that of the method using optical delay interferometer.

Secondly, the OPM based on electrical sampling technique is investigated in this thesis. The generation of the 2-dimension (2-D) phase portrait using single channel sampling technique is proposed, which reduces the monitoring system setup cost and complexity in large degree. Additionally, the related and un-related sampling schemes are studied. In the related sampling scheme, the sampling frequency is synchronized with the monitored signal, which obtains accurate sampling intervals. In the un-related sampling scheme, the software synchronization is used to synchronize the sample sequence. Once the phase difference between the samples is known, the X-Y pairs are generated by searching the nearest sample pairs with certain phase difference from the sample sequence. After the 2-D phase portrait is generated, the monitoring parameter-

s can be derived by using simple statistical pattern recognition on the phase portrait. OSNR monitoring and CD monitoring are demonstrated in several systems by using the proposed method.

At the last, time mis-alignment monitoring in return to zero (RZ) phase modulation signals is studied. The RZ pulse carver alignment and I/Q alignment monitoring based on 2-D phase portrait are proposed. By identifying the pattern distortion direction and quantifying the pattern width variation, the time mis-alignment can be monitored with the sign. Both simulation and experimental demonstration show that the proposed scheme is a simple and efficient method for the RZ phase modulation transmitter performance monitoring.

# List of Figures

# List of Tables

# List of Abbreviations

| | |
|---|---|
| 1-D | One Dimension |
| 2-D | Two Dimension |
| ADC | Analog-to-Digital Converters |
| AM | Amplitude Modulation |
| ASE | Amplified Spontaneous Emission |
| BER | Bit Error Rate |
| BPF | Band-Pass Filter |
| CD | Chromatic Dispersion |
| DGD | Differential Group Delay |
| DI | Delay Interferometer |
| DOP | Degree of Polarization |
| DQPSK | Differential Quadrature Phase-Shift-Keying |
| DSP | Digital Signal Processing |
| EAM | Electro-Absorption Modulator |
| ECL | External Cavity Lasers |
| EDFA | Erbium-Doped Fiber Amplifier |
| FFT | Fast-Fourier Transform |
| FO | Frequency Offset |
| FWM | Four Wave Mixing |

| | |
|---|---|
| ISI | Inter-Symbol Interference |
| LPF | Low-Pass Filter |
| MZM | Mach-Zehnder modulator |
| NOLM | Nonlinear Optical Loop Mirror |
| NRZ | Non-Return-to-Zero |
| OADM | Optical Add/Drop Multiplexer |
| OBPF | Optical Band-pass Filter |
| ODI | Optical Delay Interferometer |
| OEO | Optical-Electrical-Optical |
| OOK | On-Off Keying |
| OPM | Optical Performance Monitoring |
| OSNR | Optical Signal-to-Noise Ratio |
| OTF | Optical Tunable Filter |
| PD | Photo Detector |
| PDL | Polarization Dependent Loss |
| PDM | Polarization-Division-Multiplexing |
| PM | Phase Modulation |
| PMD | Polarization-Mode Dispersion |
| PolMux | Polarization-Multiplexing |
| PSK | Phase-Shift-Keying |
| PSP | Principle State of Polarization |
| QAM | Quadrature Amplitude Modulation |
| QPSK | Quadrature Phase-Shift-Keying |
| RF | Radio Frequency |
| RZ | Return-to-Zero |
| SCS | Single Channel Sampling |

| | |
|---|---|
| SE | Spectral Efficiency |
| SMF | Single-Mode Fiber |
| SNR | Signal-to-Noise Ratio |
| SPM | Self-Phase Modulation |
| TCS | Two-Channel-Sampling |
| WDM | Wavelength-Division-Multiplexing |
| XPM | Cross-Phase Modulation |

# Chapter 1

# Introduction

From 1990s, as internet service and application rapidly develop, the demand of telecommunication capacity increases continuously. More importantly, with the wide usage of multimedia applications (such as 3-D/HD TV, online gaming, telemedicine, and so on), the growth of the bandwidth demand would last for a long time. Thus, high capacity optical fiber transmission systems take over conventional coaxial transmission systems gradually, which provide ultra-broad bandwidth to satisfy the increasing demand of transmission bandwidth. Moreover, as the invention and development of Erbium-doped fiber amplifiers (EDFA), all-optical networks enter a fast developing stage, which replace the expensive transmission scheme based on the repeatable optical-electrical-optical (OEO) conversion. Additionally, wavelength division multiplexing (WDM) technique takes advantages of ultra-broad bandwidth of optical fiber, which enables the data transmission in terabit-level. Besides the full usage of optical bandwidth, polarization division multiplexing (PDM) technology further increases the transmission capacity, which employs the two polarizations of the light for data transmission.

However, as the capacity of optical fiber transmission systems increases, the system operation window is narrowed by the limited tolerance of the optical impairments

in the physical layer of optical fiber transmission systems [1]. Optical performance monitoring (OPM) offers a great assistance to optical impairment management in transmission systems, which is potential to enlarge the operation window. This thesis will focus on several basic optical impairment monitoring techniques. In this chapter, section 1.1 and 1.2 give a general introduction on optical fiber transmission systems and some basic optical impairments. Then, the necessity of OPM is discussed in section 1.3, and the literature review is presented in section 1.4. In the last section, motivation, contribution and outline of this thesis are given.

## 1.1 Optical Transmission System

Thanks for the invention of optical fiber, information can be delivered through low-loss optical fiber with high speed. Compared with radio frequency (RF) transmission, optical fiber transmission provides ultra-broad bandwidth to meet the increasing bandwidth demand. Wavelength division multiplexing (WDM) technology further increases the transmission capacity of single optical fiber from gigabit-per-second level to terabit-per-second level [2]. The general structure of optical fiber transmission system is demonstrated in Fig. 1.1. Information is modulated onto light, and transmitted through optical fiber link. The basic optical modulation format is on-off keying (OOK), which employs light intensity to carry information, while phase-shift keying (PSK) modulates the phase of light [3]. Furthermore, optical intensity and phase can be used together to carry information, such as multi-level quadrature amplitude modulation (QAM) [4, 5].

In current all-optical tranmission system, Erbium-doped fiber amplifier (EDFA) is an important element that relays information in fiber link, which replaces the expensive OEO conversion. After a certain period of fiber transmission, the EDFA compensates optical signal power loss induced by optical fiber attenuation. Thus, a piece of fiber link

is filled by the repetitive EDFAs and the optical fibers. The flat gain of EDFA realizes the thousands of kilometres of WDM transmission without OEO conversion [6].

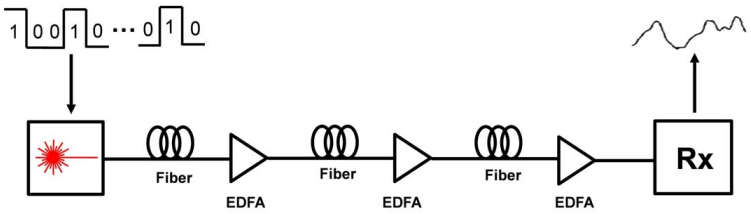


Figure 1.1: Structure of optical fiber transmission system.

In receiver end, the transmitted optical signal is converted into a electrical signal for information collection. According to the different modulation schemes, the corresponding demodulation solutions are employed to extract information from optical signals [7]. Moreover, digital signal processing (DSP) algorithms are employed to process the received electrical signal, which offer compensation to signal distortion [8, 9].

Moreover, along with the development of optical switching [10] and wavelength conversion [11], all-optical networks have flexible and transparent features, which enable network reconfiguration in optical domain. However, the dynamic optical network scheme will bring a great challenge to the system management of current optical networks, which perform under the static and well-defined scenario.

## 1.2 Optical Impairments

In optical fiber transmission systems, there are a number of factors influencing the received signal quality, which can be generally divided into two groups. One is the channel effect that is the physical effect of optical fiber link, and the other is the transceiver performance variance. For the channel effect, optical amplifiers and optical fiber in optical fiber link are the major sources that introduce optical impairments, which include additive spontaneous emission (ASE) noise, chromatic dispersion (CD), po-

larization mode dispersion (PMD), and fiber non-linearity. For the transceiver performance, there are several factors originating from the optical and electrical components in optical transceivers, which degrade system performance, including laser emission wavelength, time alignment between components, bias voltage of optical components, and so on. In this thesis, several major optical impairments are studied. The basic introduction of these optical impairments are discussed in the following paragraphs.

### Chromatic Dispersion

Chromatic dispersion (CD) is a non-catastrophic optical impairment induced by the physical characteristic of optical fiber. In brief, CD effect is illustrated as that different frequency components of light travel in optical fiber with different speed, which causes received signal distortion and pulse width broadening.

The optical fiber chromatic dispersion effect can be expressed by Taylor series expansion of mode-propagation constant $\beta$ in Eq. 1.1 [12]. $n$ is the refractive index, which is related to the wavelength. The frequency $\omega_0$ is the center frequency of the propagating light.

$$\beta(\omega) = n(\omega)\frac{\omega}{c} = \beta_0 + \beta_1(\omega - \omega_0) + \frac{1}{2}\beta_2(\omega - \omega_0)^2 + ... \tag{1.1}$$

where

$$\beta_m = \left(\frac{d^m\beta}{d\omega^m}\right)_{\omega=\omega_0} \qquad (m = 0, 1, 2, ...) \tag{1.2}$$

The parameter $\beta_1$ is the group velocity term, which is related to the group refractive index $n_g$, as Eq. 1.3 expresses. The item $\beta_2$ is the group velocity dispersion parameter that determines pulse broadening, as Eq. 1.4 demonstrates. The dispersion parameter ($D$) can be defined by Eq. 1.5, which is the refractive index and wavelength related item.

$$\beta_1 = \frac{1}{v_g} = \left(\frac{n_g}{c}\right) = \frac{1}{c}\left(n + \omega\frac{dn}{d\omega}\right) \tag{1.3}$$

$$\beta_2 = \frac{1}{c}\left(2\frac{dn}{d\omega} + \omega\frac{d^2n}{d\omega^2}\right) \tag{1.4}$$

$$D = \frac{d\beta_1}{d\lambda} = -\frac{2\pi c}{\lambda^2}\beta_2 \approx -\frac{\lambda}{c}\frac{d^2n}{d\lambda^2} \tag{1.5}$$

After a certain distance ($L$) of fiber transmission, the pulse width of the signal is broadened. The increment of the pulse width ($\Delta T$) is expressed by Eq. 1.6, where $\Delta\Lambda$ is the spectrum width of the transmitted optical signal.

$$\Delta T = DL\Delta\Lambda \tag{1.6}$$

The pulse width broadening causes inter symbol interference (ISI), which reduces transmission distance. This phenomenon has square increase as bit rate increases. Thus, dispersion management is quite important for the high-speed and dynamic optical networks [13]. Even if CD can be compensated by chromatic dispersion compensation module [14], the dynamic networks will bring an un-predicted amount of residual CD to the static compensation scheme. Moreover, CD has temperature dependent feature [15], so that the residual CD varies as the environment temperature changes. Although the temperature change of $10$ degrees centigrade ($^{\circ}C$) causes around $0.25$-$ps/nm$ residual CD variation for one-kilometer fiber transmission, one-thousand-kilometer transmission accumulates a large amount of residual CD, which causes serious system performance degradation.

**Polarization Mode Dispersion**

Polarization mode dispersion (PMD) can be generally explained by that the two polarization states of optical signal travel in optical fiber with slightly different speed. In the ideal case, optical fiber is a perfect cylindrical isotropic material, so that the two polarization states of light travel in it with same speed. However, the real optical fiber is an elliptical birefringent material, which induces the propagation deviation between the two identical polarization states. This characteristic is named as modal birefringence,

which is quantified by the dimensionless parameter as Eq. 1.7 expressed.

$$B = |n_x - n_y| \tag{1.7}$$

where $n_x$ and $n_y$ are the effective refractive indices in the x and y polarization states respectively.

Thus, in single mode fiber (SMF), the two principle states of polarization (PSPs) of light travel with different speed, which cause a certain amount of time delay between the two polarization states after a certain period of fiber transmission, as shown in Fig. 1.2. This kind of time delay is named as differential group delay (DGD), which is first order PMD. It leads to received pulse width spreading.

Since the birefringence of optical fiber changes randomly along the fiber, DGD is a stochastic quantity [16]. For the quantization of PMD effect in optical fiber, the DGD caused by a certain length of fiber transmission is utilized to express first order PMD. Moreoever, since the polarization state of light changes randomly in optical fiber, DGD is a time varying parameter. Furthermore, the fiber mechanical strain caused by the variation of environment temperature and the exterior pressure changes the birefringence of optical fiber, which is able to affect the variation of DGD.

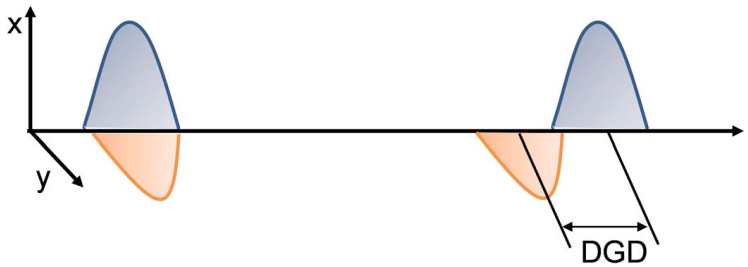


Figure 1.2: Illustration of differential group delay (DGD)

**Additive Spontaneous Emission Noise**

Optical amplifier is a key optical component in current optical fiber transmission systems, which replaces expensive OEO conversion and increases transmission distance

without electrical relay. Optical amplifier employs stimulated emission of optical gain medium to amplify optical signal. At the same time, there exists spontaneous emission that generates optical noise with optical signal amplification. The spontaneous emission noise is an additive noise, which is accumulated as the optical signal passes the cascaded optical amplifers. The power ratio between optical signal and optical noise is called as optical signal to noise ratio (OSNR), which is a key parameter in optical fiber transmission systems.

The spectrum density of ASE noise can be expressed by Eq. 1.8 [17], which is white Gaussian noise.

$$S_{sp}(v) = (G-1)n_{sp}hv \tag{1.8}$$

where $v$ is the optical frequency, $G$ is the gain of optical amplifier, $n_{sp}$ is the population inversion factor, and $h$ is the Planck constant. The SNR of the amplified signal can be expressed by Eq. 1.9, which shows the relationship between SNR and OSNR.

$$SNR \approx \frac{GP_{in}}{4S_{sp}\Delta f} \tag{1.9}$$

where $P_{in}$ is the input optical signal power, and $\Delta f$ is the receiver bandwidth.

Moreover, OSNR can be described by Eq. 1.10. It is noted that the signal input power of optical amplifier is proportional to the OSNR. In the static optical networks, the OSNR is almost kept in static status by the well defined architecture. However, in the future reconfigurable optical networks, the input signal power of EDFA might fluctuate within a certain range, so that the OSNR is not a static value any more. The signal OSNR becomes a dynamic parameter in the reconfigurable optical networks.

$$OSNR = \frac{P_{in}}{P_{ASE}} = \frac{P_{in}}{2n_{sp}(G-1)hvB_o} \tag{1.10}$$

where $B_o$ is the optical bandwidth of ASE noise.

More importantly, ASE noise is a kind of irreversible effect, which means that it can not be compensated directly. It is accumulated more and more as the signal passes

the cascaded amplifiers, which is detrimental to the received signal quality. Thus, OSNR is one of the most importance parameters, which determines the performance of optical fiber transmission systems.

### Time Alignment in Transmitter

An optical transmitter is composed of several optical and electrical components, which are employed to modulate information onto light. Generally, NRZ electrical signal is the information carrier in electrical domain, which is modulated onto light to generate optical NRZ signals, including NRZ-OOK and NRZ-PSK signals. In recent years, return to zero (RZ) signals are employed by advanced modulation formats for high-speed transmission, which shows better receiver sensitivity than NRZ signals [3]. Additionally, RZ format is adopted in polarization division multiplexing (PDM) systems [18]. The typical method of RZ signal generation is to use RZ pulse carver that modulates NRZ signals by sinusoidal-like clock signal. The modulated clock signal should be aligned with the modulated data, as the schematic diagram of RZ-OOK signal generation shows in Fig. 1.3. The NRZ-OOK signal is modulated by 50% RZ pulse carver to generate 50% RZ-OOK signal. The waveform valley of the pulse carver is aligned with the bit transition center of the NRZ signal, while the peak is aligned with the bit center. The RZ suppression can reduce inter-symbol interference (ISI). In the optical RZ signal transmitter, the data modulator should be synchronized with the RZ pulse carver. However, as component ages or environment temperature changes, the optimized working condition would be eroded, which may induce the time mis-alignment between components. The time mis-alignment between the pulse carver and the modulated data will cause waveform distortion, which finally degrades bit error rate (BER) [19].

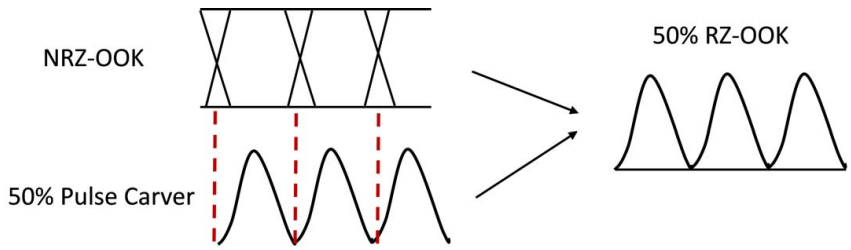


Figure 1.3: Schematic diagram of 50% RZ-OOK generation process.

Moreover, for RZ-DQPSK system, an I/Q modulator is used to generate DQPSK signal, which has in-phase (I) and quadrature-phase (Q) data modulation branches. The I and Q branches need to be aligned with each other, which can be considered as the synchronization between the I/Q branches and the RZ pulse carver respectively. A certain amount of the time mis-alignment between I and Q branches would cause serious system performance degradation [20]. Thus, for the modulation formats generated by using the I/Q modulator, the time alignment between I and Q branches is an important issue for the transmitter performance.

## 1.3 Necessity of Optical Performance Monitoring

Current optical fiber transmission networks are performing in well-defined and static specifications, where the light path is fixed. As the optical networks enter the dynamic era [21], the reconfigurable fashion promotes dynamic optical networks that maximize and optimize the usage of network resources. Thus, the system management is facing a great challenge from the dynamic networks, where the optical impairments are not in the static status any more. Moreover, as the transmission data rate increases, the transmission systems become more vulnerable to the optical impairments. Optical performance monitoring (OPM) is a potential mechanism that provides helpful and useful assistance to the system management of the dynamic networks [1, 22, 23].

In the reconfigurable optical networks, OPM is not a simple module to generate the fault alarm of optical networks any more. It is required to isolate and quantify the optical impairments in the physical layer of optical fiber transmission systems as well as to locate the impairment resource, which provides useful assistance to the intelligent system management of optical networks. However, several optical impairments co-exist in the systems, which are difficult to be distinguished, because several optical impairments cause similar impact on the tested signal. Thus, independent impairment monitoring is an indispensable requirement for a robust monitoring scheme. Secondly, the cost of OPM system is another significant factor, which is a non-negligible part of the whole network budget. The cost of the monitoring system not only includes the setup cost, but also contains the expense of operation and maintenance, such as power consumption. Thirdly, the complexity of the OPM setup and its operation procedure should be considered, which is better to be as simple as possible. These features are significant for the design of OPM system. However, for the OPM mechanism in the whole optical network, OPM module is not restricted to be applied in receiver end. The deployment in fiber link or switching center can collect the detailed and distributed monitoring information of optical impairments, which is beneficial to locate the impairment source. For the real applications, network administrators may bring the portable OPM device to a suspected failure point for testing and diagnosis, while the real-time monitoring module would operate persistent listening in switching center. Thus, the integratability of the monitoring system and the power consumption are the important aspects for the OPM system design.

So far, there are several OPM techniques have been proposed and demonstrated [22], which are based on different techniques and purposes. In the next section, we will make a general review of some major OPM techniques.

## 1.4 Literature Review of Optical Performance Monitoring

Among various OPM techniques, OSNR monitoring and CD monitoring are the two hot topics that have been studied by a number of researchers [22], since OSNR and CD are the two major factors that impact the transmission performance of optical networks. Moreover, the monitoring techniques of PMD, optical power, optical spectrum, and so on, are also investigated by several researchers [24–26]. This thesis focuses on the study of OSNR monitoring and CD monitoring techniques. In addition, time alignment of optical transmitter is also investigated.

**Optical Signal to Noise Ratio Monitoring**

Among the proposed OSNR monitoring methods, a number of methods rely on the optical or electrical characteristics of signal and noise. The most effective and direct OSNR monitoring method is the out-band noise measurement method [27]. This method is based on the fact that the ASE noise spectrum is flat in the tested frequency range. The out-band noise power and the signal power are extracted from the obtained optical spectrum directly. However, in WDM systems, due to the narrow channel spacing, it is difficult to derive the out-band noise between channels with acceptable accuracy. Moreover, the major part of out-band noise is removed by optical add/drop multiplexers (OADM) in networks, so that it is difficult to obtain the noise power by this way. Thus, in-band OSNR monitoring technique is more important and necessary for WDM systems. In the following paragraphs, we will discuss several in-band OSNR monitoring methods based on different techniques.

Firstly, pilot tone and sub-carrier were proposed to be transmitted with data for OSNR monitoring [28, 29]. Low-speed components are used to generate small amplitude pilot tone, which is a cost-effective solution. For this method, the optical transmit-

ter is modified to insert pilot or sub-carrier. However, the modification of transmitter increases the system complexity. Moreover, the pilot tone and sub-carrier interact with the modulated data, which causes crosstalk to the transmitted data. Thus, this scheme brings an additional optical impairment to the network, and increases the complexity of the network, which is not recommended for the high-speed optical transmission systems with narrow operation window. The method that directly processes the monitored signal would be preferred, which is flexible to be operated at any locations in networks.

The OSNR monitoring methods based on the polarization nulling technique were studied in [30–32], which analyzed optical signal directly. This kind of method relies on the fact that optical signal is linear polarized and optical noise is de-polarized, so that the tested optical signal with noise can be split into the polarized signal with polarized noise and the polarized noise by a polarization splitter. This method has a simple and low-cost setup, which is easy to be operated. However, it is not practical for the real optical fiber transmission systems with PMD and polarization dependent loss (PDL). Moreover, as the polarization state of the incoming light rotates, the incoming angle of the monitoring system should be tuned to compensate the polarization rotation.

For the polarization independent monitoring, optical delay interferometer (ODI) was widely studied in OSNR monitoring [33–38]. The two outputs of ODI have different optical filtering effects. While one output shows band-pass filtering effect, the other output exhibits stop-band filtering effect. Thus, the ODI can tailor the optical signals with different optical spectra, which contain different signal to noise power ratios. The power ratio between these two outputs is a function of OSNR, which can be used as OSNR monitoring parameter. Moreover, by using different time delay of ODI [33,35], the bandwidth of the pass-band and stop-band of ODI is tuneable, which causes different OSNR monitoring dynamic ranges. More importantly, the ODI based OSNR monitoring method is also applicable to polarization division multiplexing (PDM) systems [39,40]. However, the optical interference based method is sensitive to the optical

phase deviation induced by environment temperature change. The optical phase variation will lead to the center frequency shift of the pass-band and stop-band, which causes OSNR monitoring error. Although the ODI based OSNR monitoring method has the advantages of simple and cost-effective all-optical setup, easy operation procedure, incoming polarization independence, and dispersion insensitivity, the temperature sensitive feature requires an additional temperature control, which restricts its application in a temperature stabilized environment.

Moreover, in recent years, the OSNR monitoring method based on optical non-linear effect was reported in several papers. Self-phase modulation (SPM) was proposed for OSNR monitoring, since the SPM induced spectrum evolution is related to signal OSNR [41]. Moreover, the OSNR monitoring method using nonlinear optical loop mirror (NOLM) was proposed [42, 43], which relies on the power transfer profile of NOLM. In addition, four wave mixing (FWM) is another optical non-linear effect that has been used for OSNR monitoring [44–47]. The generated wavelength spectrum or optical power has an OSNR-dependent feature. The OSNR monitoring method based on non-linear effect is all-optical monitoring method, which has quite fast monitoring speed. However, these schemes require high power optical amplifiers and highly non-linear mediums, which is a complicated scheme. Thus, this method would not be applicable for the portable monitoring device to provide a flexible monitoring capability in the whole optical network. Even if it works in switching center or receiver end, its high energy consumption increases the operation cost of the monitoring system.

### Chromatic Dispersion Monitoring

As discussed in the previous section, the pilot-tone was used in OSNR monitoring [28], which was also applicable to CD monitoring. The CD monitoring methods using pilot tone and sub-carrier were investigated by several researchers [14, 48–52]. These

methods are based on the fact that CD causes the time delay between the inserted sub-carrier and the baseband. It is a simple and low-cost method, which can be used in WDM system. However, the insertion of sub-carrier needs the modification of the existing optical transmitter. Additional, the sub-carrier interferes with the transmitted data to degrade the BER. Thus, this method is also not recommended for real application. Moreover, since CD induces the phase mis-match between the two side-bands of the signal, CD effect causes the RF tone fading or re-generation of the received signal. Thus, the RF tone power of the transmitted signal was proposed and demonstrated for CD monitoring, which does not require the insertion of sub-carrier [25, 53–55]. By measuring the RF tone power at different frequencies, the CD monitoring dynamic range is diverse. The monitoring scheme using the low frequency RF tone power has larger monitoring range and smaller dynamic range, while the high frequency scheme has contrary performance. However, the RF power is also affected by OSNR value. Thus, this method is not an independent CD monitoring scheme, which needs simultaneous OSNR monitoring. Furthermore, fiber non-linear effect was also used for CD monitoring. CD monitoring was demonstrated by using SPM, 2R regenerator, FWM, and XPM [41, 56–59]. For CD monitoring, the method based on fiber non-linear effect has limited CD measurement range, and requires high power optical amplifier and highly non-linear medium.

**Multi Optical Impairment Monitoring**

As discussed in the previous paragraphs, the monitoring methods have simple working principle and fast measurement speed, which are based on the physical effects of the optical impairments. However, most of them require the precise control of the optical components in the monitoring systems, which increases the operation complexity. Since various optical impairments cause the received signal waveform distortion in different degree and forms, OSNR and CD can be identified and quantified from electrical

waveform distortion, which uses electrical sampling technique to convert waveform information into data sequence for computer processing.

Firstly, Q-fator and OSNR were estimated by using a one dimension (1-D) histogram of signal amplitude, which was derived by the synchronized or asynchronized sampling scheme [60–66]. By using statistical analysis on the sampled signal amplitude, the monitoring parameters can be derived from the amplitude distribution. For this type of method, electrical sampling and digital signal processing (DSP) are in charge of the major function of the monitoring module, instead of the precise control of optical components. Thus, the monitoring system is easy to be operated and maintained. Moreover, the OSNR monitoring method based on 1-D histogram is also applicable for advanced phase modulation format [67, 68]. Additionally, the 1-D histogram was proposed and demonstrated for CD monitoring [69–71]. However, the CD monitoring results are affected by the OSNR variation. It is difficult to distinguish CD and OSNR from 1-D statistical analysis, due to its limited information. Thus, this method is not practical to the systems where there are multiple optical impairments.

In order to derive more information from the waveform, the two dimension (2-D) histogram was proposed for multiple optical impairment monitoring, which provided fruitful statistical information [72, 73]. The 2-D histogram is also named as 2-D phase portrait or delay-tap sampling plot. It is an alternative plot of eye diagram for the demonstration of electrical waveform. This method employs two samplers that work simultaneously with short internal time delay to derive samples. The samples from these two samplers are formed as X-Y pairs successively, which are depicted in 2-D coordinate system. The X-Y pairs display the relative intensity between the two addresses on electrical signal, which are with fixed time delay. The time delay can be considered as the phase difference on the waveform. Since the phase portrait pattern evolutions induced by different optical impairments are diverse, it is possible to separate and quantify multiple impairments by monitoring the pattern evolution of the 2-D

phase portrait [74].

According to the particular waveform of difference modulation formats, half symbol or tenth symbol delay was used to generate 2-D phase portrait for OSNR monitoring parameter derivation [75–79]. By using different time delay, the phase portraits exhibit different features of the electrical waveform. Although the phase portrait pattern is different in various modulation formats, the common method is to derive the ASE-noise induced corresponding pattern evolution. The most notable feature is that the "mark" level amplitude is sensitive to the noise power variation, so that the sample pairs from the "mark" level are extracted for the monitoring parameter calculation.

Since residual CD induces pulse width broadening, the pattern width of the phase portrait is changed by residual CD [80–83]. Additionally, since the pattern width is related to the monitored signal power, the width ratio of the pattern in the two specific directions is employed to estimate CD variation. Moreover, for DPSK and DQPSK signals, the sign of CD can be determined after applying the imperfect phase demodulation to the phase modulated signal [80, 81].

In sum, the OSNR monitoring and CD monitoring parameters can be derived from the 2-D phase portrait by using simple statistical pattern recognition technique. The key part of the monitoring system is signal processing, which reduces the complexity of maintenance and operation in large degree, compared with the methods using analog signal processing, which need the precise control of optical components. Moreover, this method has a much simple system setup, which is easy to be maintained. However, the 2-D phase portrait generation using two sampling channels is not a cost-effective method, which is another important factor for the system design. In addition, electrical sampling and data processing are power consuming.

#### Time Alignment Monitoring

For the time alignment monitoring in RZ phase modulation system, RZ pulse carver

monitoring and I/Q alignment monitoring were studied by several researchers. In [19], a pulse carver alignment monitoring method of RZ-DPSK signal was proposed by using the degree of polarization (DOP) of the monitored signal, which varied with the time mis-alignment in the presence of finite differential group delay (DGD). It is a simple and cost-effective method that employs few passive optical components. However, this method requires the polarization alignment of the monitored signal, which increases the operation complexity of the monitoring system. In [84], since the time mis-alignment broadens the optical spectrum of the modulated signal, the authors proposed to use the optical side-band power variation to monitor the time mis-alignment by filtering out a narrow side-band from the optical spectrum. However, the monitoring accuracy is dependent on the filter performance, which would be affected by the detuning of filter's center frequency and bandwidth. Moreover, the RF spectrum evolution induced by the RZ pulse carver mis-alignment was proposed and demonstrated for the time alignment monitoring [85].

For I/Q branch alignment monitoring, the radio frequency (RF) clock tone power was proposed to be used in the time alignment monitoring for both RZ pulse carver and I/Q branch in RZ-DQPSK system [86]. However, this method cannot identify the sign of the time mis-alignment of RZ phase modulated signals, and neither do the methods in [19,84,85]. In [87], the time alignment monitoring method based on delay-tap sampling technique was proposed for RZ-OOK signal. The sign and degree of the time alignment can be determined by quantifying the average angle of the sample pairs that is located at the certain area of the plot. Thus, the sign of the time mis-alignment can be identified through the analysis on the waveform.

## 1.5 Motivation and Contribution of the Thesis

In the previous section, the discussed OPM techniques can be divided into two groups. One is based on analog signal processing, which relies on the physical characteristics of optical impairments. The other is based on digital signal processing, which investigates the signal waveform distortion induced by optical impairments.

For the methods using analog signal processing, they have fast monitoring speed and good monitoring dynamic range. Moreover, this type of monitoring systems employs several cost effective components to estimate single optical impairment. The monitoring system is able to be integrated to a compact monitoring module, which is flexible to be implemented in networks. Thus, in this thesis, we will firstly investigate the method using analog signal processing for single OSNR monitoring, which is the most important function in OPM system. In practical systems, since optical signal is with CD, PMD, and PDL, a robust OSNR monitoring scheme should be able to isolate OSNR with other effects. Moreover, the OSNR monitoring system does not require the modification of optical transmitter. One of the good solutions is to use optical filtering effect, such as the ODI based method [34]. However, the key drawback of this method is its phase sensitive feature. Additionally, its limited bandstop effect limits the monitoring dynamic range. In this thesis, we will further investigate the OSNR monitoring method using optical filtering effect.

For the OPM method using digital signal processing, it relies on the fact that optical impairments cause the received waveform distortion in different forms and degree, so multiple optical impairments could be derived from the pattern evolution of the 2-dimension (2-D) phase portrait [72]. Thus, it is a good candidate for multiple optical impairments monitoring, which would be a monitoring solution in switching center or receiver end. This method was studied in OSNR monitoring and CD monitoring with the co-operation of simple pattern recognition technique [75, 77]. However, the

2-D phase portrait is depicted by using two high bandwidth samplers. It is a quite expensive method, even if several optical impairments could be derived simultaneously. Since the two samples of two sampling channels generate the X-Y pair, which are located in the waveform with certain phase difference, it is possible to derive the X-Y pair from the sample sequence with known time interval by using single sampler. By using this approach, the monitoring system cost could be reduced in large degree. More importantly, the monitoring system setup can be simplified further. It would be easily implemented in real systems. Thus, in this thesis, we will investigate the 2-D phase portrait generation using single sampler. Moreover, based on the generated 2-D phase portrait, the monitoring methods of OSNR, CD and time alignment are investigated.

In sum, the contributions of this thesis are listed as below:

- For single optical impairment monitoring, optical signal to noise ratio (OSNR) is a quite important parameter that desires an effective monitoring solution. In this work, we propose to use the uncorrelated signal power to monitoring OSNR variation. The uncorrelated signal is generated by removing the correlated signal, which is generated by a narrow-bandwidth optical filter. The removal of correlated signal is proposed to utilize balanced subtraction or optical interference. In both simulation and experimental demonstration, the uncorrelated signal is successfully derived by using electrical balanced subtraction. Moreover, after using low bandwidth receiver, the proposed OSNR monitoring scheme can be insensitive to both CD and PMD. Additionally, the usage of low bandwidth receiver reduces the monitoring setup cost in large degree. Further more, in the simulation demonstration, the uncorrelated signal is also derived by using optical interference, which shows better OSNR monitoring dynamic range.

- In order to reduce the cost of the 2-D phase portrait generation for OPM, single channel sampling technique is proposed to generate the X-Y pairs, which saves

the cost of one high bandwidth sampler. In the experimental demonstration, a low-speed related sampling clock is used to trigger the sampler to generate the sample sequence with known time interval. Then, the proposed self-delay scheme generates the X-Y pairs for the 2-D phase portrait depiction. By using simple statistical pattern recognition, the OSNR monitoring parameter is derived from the 2-D phase portrait in all the demonstrated modulation formats, while the CD monitoring parameter is derived in the demonstrated NRZ phase modulation systems.

- In order to further reduce the monitoring setup cost and extend the application scope, a un-related sampling clock is used to trigger the single sampling channel. In this case, the software based synchronization technique is used for the 2-D phase portrait generation. In the experimental demonstration, the OSNR monitoring method based on the software synchronized 2-D phase portrait is successfully demonstrated. Moreover, in order to loosen the requirement of the software synchronization accuracy, a tolerated phase difference phase portrait is proposed. Compared with the conventional X-Y pairs with fixed phase difference, the phase difference of the X-Y pairs is proposed to be within a tolerated range. This scheme is verified by experimental demonstration for OSNR monitoring.

- In this thesis, we also investigate the time alignment of optical transmitter. We propose to use the 2-D phase portrait to monitor RZ pulse carver alignment and I/Q branch alignment in RZ phase modulation systems. By identifying the pattern distortion direction of the 2-D phase portrait, the sign and degree of the time mis-alignment are estimated. More importantly, the time alignment monitoring is also demonstrated by using the proposed single channel sampling method, which extends the application scope.

## 1.6 Outline of the Thesis

The following contents of this thesis are as follows.

In chapter 2, we will review the generation of different modulation formats in high-speed optical transmission systems, which use Mach-Zehnder modulator (MZM). Moreover, RZ pulse carver generation, demodulation of differential phase-shift keying (DPSK) and differential quadrature phase-shift keying (DQPSK) signals, and electrical sampling technique are introduced.

In chapter 3, the OSNR monitoring method based on filtering effect is investigated. By using electrical subtraction or optical interference, the generated uncorrelated signal can be used for OSNR monitoring. Both experimental demonstration and simulation work are employed to investigate the proposed OSNR monitoring method.

In chapter 4, single channel sampling technique is proposed for OSNR monitoring and CD monitoring. Single channel sampling scheme is employed to depict the 2-D phase portrait, from which the monitoring parameters are derived. The OSNR monitoring and CD monitoring in different modulation formats are experimentally demonstrated and discussed in this chapter.

In chapter 5, software synchronized single channel sampling technique is proposed for OSNR monitoring, where the sampler is triggered by un-related sampling frequency. In this scheme, the sampling sequence is synchronized by software algorithm. Moreover, the tolerated phase difference phase portrait is proposed, which can further increase the tolerance to the aliasing frequency estimation offset.

In chapter 6, time alignment monitoring is investigated by using the proposed sampling technique. With the cooperation of simple statistical pattern recognition, the monitoring of RZ pulse carver alignment and I/Q branch alignment are demonstrated in RZ phase modulation systems.

Finally, conclusion and future work are discussed in chapter 7

# Chapter 2

# Fundamental of Optical Transmission System and Optical Performance Monitoring

In this chapter, the basic knowledge of optical fiber transmission systems and electrical sampling technique are studied. In optical fiber transmission systems, several optical modulation formats are employed to carry information travelling in optical fiber link [3]. Among these formats, on-off keying (OOK) is the basic one that modulates light intensity. Compared with OOK, phase-shift-keying (PSK) provides better receiver sensitivity and robustness to fiber non-linearity [3]. Among various advanced modulation formats, differential-phase-shift keying (DPSK) and differential-quadrature-phase-shift keying (DQPSK) signals are the candidates that can be utilized in both coherent and non-coherent detection systems [88]. Moreover, return to zero (RZ) format shows better receiver sensitivity than non-return to zero (NRZ) one, which is also employed by advanced polarization division multiplexing (PDM) systems [18, 89]. Moreover, multi-level modulation formats and multi-carrier systems are employed to improve spectra efficiency (SE) [4, 90]. In this thesis, we focus on the

OPM methods for single carrier systems. Moreover, the optical performance monitoring (OPM) methods using analog signal processing and digital signal processing are investigated. Thus, in this chapter, the working principle of the related optical effects, optical transceiver and electrical sampling are studied.

## 2.1 Application of Mach-Zehnder Modulator

Mach-Zehnder modulator (MZM) is an important and fundamental optical device that is used for optical modulation in optical transmission systems, including amplitude modulation (AM) and phase modulation (PM). The structure of MZM is demonstrated in Fig. 2.1. The light is identically split into two branches in the MZM at first. Two phase modulators are applied to add phase shift in the two branches separately, which are controlled by the modulation driving voltages $V_1(t)$ and $V_2(t)$ separately. Then, the two-branch signals interference with each other at the second coupler [91]. The output of the second coupler can be expressed by Eq. 2.1, where $\phi_1(V(t))$ and $\phi_2(V(t))$ are the modulated phase in the two branches [92]. $V_{bias}$ is the bias voltage of the modulator.

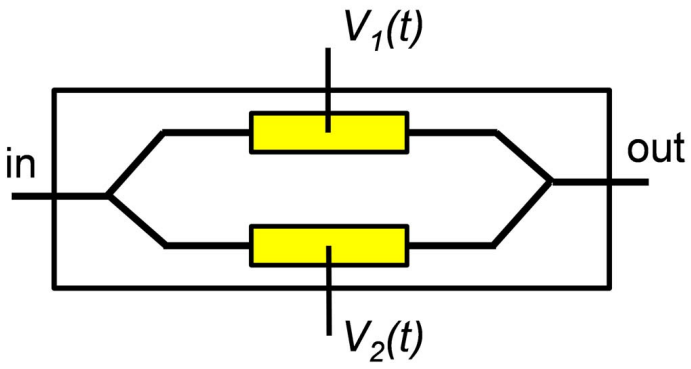


Figure 2.1: Structure of Mach-Zehnder modulator.

$$E_{output} = \frac{E_{input}}{2}\left[\exp\left(j\phi_1(V(t))\right) + \exp\left(j\phi_2(V(t))\right)\right]$$

$$= E_{input} \cos\left(\frac{V_1(t) - V_2(t)}{4V_\pi} \cdot \pi\right) \cdot \exp\left(j\frac{V_1(t) + V_2(t)}{4V_\pi} \cdot \pi\right). \quad (2.1)$$

The output power of the MZM can be expressed as Eq. 2.2.

$$E^2_{output} = E^2_{input} \cdot cos^2\left(\frac{V_1(t) - V_2(t)}{4V_\pi}\pi\right) \quad (2.2)$$

In order to obtain chirp free operation, the MZM works in push-pull mode, where the driving voltages have the relationship as $V_1(t) = -V_2(t)$ [92]. Thus, Eq. 2.1 can be represented as Eq. 2.3

$$E_{output} = E_{input} \cdot cos\left(\frac{\pi V_1(t)}{2V_\pi}\right) \quad (2.3)$$

The power transmission function of the MZM is shown in Fig. 2.2. The output power is a periodic function of the modulation voltage. For intensity modulation, the bias voltage is placed at the quadrature point, so that the modulated signal can manipulate the output from the maximum transmittance to the minimum transmittance [93]. For phase modulation, the bias voltage is set to the null point, which is the minimum transmittance point. The optical phase is modulated by $\pi$, when the driving voltage crosses the null point.

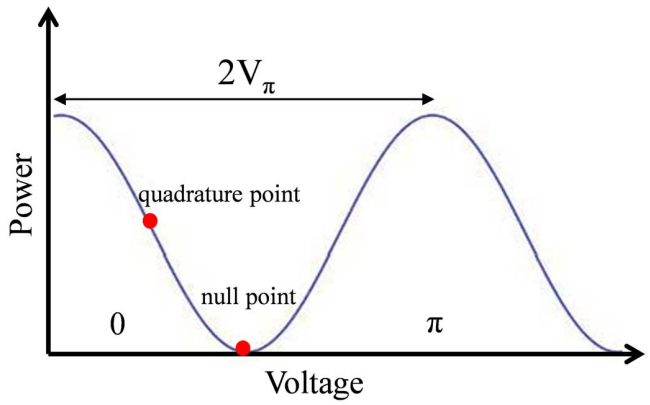


Figure 2.2: Power transmission function of MZM.

MZM can not only be used for binary phase modulation, but also for quadrature phase modulation using the parallel structure MZM. The schematic diagram of the

parallel structure MZM is composed of two push-pull mode MZMs and one $90^\circ$ phase shift, which is named as I/Q modulator, as shown in Fig. 2.3.

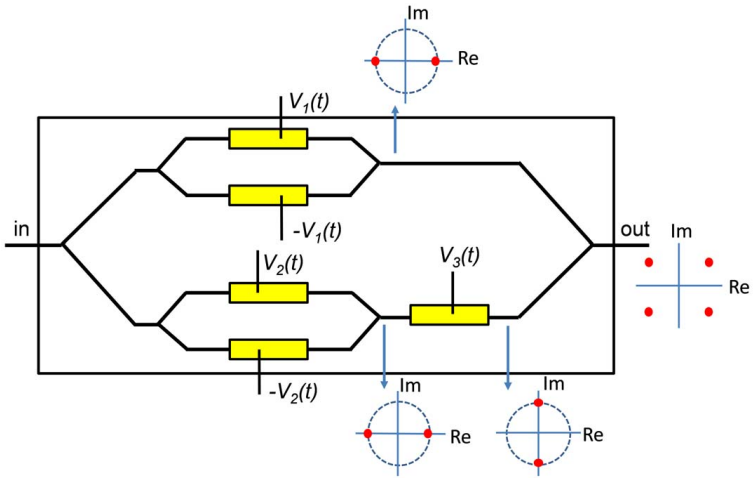


Figure 2.3: Schematic diagram of I/Q modulator.

The incoming light is equally split into two branches, which are processed by the two MZMs. These two MZMs are biased at the null point for binary phase modulation. The $90^\circ$ phase shift is applied at one branch to generate $90^\circ$ phase difference between the two branches. Finally, the phase modulated signals of these two branches are coupled to generate quadrature phase modulated signal [94]. Moreover, the parallel-structure I/Q modulator is also employed for the generation of multi-level advanced modulation formats [95].

## 2.2 Optical Pulse Carver Generation

In optical communication systems, return to zero (RZ) format can be generated by several methods [3,96,97]. The optical data modulation drived by electrical RZ signal is a direct method to generate optical RZ signal, which has been demonstrated in 10-Gb/s system. Moreover, optical RZ waveform can be also generated by using a RZ pulse carver, which is realized by driving electro-absorption modulator (EAM) or MZM with

sinusoid signal. In high-speed optical transmission systems, the MZM based RZ pulse carver is preferable for chirp free modulation, compared with the method using RZ driving signal or EAM generated RZ pulse carver [96, 97]. For the MZM based RZ pulse carver, the duty ratio of the RZ signal is tuned by using different driving schemes. The detailed configuration of these schemes are listed in table 2.1, while the corresponding RZ pulse carver waveform is demonstrated in Fig. 2.4. The RZ pulse carver is applied in the NRZ signal to generate a RZ signal, which suppresses the bit transition of the NRZ signal.

Table 2.1: RZ Format

| Format | Bias Voltage | Amplitude | Frequency |
|---|---|---|---|
| $33\%$ RZ | $2V_\pi$ | $2V_\pi$ | $f_{symbol}/2$ |
| $50\%$ RZ | $V_\pi/2$ | $V_\pi$ | $f_{symbol}$ |
| $67\%$ RZ | $V_\pi$ | $2V_\pi$ | $f_{symbol}/2$ |

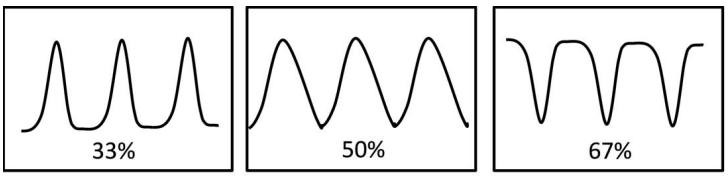


Figure 2.4: RZ pulse carver waveform with different duty ratios.

## 2.3 Demodulation of DPSK and DQPSK Signals

In optical fiber transmission systems, photo detectors (PD) convert optical intensity to electrical signal. For the intensity modulated signals, such as OOK, a single PD can directly demodulate optical signal. However, the phase-modulated optical signal

carries the information by using the phase of light, so that the phase information cannot be obtained by detecting the light intensity directly. In order to extract the information from the optical phase, a phase demodulation is required. The phase demodulation methods of DPSK and DQPSK can be divided into two types. One is direct detection, the other is coherent detection [7, 98, 99]. For coherent detection, coherent local light is employed to beat with the received light, which converts the phase-modulated signal to the light intensity, where the local light provides the reference phase. However, for direct detection, the reference phase is provided by the received light itself. The optical demodulator structures of DPSK and DQPSK signals are demonstrated in Fig. 2.5. The 1-bit delay optical delay interferometer (DI) is used to enable the beating between the neighbour bits, which provides the reference phase to each other in DPSK system. For the quadrature phase modulated system, two DIs are used to demodulate the in-phase and quadrature-phase branches separately. In fact, one output of single DI contains the transmitted data, but the balanced detection provides the benefit of 3-dB receiver sensitivity [100].

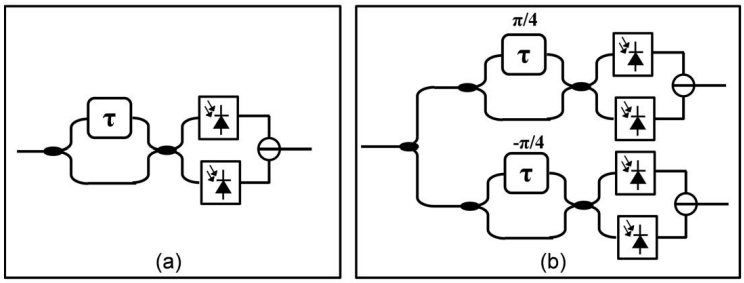


Figure 2.5: Demodulator structure of (a) DPSK, (b) DQPSK.

## 2.4 Electrical Sampling Technique

In the nature, both optical and electrical signal exist and propagate in analog fashion. However, signal processing can be realized by either analog method or digital way.

Optical signal processing is carried out by optical effects, which performs in continuous manner [101]. However, for electrical signal processing, it works in continuous or discrete ways. In the continuous way, the signal processing is based on the electrical effect of electrical components, while digital signal processing (DSP) processes discrete signal in a mathematical way [102]. DSP has been widely implemented in several areas. Since the electrical signal exists in a continuous way, it requires an analog to digital converter (ADC) to transform the continuous signal into the digital sequence for mathematical computation. Thus, ADC is an important component for DSP.

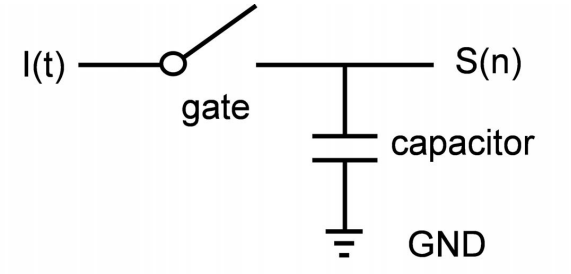


Figure 2.6: Schematic diagram of ADC.

The typical ADC employs a sample-and-hold circuit, which is generally composed of a sampling gate and a capacitor, as shown in Fig. 2.6. The sampling gate is controlled by the sampling frequency, which is also considered as a switching period. After the sampling gate is closed, the incoming electrical signal ($I(t)$) charges the capacitor. The accumulated charges is related to the signal amplitude, which is used to quantize the analog signal. After the sampling gate is open, the capacitor is discharged and prepared for the next sampling time slot.

In practical systems, the sampling gate closing time is an important parameter that determines the analog bandwidth of the sampler. The mathematical model of electrical sampler is expressed by Eq. 2.4. The closing process of the sampling gate is represented by the sampling pulse ($g(t)$). In ideal case, the sampling pulse ($g(t)$) is expressed by Dirac function, which is with infinite analog bandwidth. However, in

practical case, the sampling pulse has a certain duration, so that the analog bandwidth of sampler is finite. For further explanation, the Gaussian pulse is employed as an example to represent the sampling pulse. In this model, the sampling pulse ($g(t)$) is expressed by Eq. 2.5 in time domain, where $T_{gate}$ is the sampling pulse width. In frequency domain, it is expressed by Eq. 2.6. The sampling pulse width determines the analog bandwidth of the sampler. The sampling pulse width is inversely proportional to the analog bandwidth of the sampler.

$$S(n) = \int I(t) \cdot g(t) \cdot dt \tag{2.4}$$

$$g(t) = exp\left(-\frac{t^2}{T_{gate}^2}\right) \tag{2.5}$$

$$G(f) = T_{gate}\pi^2 exp(-(T_{gate} \cdot \pi \cdot f)^2) \tag{2.6}$$

# Chapter 3

# Optical Signal to Noise Ratio Monitoring Using Filtering Effect

For single optical signal to noise ratio (OSNR) monitoring, robustness of incoming signal polarization state variation, isolation from other optical impairment, and monitoring system setup cost are the three key concerns for the system design. Thus, the OSNR monitoring method using the filtering effect of optical delay interferometer (ODI) would be an effective solution. This method adopts passive optical components and measures the optical power, which is a cost-effective and dispersion insensitive OSNR monitoring method [34]. This method is based on the advantage of band-stop and band-pass effect of ODI. However, the ODI is sensitive to its phase shift, which induces OSNR monitoring error. In [103], the authors proposed a OSNR monitoring method using uncorrelated signal. By placing two optical filters symmetrically at the two side-bands of the monitored signal separately, the optical spectra of the two filtered side-band signals partially overlap at the center frequencies. The overlapped frequency components are correlated, which are removed by balanced subtraction after photo detection. The remaining part is the uncorrelated signal, whose high frequency power density is derived to estimate in-band OSNR. The generation of the uncorrelated

signal is an alternative method to generate band-stop effect. The electrical balanced subtraction is not sensitive to the optical phase variation between the two branches. However, the method using high-frequency signal power is affected by CD and PMD, since both CD and PMD induce high-frequency RF tone power variation. Moreover, the two-filter based setup is complicated.

In this chapter, we propose to use a single optical band-pass filter (OBPF) to generate uncorrelated signal, where the correlated signal is removed by balanced electrical subtraction or optical interference. The power ratio of the uncorrelated signal and the original signal is a function of the OSNR, which is used for OSNR monitoring. More importantly, after using low bandwidth receiver, the proposed OSNR monitoring method can be insensitive to CD and PMD. For the demonstration of the proposed method, numerical simulation and experimental demonstration are employed to investigate the OSNR monitoring method using the uncorrelated signal power generated by balanced subtraction in both single and dual polarization systems. Moreover, the OSNR monitoring performance is studied in the presence of CD and PMD effect.

In addition, the uncorrelated signal generated by using optical interference is proposed for OSNR monitoring, which is demonstrated by simulation work. The proposed scheme exhibits novel notch filtering (band-stop) effect, which removes the correlated signal. The proposed OSNR monitoring method is investigated in different systems.

# 3.1 OSNR Monitoring Using Uncorrelated Signal Generated by Balanced Subtraction

## 3.1.1 Working Principle of the Proposed Method and Simulation Setup

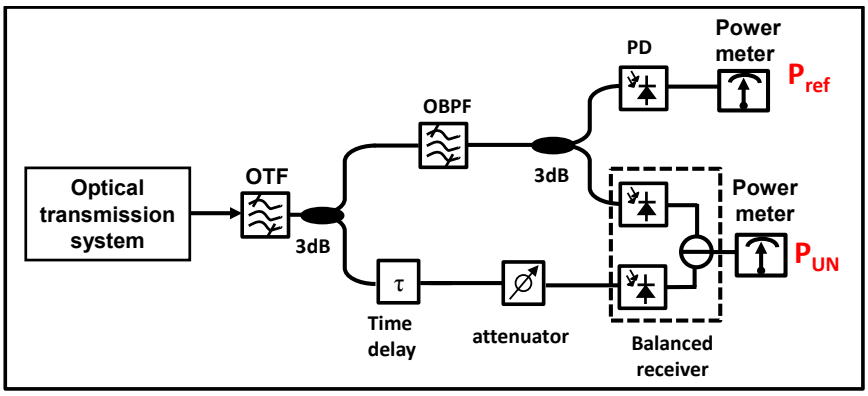


Figure 3.1: Simulation setup of the proposed OSNR monitoring method using the uncorrelated signal power generated by balanced subtraction.

Fig. 3.1 shows the simulation setup of the OSNR monitoring method using the uncorrelated signal power generated by balanced subtraction. In the setup, an optical tuneable filter (OTF) is used as a de-multiplexer to select the monitored channel with certain bandwidth. Then, the optical signal is split into two identical branches by a 3-dB coupler. One branch signal passes a relatively narrow bandwidth optical band-pass filter (OBPF), whose center frequency is the same as the monitored signal center frequency. After that, the filtered signal is split by another 3-dB coupler into two branches. One output is sent into a single photo detector (PD), and the other is connected with one input of a balanced receiver. The other output of the first 3-dB coupler is connected with the other input of the balanced receiver after passing an optical time delay line and an attenuator. These two components are used to keep the two input signals matched

before the balanced receiver. The output power of the two receivers are measured as the uncorrelated signal power and the reference signal power ($P_{UN}$ and $P_{ref}$).

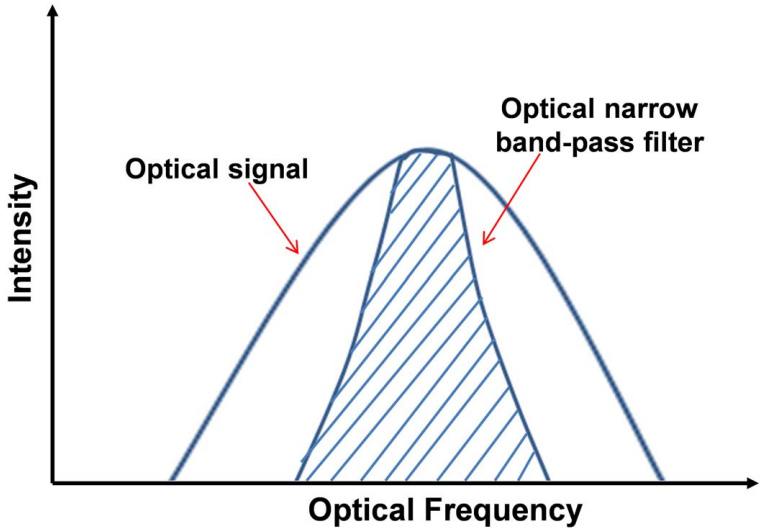


Figure 3.2: Optical spectra of the two input signals of the banlanced receiver.

The optical spectra of the two inputs of the balanced receiver are demonstrated in Fig. 3.2. The shadow one is the optical spectrum of the signal at the upper branch of the balanced receiver, which is overlapped with the outer optical spectrum that is from the signal of the balanced receiver lower branch. The bandwidth and shape of the OBPF determine the overlapped area. The overlapped frequency components are correlated, which are cancelled out after balanced detection and subtraction. The remainder is the uncorrelated signal, whose power contains a certain amount of signal and noise. The uncorrelated signal power can be expressed by Eq. 3.1, while the reference signal power can be expressed by Eq. 3.2.

$$P_{UN} \propto \alpha \cdot P_S + \beta \cdot P_N \tag{3.1}$$

$$P_{ref} \propto \phi \cdot P_S + \gamma \cdot P_N \tag{3.2}$$

$$OSNR = \frac{P_S \cdot NEB}{P_N \cdot B_r} = f(\frac{P_{ref}}{P_{UN}}) \tag{3.3}$$

$P_S$ and $P_N$ represent the optical signal and the noise power respectively. The coefficient $\alpha$ and $\beta$ are related to the shape and bandwidth of the OTF and OBPF, while the coefficient $\phi$ and $\gamma$ are related to the OTF. Since the majority of the signal power is removed by balanced subtraction, $\alpha$ is much smaller than $\phi$. Moreover, due to the different signal-to-noise power ratios of these two equations, the OSNR is a function of the power ratio between the reference power and the uncorrelated signal power, as shown in Eq. 3.3, where NEB and $B_r$ are the noise equivalent bandwidth and the resolution bandwidth separately.

The simulation setup of the proposed OSNR monitoring system is shown in Fig.3.3. The modulated optical signal is coupled with the ASE noise, whose power level is tuned by using an optical attenuator, which emulates different OSNR values. During the fiber transmission, a section of single model fiber (SMF) and a PMD emulator are used to introduce CD and PMD into the system. Finally, the signal is tested by the proposed OSNR monitoring module.

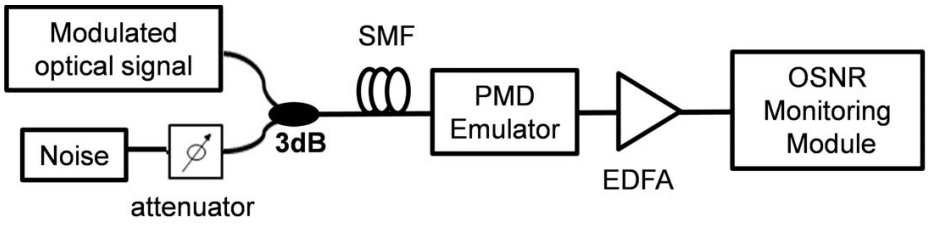


Figure 3.3: System setup of the tranmission system for the OSNR monitoring demonstration.

The proposed OSNR monitoring method is demonstrated in 10-Gb/s NRZ-OOK, DPSK and Duo-binary systems by using VPI transmission maker 7.6. The bandwidth of the OTF and the OBPF are investigated from 30 GHz to 100 GHz, and from 10 GHz to 40 GHz separately. Moreoever, the low bandwidth receiver scheme is also studied in the simulation work.

### 3.1.2 Simulation Results and Discussions

**Modulation Format**

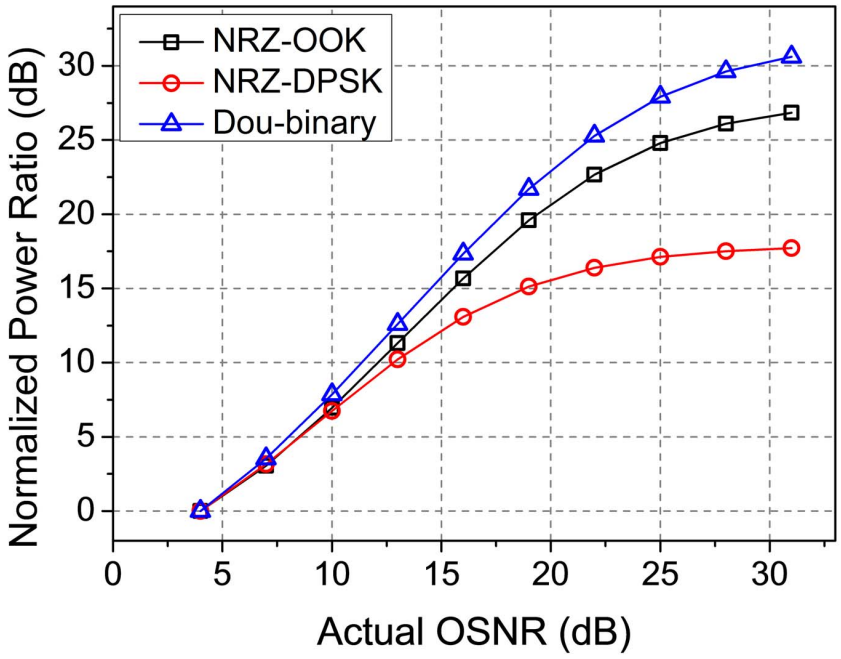


Figure 3.4: Simulation results of the OSNR monitoring performance comparison among the three tested formats.

Three modulation formats are tested in the proposed OSNR monitoring method, and the performance comparison are shown in Fig. 3.4. In this work, the OTF and the OBPF are 1st order Gaussian filters, with 50-GHz and 25-GHz bandwidth separately. The receivers bandwidth is 500 MHz. When the three modulation formats are tested under the same monitoring system setup and condition, the OSNR monitoring dynamic ranges are different. The monitoring dynamic range discussed in this chapter is the power ratio increment for the OSNR from 4 dB to 30 dB, which is used to compare the OSNR monitoring performance. Since the three tested modulation formats have their different spectrum shape, the coefficients are different for different systems, which lead to different OSNR monitoring dynamic ranges. As the OSNR increases to a high

value, signal power is dominant in $P_{UN}$ and $P_{ref}$. Thus, the ratio between $P_{UN}$ and $P_{ref}$ would converge to a saturation value, which is related to the filters' shape and bandwidth.

**Channel Bandwidth**

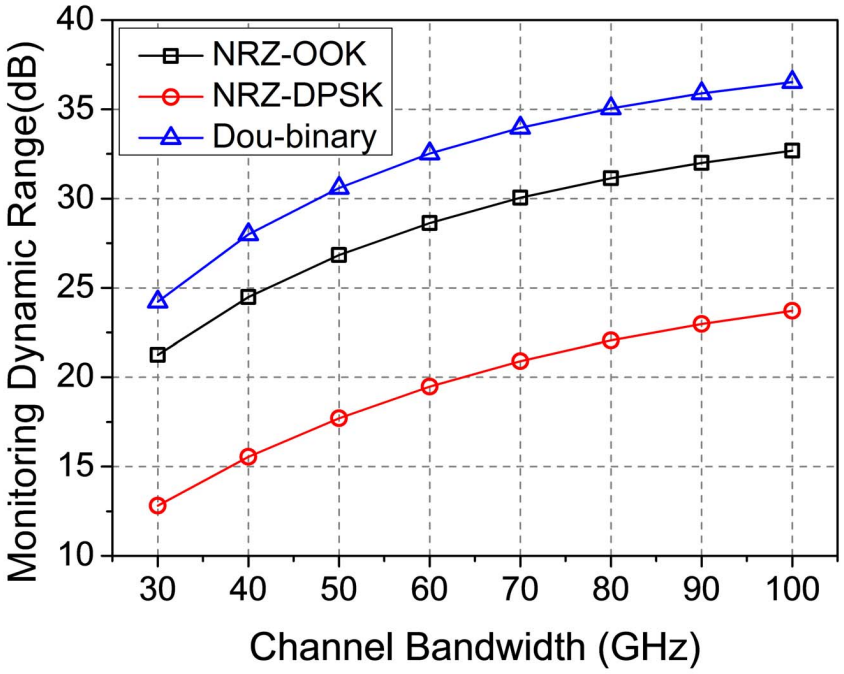


Figure 3.5: Simulation results of the monitoring dynamic range versus the channel bandwidth. The monitoring dynamic range is the normalized power ratio increment when the OSNR is from 4 dB to 30 dB. OBPF: 25 GHz, $1^{st}$ order Gaussian filter; PD: 500 MHz.

The monitored channel bandwidth is determined by the performance of de-multiplexer. In the simulation work, the OTF is used as de-multiplexer, whose bandwidth is studied from 30 GHz to 100 GHz, as shown in Fig. 3.5. The OSNR monitoring dynamic ranges increase as the channel bandwidth increases for all the tested formats, when the OSNR varies from 4 dB to 30 dB. The larger bandwidth of the OTF increases coefficient $\gamma$ in

the $P_{ref}$, which enlarges the noise power portion in $P_{ref}$, so that the OSNR monitoring dynamic range increases. However, in some cases, the larger channel bandwidth would bring more noise from neighbour channels, which may induces some monitoring errors. Thus, there is a trade-off between the monitoring dynamic range and the reliability.

**Bandwidth of the OBPF**

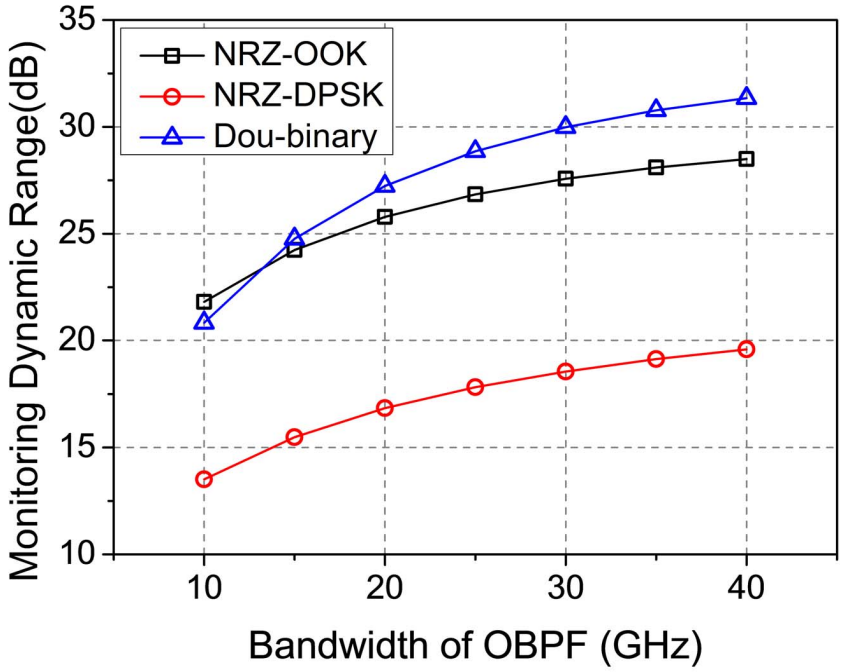


Figure 3.6: Simulation results of the OSNR monitoring dynamic range versus the bandwidth of the OBPF. The monitoring dynamic range is the normalized power ratio increasement when the OSNR varies from 4 dB to 30 dB. OTF: 50 GHz; PD: 500 MHz.

In Fig. 3.6, the OBPF bandwidth versus the OSNR monitoring dynamic range is demonstrated. As the OBPF bandwidth increases from 10 GHz to 40 GHz, the OSNR monitoring dynamic range is enlarged. The larger bandwidth of the OBPF reduces the

signal power weighting in $P_{UN}$, while the noise portion in $P_{UN}$ is increased, which leads to that the power ratio is more sensitive to noise power variation. Consequently, the OSNR monitoring dynamic range is increased.

**Receiver Bandwidth**

The receiver bandwidth is investigated in the proposed OSNR monitoring method. A high bandwidth receiver scheme is tested for the performance comparison with the low bandwidth scheme, whose bandwidth is equal to the bit rate. As Fig. 3.7 shows, the high bandwidth receiver scheme suffers serious OSNR monitoring errors, since the high frequency RF power variation induced by CD effect is included into the measured signal power. Moreover, in the high OSNR case, the CD induced power variation is more significant than the noise power variation, which leads to larger OSNR estimation errors. However, the low bandwidth receiver scheme minimizes CD induced OSNR monitoring error, since the low bandwidth receiver removes CD induced high frequency signal power variation. For PMD effect, since DGD also causes high frequency RF signal power variation, the low bandwidth receiver can also reduce DGD induced OSNR monitoring errors, as the simulation results show in Fig. 3.8. Hence, the receiver with the bandwidth of twentieth symbol rate is able to minimize the monitoring errors induced by dispersion effect. Although the receiver with narrower bandwidth is able to remove the dispersion induced power variation, it might cause that the output power is too small to be detected by the power meter with limited sensitivity. Thus, there is a tradeoff between the receiver bandwidth and the power meter sensitivity. More importantly, the low bandwidth receiver reduces the OSNR monitoring setup cost.

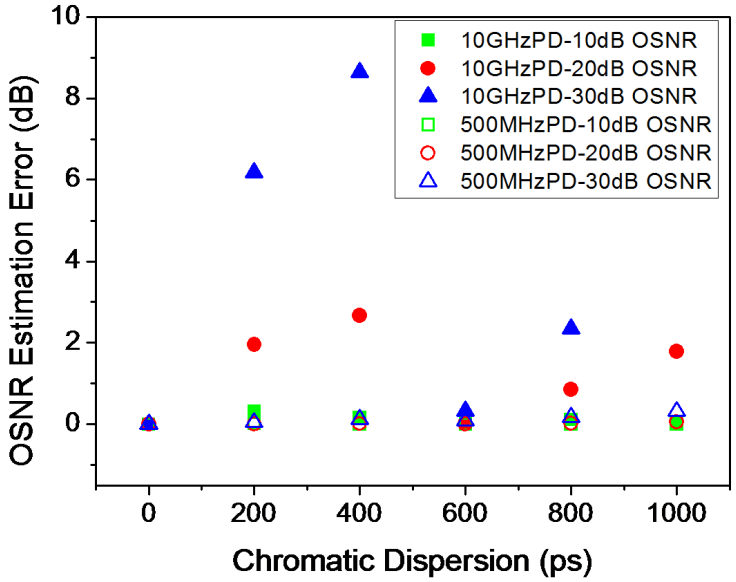


Figure 3.7: Simulation results of the OSNR monitoring accuracy versus CD effect in 10-Gb/s NRZ-OOK system. OTF: 50 GHz; OBPF: 25 GHz, $1^{st}$ order Gaussian filter.

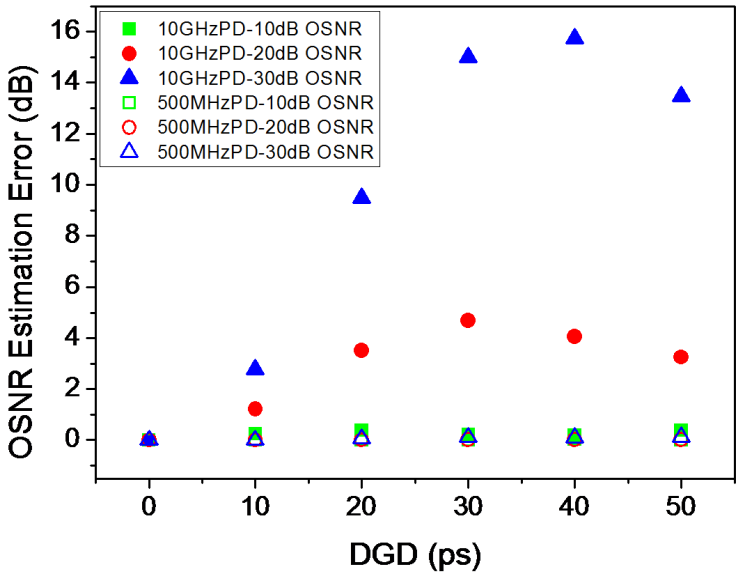


Figure 3.8: Simulation results of the OSNR monitoring accuracy versus DGD in 10-Gb/s NRZ-OOK system; OTF: 50 GHz; OBPF: 25 GHz, $1^{st}$ order Gaussian filter.

### 3.1.3 Experimental Setup

The experimental setup of the proposed OSNR monitoring method is shown in Fig. 3.9. The monitored signal is selected by a 0.4-nm optical tunable filter (OTF), and then, split into two branches by a 90:10 coupler. The $10\%$ optical signal is directly detected and measured as the reference signal power $P_{ref}$, while the $90\%$ optical signal is split into two branches by another 3-dB coupler. One branch is connected with a 0.2-nm OBPF with the same center frequency as the monitored signal. The other branch is connected with an optical attenuator and an optical time delay line, which are used to keep time and power matched between the two branches of the balanced receiver.

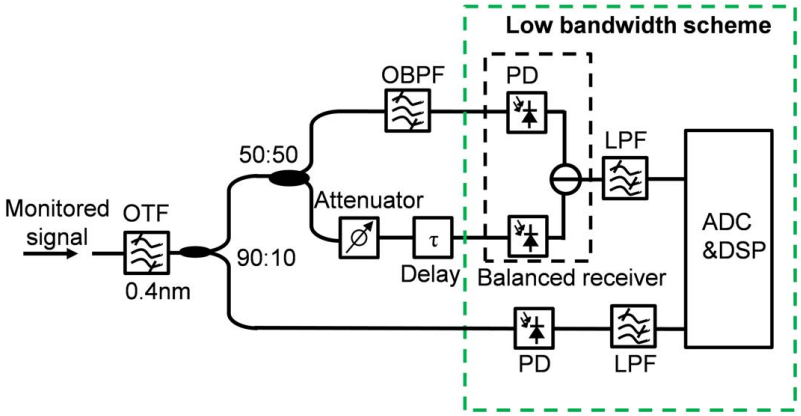


Figure 3.9: Schematic diagram of the experimental setup for the uncorrelated signal generation using balanced subtraction.

In the simulation work, the filter bandwidth and shape are investigated for their impact on the monitoring dynamic rang. In this section, the bandwidth of the OTF and the OBPF are fixed at 0.4 nm and 0.2 nm individually for experimental demonstration. More importantly, since the low bandwidth receiver and measurement equipment are adopted to achieve a low-cost OSNR monitoring scheme, two 465-MHz low-pass filters (LPF) are placed after the DC-coupled high-speed balanced receiver and the sin-

gle DC-coupled high-speed photo detector to emulate the low bandwidth receivers, as shown in Fig. 3.9. Additionally, the LPF can reject the high frequency RF components that are affected by dispersion effect, so it can reduce the signal power variation caused by dispersion. For the power measurement, since we do not have power meter, we use a 20-GHz sampling oscilloscope that works as an analog-digital-converter (ADC) to derive the amplitude of electrical signals, which can be converted into signal power. Since the LPF is placed before the sampling oscilloscope, the bandwidth of the ADC can be as low as the receiver bandwidth. Thus, it is possible to use a low bandwidth receiver and an ADC to fabricate a cost-effective OSNR monitoring module.

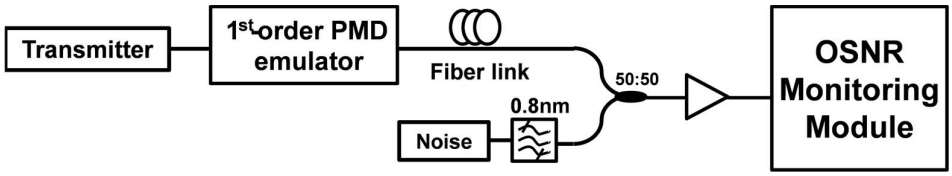


Figure 3.10: Experimental setup of the optical transmission system for the OSNR monitoring demonstration.

The whole experimental setup of the OSNR monitoring method is shown in Fig. 3.10. In the experimental demonstration, single polarization 10-Gb/s NRZ-OOK, 10-Gb/s NRZ-DPSK and 50-Gb/s NRZ-QPSK are tested. Moreover, 100-Gb/s PDM-QPSK is also investigated in detail in this work. For the generation of 10-Gb/s NRZ-OOK and DPSK, an MZM works at the quadrature and null point separately by applying different bias and driving voltage. 50-Gb/s single polarization QPSK signal is modulated by an I/Q modulator, while Pol-Mux is used to push 50-Gb/s signal to 100-Gb/s PDM signal. A first order PMD emulator is used to introduce differential group delay (DGD) into the system. Additionally, the different values of CD in the system are emulated by using different lengths of single mode fiber (SMF). The OSNR value in the system is varied by tuning the output power of the ASE noise source, which is coupled

with the optical signal by a 3-dB coupler. The bandwidth of the noise source is 0.8 nm. Before the monitoring module, an Erbium-doped fiber amplifier (EDFA) is used to compensate power loss during fiber transmission.

The optical spectra of 100-Gb/s PDM-QPSK signal before the two branches of the balanced receiver are shown in Fig. 3.11. The optical spectrum of the upper branch is overlapped with the center frequencies of the lower branch. The overlapped area can be tuned by varying the bandwidth of the OBPF. The overlapped frequency components of these two signals are correlated, which are cancelled out by balanced subtraction after photo detection. Therefore, the output of balanced receiver is the uncorrelated signal, which is measured as $P_{UN}$. It can be generally expressed by Eq. 3.1. Moreover, the detected reference signal power ($P_{ref}$) is expressed by Eq. 3.2.

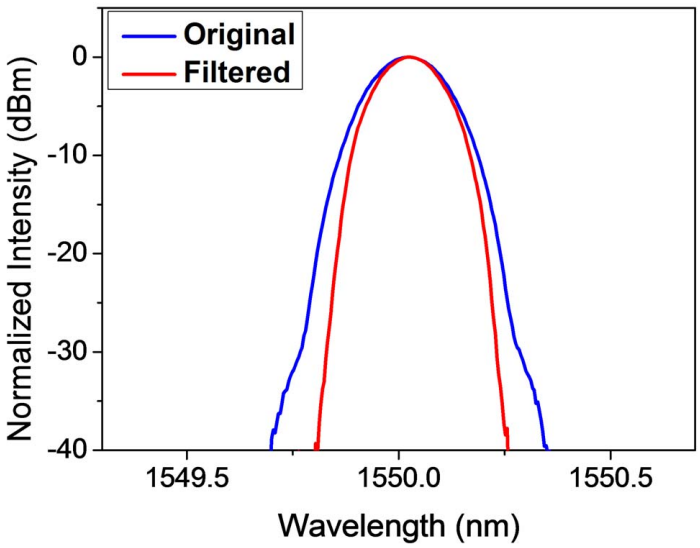


Figure 3.11: Optical spectra of the input signals of the balanced receiver.

Since the majority of the signal power is removed by balanced subtraction, $\alpha$ is much smaller than $\phi$. Moreover, due to the different signal-to-noise power ratios of these two equations, the OSNR is a function of the power ratio between the reference power and the uncorrelated signal power, as shown in Eq. 3.3. The signal OSNR is

estimated by using the power ratio between the reference signal and the uncorrelated signal. The exact OSNR can be estimated by the measured power ratio after data fitting and one-time calibration based on the actual performance of the filters in the monitoring setup.

### 3.1.4 Experimental Results in Single Polarization Systems

As the experimental and simulation results in Fig. 3.12 show, the proposed OSNR monitoring method using the power ratio is successfully demonstrated in 10-Gb/s NRZ-OOK and NRZ-DPSK systems from 10 dB to 30 dB. The simulation results demonstrated in this figure are generated by using the same setup and configuration as the experiment. The two modulation formats have different OSNR monitoring performances, due to different optical spectra. When the OSNR is at high level (larger than 25 dB), signal power becomes dominant in $P_{UN}$, which is insensitive to noise power variation, so that the OSNR monitoring dynamic range decreases. The divergences between the experimental results and the simulation results would be attributed to the performance difference of the filters. More importantly, the low bandwidth receiver scheme is not only compatible to our proposed OSNR monitoring method, but also able to increase the monitoring dynamic range, compared with the high bandwidth receiver scheme. When the OSNR is from 10 dB to 30 dB, the total monitoring dynamic range is increased by around 4 dB for these two signals. The monitoring dynamic range can also be tuned by varying the bandwidth of the OTF and the OBPF, as discussed in the previous sections.

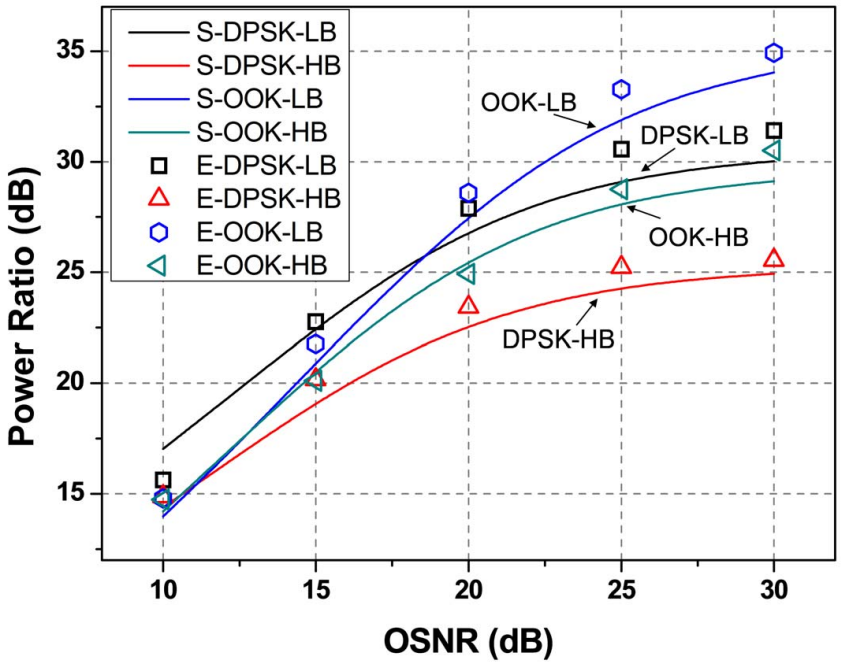


Figure 3.12: Experimental and simulation results of the proposed OSNR monitoring method. S: simulation results (line); E: experimental results (symbol); LB: low bandwidth receiver (465 MHz); HB: high bandwidth receiver (42 GHz).

### 3.1.5 Experimental Results in Polarization Division Multiplexed System

In this work, the proposed OSNR monitoring method is demonstrated in 50-Gb/s QPSK and 100-Gb/s PDM-QPSK systems. As the experimental results in Fig. 3.13 show, the proposed power ratio is a function of OSNR value in both 50-Gb/s QPSK and 100-Gb/s PDM-QPSK systems. The demonstrated OSNR monitoring range is from 5 dB to 27.5 dB. For real system monitoring, it is profound to monitor the signal OSNR from 10 dB to 25 dB. The OSNR monitoring performances in the two tested systems are the same, due to the same optical spectra, even if the 100-Gb/s signal uses PDM technique.

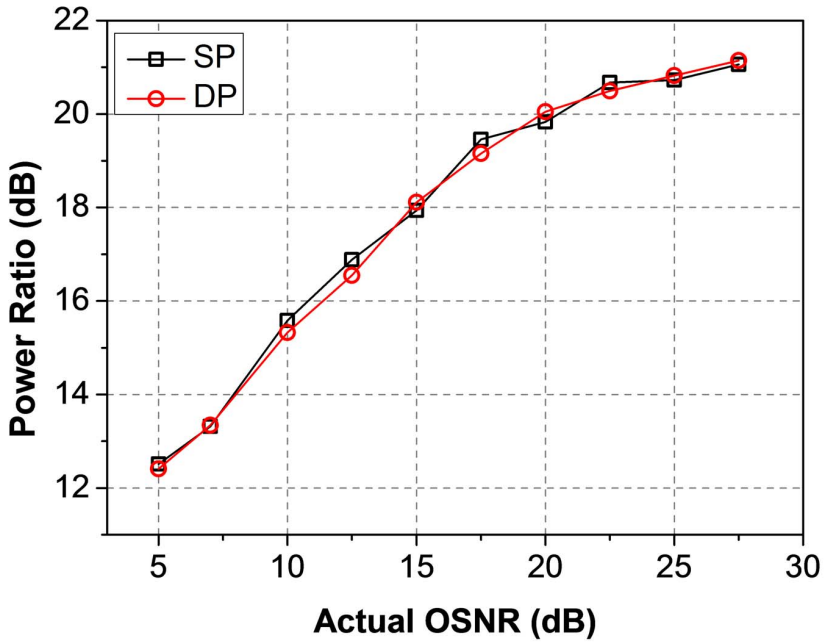


Figure 3.13: The experimental results of the signal power ratio versus the OSNR value in both single and dual polarization systems. SP: 50-Gb/s QPSK; DP: 100-Gb/s PDM-QPSK.

Since the proposed method is based on the electrical signal power, both CD and PMD induced high frequency RF power variation will reduce monitoring accuracy. Thus, by using the low bandwidth receiver, the OSNR monitoring errors induced by CD and PMD can be minimized. As the experimental results show in Fig. 3.14, in the demonstrated OSNR monitoring range (from 5 dB to 27.5 dB) of 100-Gb/s PDM-QPSK signal, the OSNR monitoring performance is robust to 1st order PMD. As the DGD increases from 0 ps to 50 ps, the OSNR monitoring errors are within 1-dB all the time.

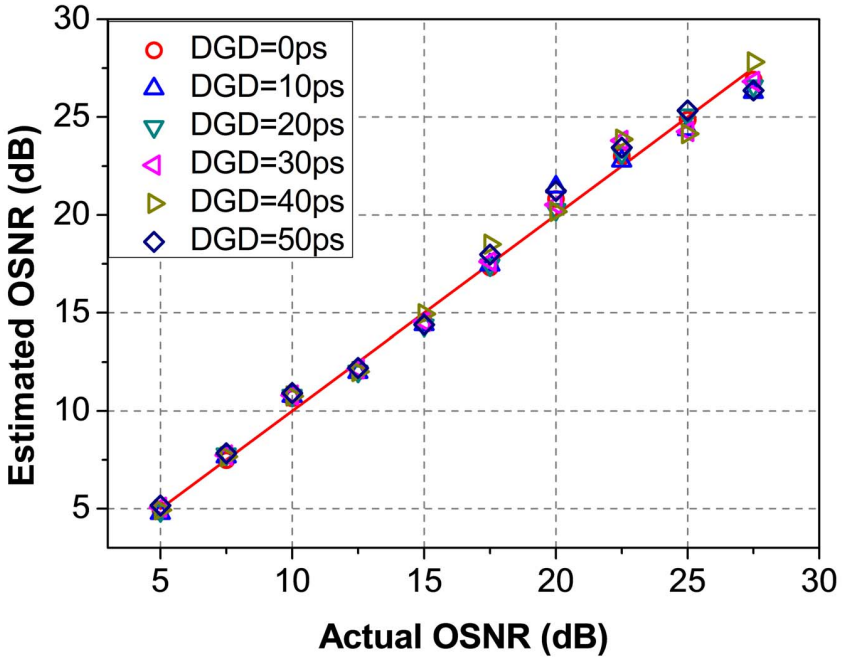


Figure 3.14: The OSNR monitoring performance of 100-Gb/s PDM-QPSK signals in the presence of 1st order PMD,

For investigation of the CD influence on the OSNR monitoring accuracy, the residual CD value is changed from 0 ps/nm to 1360 ps/nm in 100-Gb/s PDM-QPSK system. In Fig. 3.15, the experimental results show that the OSNR monitoring errors can always be kept below 1 dB. Since the low bandwidth receiver successfully removes the CD induced high frequency power variation, this scheme can be insensitive to the CD value which is much larger than the demonstrated one.

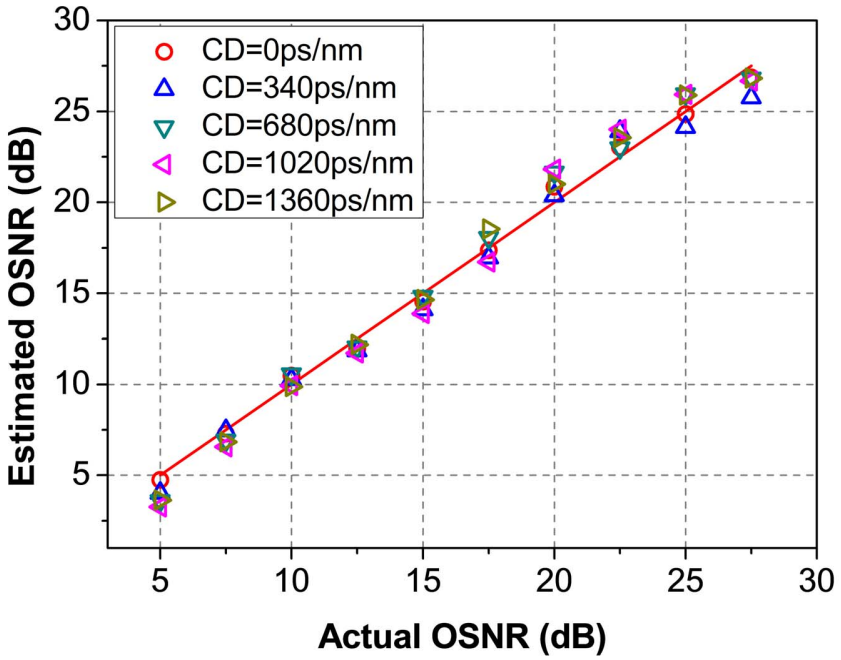


Figure 3.15: The OSNR monitoring performance of 100-Gb/s PDM-QPSK signals in the presence of CD.

In Fig. 3.16, the 1st order PMD influences on the OSNR monitoring accuracy in the low bandwidth receiver (465 MHz) and the high bandwidth receiver (42 GHz) systems are demonstrated and compared. As the DGD varies from 0 ps to 50 ps, the signal OSNR is tested in 10 dB, 15 dB, and 20 dB. By using the high bandwidth receiver, the OSNR monitoring performance is seriously affected by DGD, especially for the high OSNR cases. It is due to that the DGD induced power variation is greater than the noise power variation in the uncorrelated signal. In the low bandwidth receiver scheme, the OSNR monitoring errors are minimized below 1 dB for all cases.

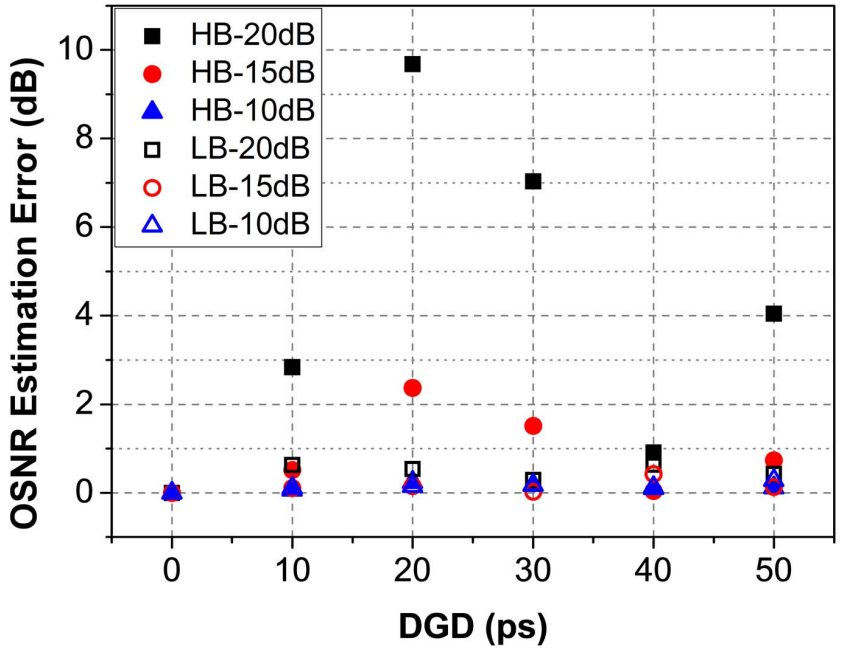


Figure 3.16: 1st order PMD induced OSNR monitoring errors in the low bandwidth scheme and the high bandwidth scheme for different OSNR cases (10 dB, 15 dB and 20 dB) in 100-Gb/s PDM-QPSK system. LB: low bandwidth receiver; HB: high bandwidth receiver.

In Fig. 3.17, the OSNR monitoring accuracy in the low bandwidth receiver and high bandwidth receiver systems is studied in the presence of CD effect. The residual CD is changed from 0 ps/nm to 1360 ps/nm by using different lengths of fiber. The signal OSNR is tested in 10 dB, 15 dB, and 20 dB individually. The high bandwidth receiver scheme suffers the CD induced OSNR monitoring performance errors seriously, especially for the high OSNR cases. As same as DGD, the CD induced power variation is greater than the noise power variation in the uncorrelated signal. In the low bandwidth receiver scheme, the OSNR monitoring errors are almost kept below 1 dB as the CD varies.

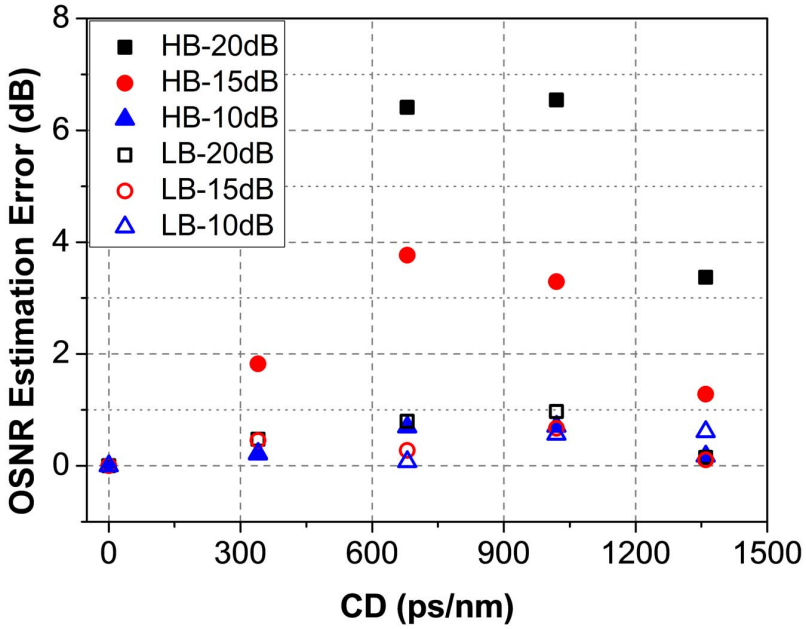


Figure 3.17: CD induced OSNR monitoring errors in the low bandwidth scheme and the high bandwidth scheme for different OSNR cases (10 dB, 15 dB and 20 dB) in 100-Gb/s PDM-QPSK system. LB: low bandwidth receiver; HB: high bandwidth receiver.

The low bandwidth scheme cannot only reduce the DGD and CD induced monitoring errors, which also increases the time mismatch tolerance between the two branches of the balanced receiver. As the experimental results show in Fig. 3.18, the 1-dB OSNR monitoring error tolerance of the time mismatch is less than 4 ps in the high bandwidth scheme. The time mismatch induced OSNR monitoring error is larger in the higher OSNR case (20 dB). After using the low bandwidth receiver, the 1-dB OSNR monitoring error tolerance can be increased to 40 ps in the high OSNR case.

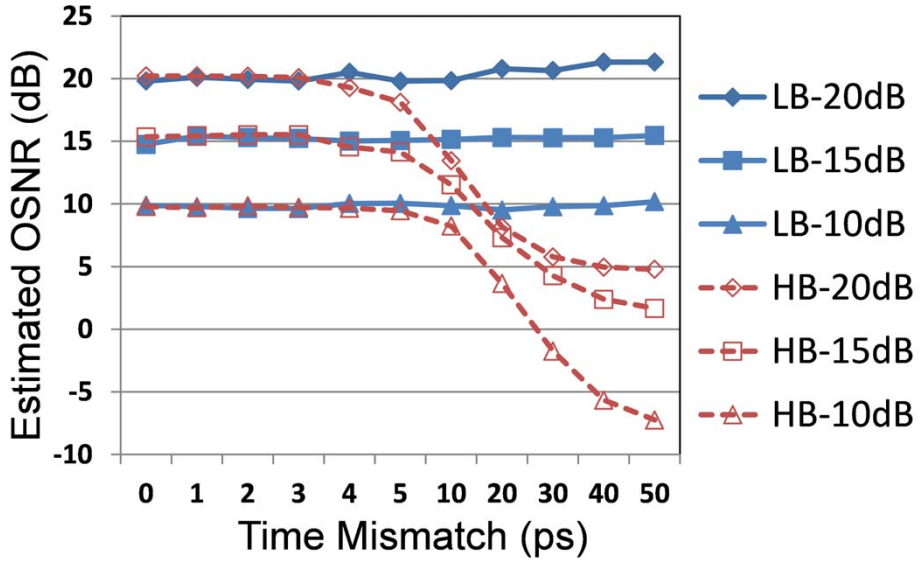


Figure 3.18: The time mismatch tolerance comparison between the low bandwidth scheme and the high bandwidth scheme at different OSNR values (10 dB, 15 dB, and 20 dB) in 100-Gb/s PDM-QPSK system.

## 3.2 OSNR Monitoring Using Uncorrelated Signal Generated by Optical Interference

In this section, we propose an OSNR monitoring scheme using the uncorrelated signal generated by optical interference. Compared with the uncorrelated signal generation using balanced subtraction, an optical coupler is employed to replace the balanced receiver to remove the correlated signal. The destructive port of the optical coupler generates novel notch filtering effect, while the constructive port serves as a combiner. This novel filter scheme is proposed for OSNR monitoring, because the two outputs contain the different ratios of signal and noise power. Consequently, the signal power ratio between the destructive and constructive branches can be a function of OSNR value. Moreover, a low bandwidth photo detector used in this monitoring scheme

provides low-cost and dispersion insensitive merits. The proposed OSNR monitoring method is demonstrated in 10-Gb/s and 40-Gb/s systems by using VPI transmission maker 7.6.

### 3.2.1 Working Principle of the Proposed Method

The conventional notch filtering effect is generated by FBG filter or delay interferometer (DI). In this section, we propose a new scheme to generate notch filtering effect. The schematic diagram of the setup is shown in Fig. 3.19. The incoming optical signal is split into two branches by a 3-dB coupler at first. Then, the upper branch is sent into a narrow bandwidth optical band-pass filter (OBPF), whose center frequency is same as the monitored signal center frequency. The filtered signal in the upper branch is coupled with the signal in the lower branch by another 3-dB coupler. Both the intensity and the time delay of the two-branch signals are matched before the second 3-dB optical coupler.

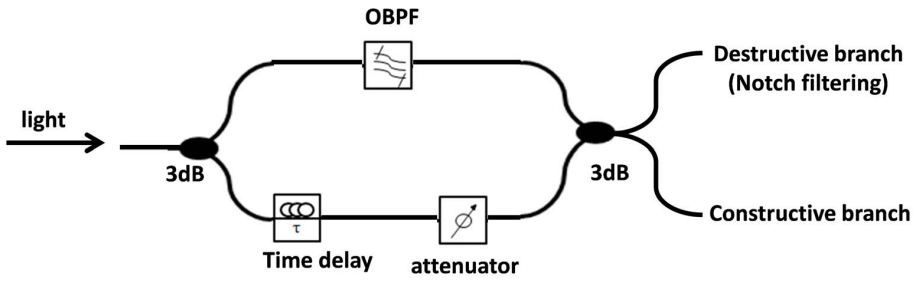


Figure 3.19: Schematic diagram of the proposed notch filtering scheme.

In Fig. 3.20, the optical spectrum of ASE noise is used to illustrate the generated filtering effect. The optical spectrum of ASE noise is assumed to be constant at the demonstrated frequency range. After it enters the proposed setup, the ASE noise in the upper branch is tailored by the narrow bandwidth OBPF, while the lower branch signal keeps intensity and time matched with that of the upper branch. The filtered

signal and the un-filtered signal are correlated at the overlapped frequencies. After optical interference between these two branches, the correlated signal components are removed by destructive interference at one output, which generates band-stop effect, as notch filter.

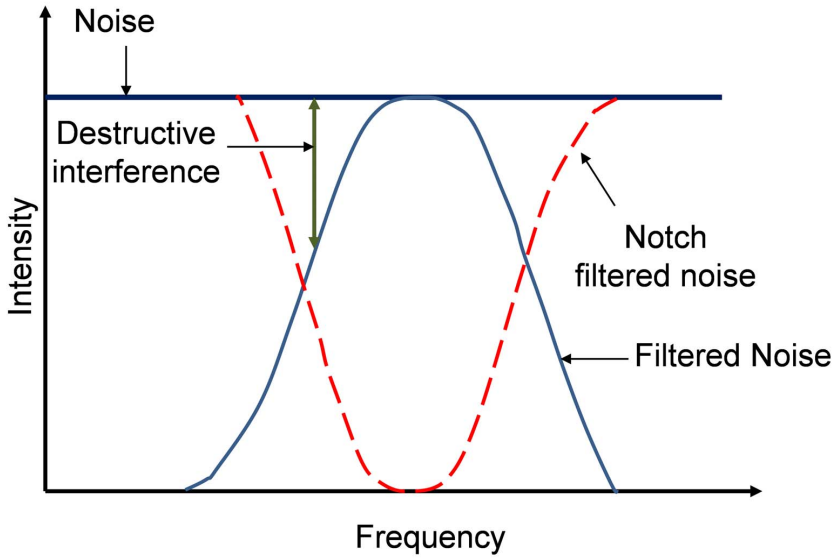


Figure 3.20: The illustration of the proposed filtering effect generation using ASE noise.

In Fig. 3.21, the simulated optical spectra demonstrate the proposed notch filtering effect, which employ ASE noise as an example. In Fig. 3.21(a) and (b), the optical spectra are the noise spectra in the upper (filtered) and lower (un-filtered) branches of the proposed scheme separately. Fig. 3.21(c) and (d) show the optical spectra of the destructive and constructive ports of the proposed scheme. As Fig. 3.21(c) shows, there generates band-stop effect at the correlated frequency, where the correlated signal is removed. In Fig. 3.21(d), the optical spectrum shows that the constructive interference combines the two signals.

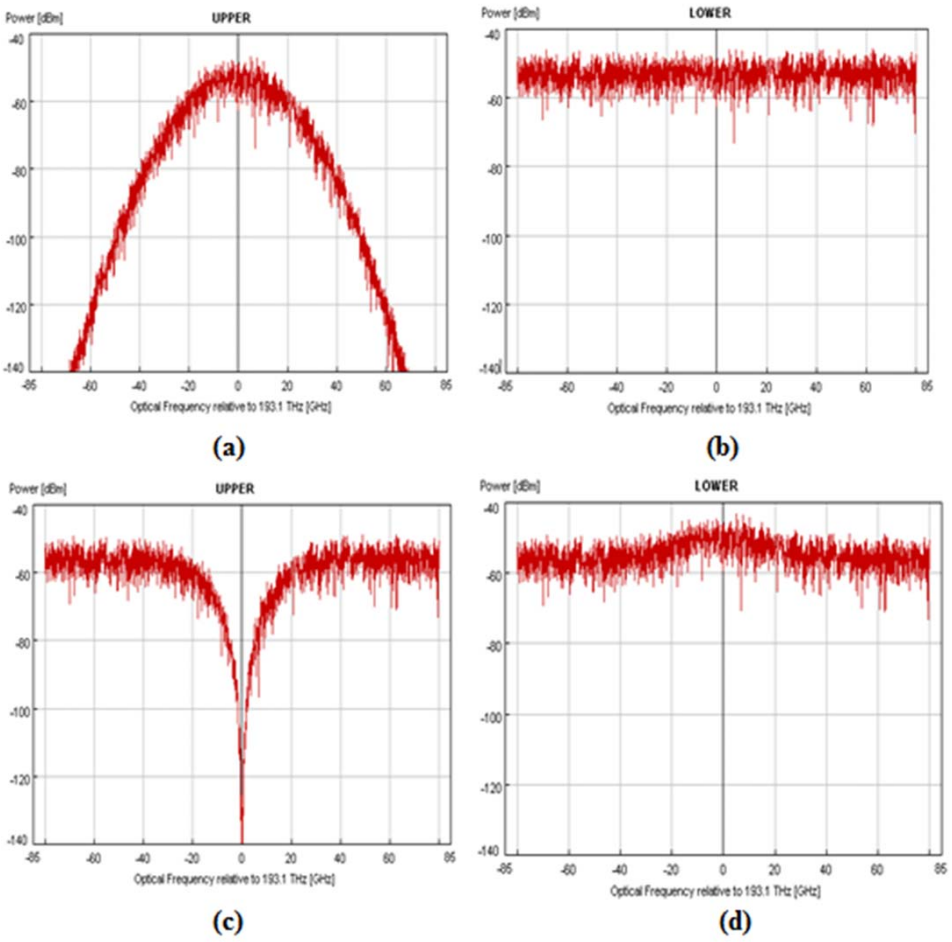


Figure 3.21: Optical spectra at the different locations of the proposed scheme, which use ASE noise as an example. (a) the upper branch before the second coupler , (b) the lower branch before the second coupler, (c) the upper branch after the second coupler, (d) the lower branch after the second coupler.

The system setup of the OSNR monitoring method using the proposed notch filtering effect is shown in Fig. 3.22. The modulated optical signal is coupled with the ASE noise before launching into fiber link. A section of single mode fiber (SMF) and a PMD emulator are used to induce CD and PMD into the transmission system. The optical tuneable filter (OTF) is employed as a channel selector to pick up the monitored channel from WDM system. Then, the optical signal goes through the proposed notch

filter scheme, and is detected by a low bandwidth photo detector. A power meter is used to measure the received signal power.

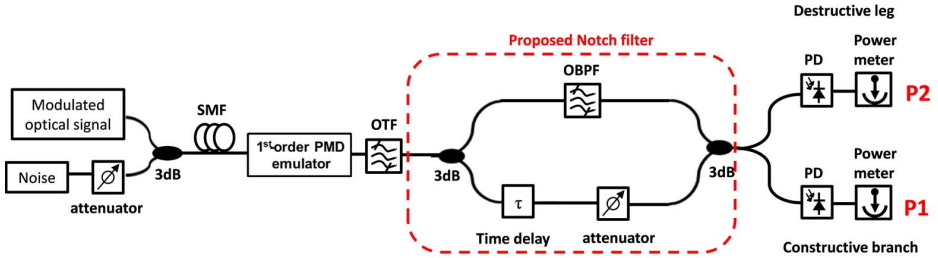


Figure 3.22: The system setup of the OSNR monitoring method using the proposed notch filtering scheme.

Firstly, the signal at the lower branch of the second coupler input is the original monitored signal, whose optical power ($P_0$) can be expressed by Eq. 3.4. Additionally, the upper branch filtered signal power ($P_c$) can be expressed by Eq. 3.5. The whole filtered signal is correlated with a part of the original signal. After the optical interference between these two signals, the correlated signals between these two branches are cancelled out at the destructive port, which can be expressed by Eq. 3.7, while the signal at the constructive port is the summation of the two signals, whose power can be expressed by Eq. 3.6.

$$P_0 \propto \phi \cdot P_S + \gamma \cdot P_N \tag{3.4}$$

$$P_c \propto \alpha \cdot P_S + \beta \cdot P_N \tag{3.5}$$

$$P_1 \propto 0.5 \cdot ((\phi + \alpha) \cdot P_S + (\gamma + \beta) \cdot P_N) \tag{3.6}$$

$$P_2 \propto 0.5 \cdot ((\phi - \alpha) \cdot P_S + (\gamma - \beta) \cdot P_N) \tag{3.7}$$

$$OSNR = \frac{P_S \cdot NEB}{P_N \cdot B_r} = f\left(\frac{P_1}{P_2}\right) \tag{3.8}$$

$P_S$ and $P_N$ represent the signal power and the noise power, respectively. The coefficients $\alpha$ and $\beta$ are related to the shape and bandwidth of the OBPF separately, which

determine the spectrum of the correlated signal, while $\phi$ and $\gamma$ are defined by the OTF performance. Since the correlated signal contains the major part of signal power, $\phi - \alpha$ is much smaller than $\phi + \alpha$. Thus, the ratio between $P_1$ and $P_2$ is a function of OSNR, as expressed in Eq. 3.8.

In this work, NRZ-OOK, NRZ-DPSK, and Duo-binary signals are investigated for the proposed OSNR monitoring scheme in 10-Gb/s and 40-Gb/s systems by using VPI transmission maker 7.6. The bandwidths of OTF, OBFP and photo detector (PD) are also investigated for their influence on the OSNR monitoring.

### 3.2.2 Simulation Results and Discussions

#### Modulation Format and Transmission Rate

In this section, three modulation formats in 10-Gb/s and 40-Gb/s systems are demonstrated and compared in the proposed monitoring setup, as shown in Fig. 3.23. The bandwidths of OTF, OBF, and PD are 50 GHz, 25 GHz, and 1 GHz separately in this setup. The OSNR monitoring in the three modulation formats are successfully demonstrated, but their monitoring dynamic ranges are diverse, due to the different spectrum shapes. The monitoring dynamic range being discussed in this section is the power ratio increment as the OSNR from 5 dB to 30 dB. When the OSNR increases to a certain high value, $P_1$ and $P_2$ become signal power dominant. Thus, the power ratio approaches to a fixed value, like saturation. When the data rate is increased from 10-Gb/s to 40-Gb/s, the signal optical spectrum is broaden, which increases the difference between $\phi$ and $\alpha$. It increases the weight of the signal power in the uncorrelated signal, which reduces the monitoring dynamic ranges.

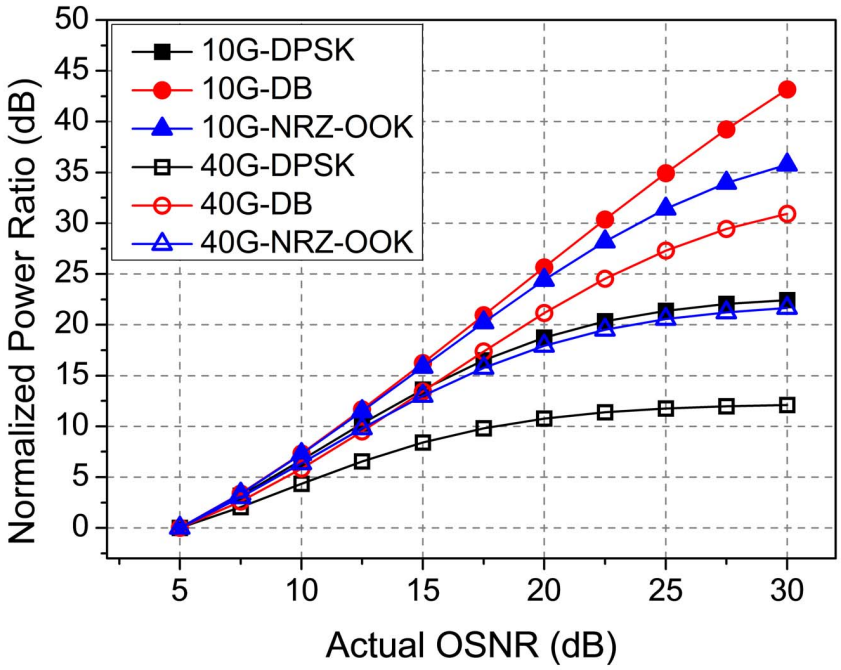


Figure 3.23: Simulation results of the comparison among different modulation formats with different data rates. OTF: 50 GHz; OBPF: 25 GHz; PD: 1 GHz.

**Monitoring Scheme Comparison**

In this work, the DI based OSNR monitoring performance is compared with the proposed OSNR monitoring performance. The time delay of the demonstrated DI is 25 ps. The power ratio between the constructive port and the destructive port of the DI is used to estimate OSNR. In Fig. 3.24, the monitoring performances of the proposed method and the DI based method are compared in 10-Gb/s and 40-Gb/s NRZ-OOK systems. The proposed OSNR monitoring method has a larger monitoring dynamic range. It is due to that the stop-band bandwidth of the notch filter is larger than that of the ODI. Thus, more signal power is removed in the proposed scheme, which contributes to the larger monitoring dynamic range.

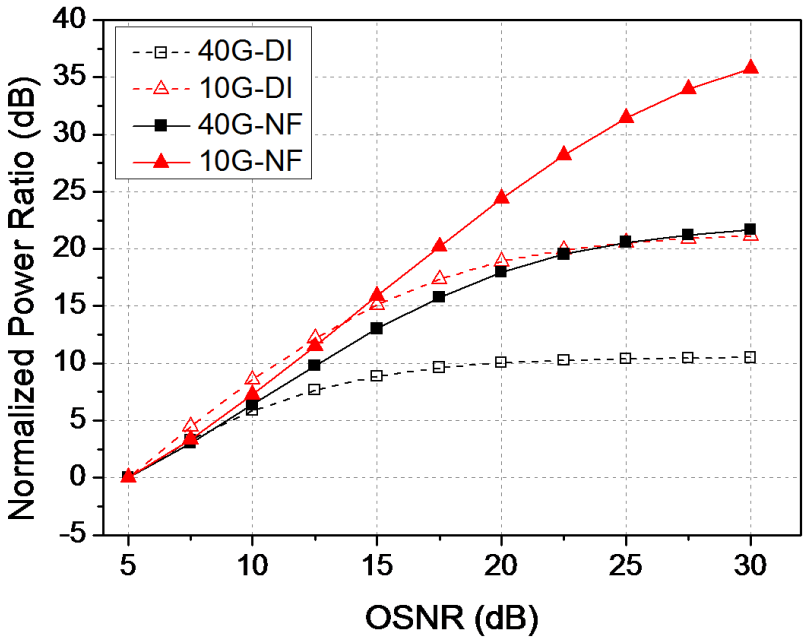


Figure 3.24: Simulation results of the OSNR monitoring performance comparison between the proposed notch filter based method and the DI based method. DI: the DI based method; NF: the proposed notch filter based method. OTF: 50 GHz; OBPF: 25 GHz; PD: 1 GHz.

### Channel Bandwidth

The bandwidth of the OTF is tuneable for different channel spacing and various system configuration requirements. The monitored channel bandwidth is another factor that determines the monitoring dynamic range. As Fig. 3.25 shows, the OSNR monitoring dynamic range increases as the OTF bandwidth increases from 30 GHz to 80 GHz, which is quite important to improve the OSNR monitoring dynamic range for the 40-Gb/s systems. Since more noise power is included in $P_1$ and $P_2$, the signal power dynamic range is improved.

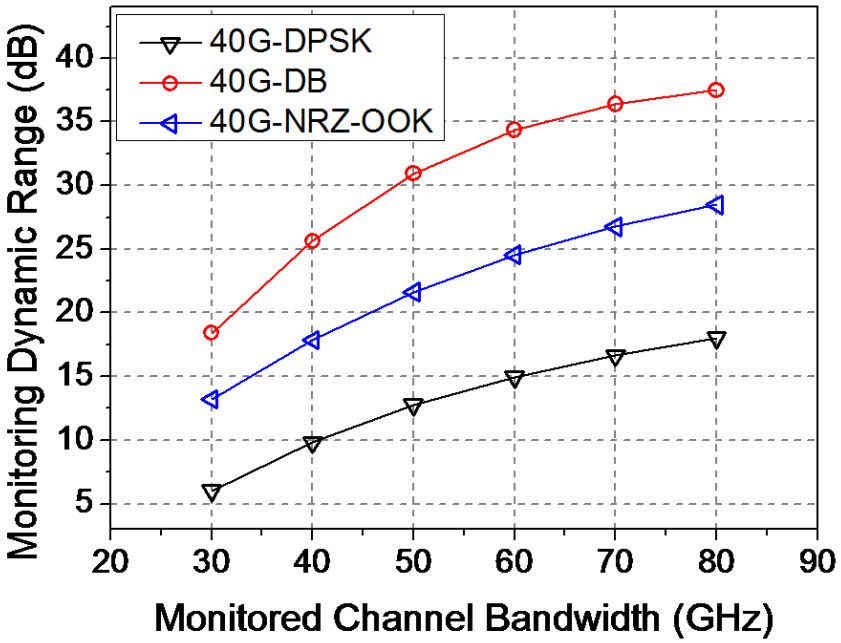


Figure 3.25: Simulation results of the OTF bandwidth versus the monitoring dynamic range. OBPF: 25 GHz; PD: 1 GHz.

**Bandwidth of OBPF**

The bandwidth of the OBPF is another key factor that affects the OSNR monitoring performance. As the simulation results show in Fig. 3.26, the scheme using larger bandwidth OBPF has a larger monitoring dynamic range. The larger bandwidth OBPF increases $\alpha$ in Eq. 3.5, which reduces the signal power portion in $P_2$, so that the saturation point of the power ratio curve is also increased. The monitoring dynamic range is increased as well.

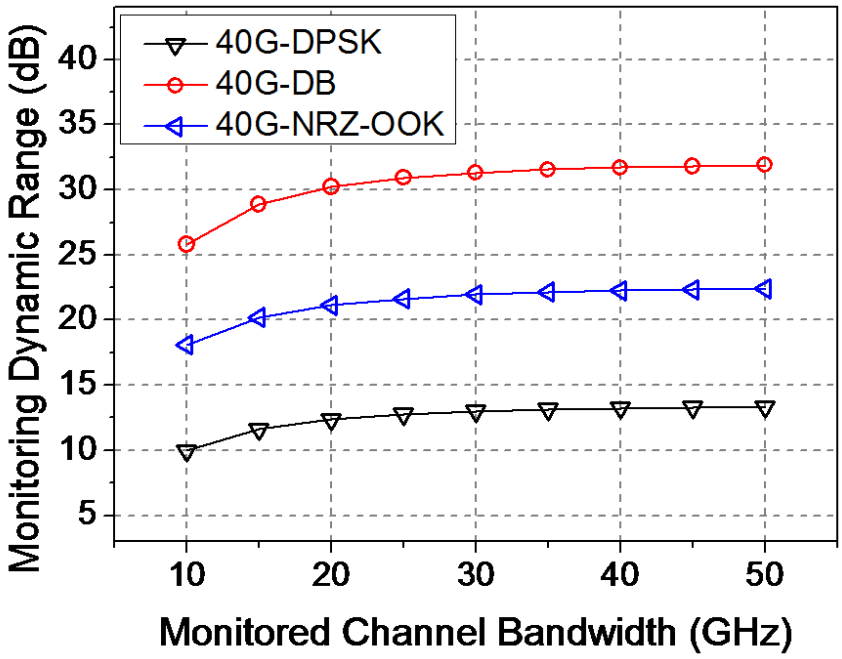


Figure 3.26: Simulation results of the relationship between the monitoring dynamic range and the bandwidth of OBPF. OTF: 50 GHz; PD: 1 GHz.

**Bandwidth of Photo Detector**

In this method, low bandwidth photo detectors are used to minimize the CD and PMD induced OSNR monitoring errors, which is also a low-cost solution. Thus, the high bandwidth (40 GHz) scheme and the low bandwidth (1 GHz) schemes are investigated in the OSNR monitoring in the presence of CD and PMD. As Fig. 3.27 and 3.28 show, the low bandwidth scheme is robust to CD and PMD impairments, since the low bandwidth receiver removes the dispersion induced high frequency power variation. However, the high bandwidth scheme suffers from the CD and PMD induced monitoring errors. Moreover, the monitoring errors introduced by CD and PMD are significant in the high OSNR case, because the CD and PMD induced power variation is greater than the noise power variation.

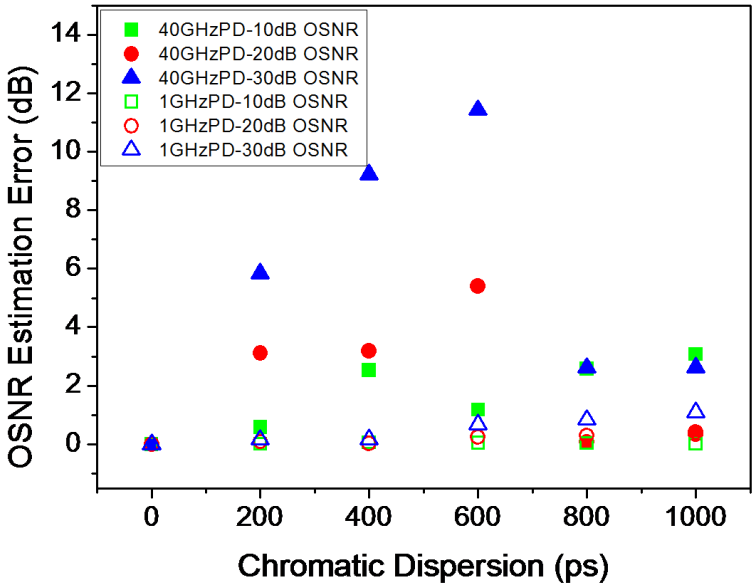


Figure 3.27: Simulation results of CD versus OSNR monitoring error in 40-Gb/s NRZ-OOK system for difference receiver schemes. OTF: 50 GHz; OBPF: 25 GHz.

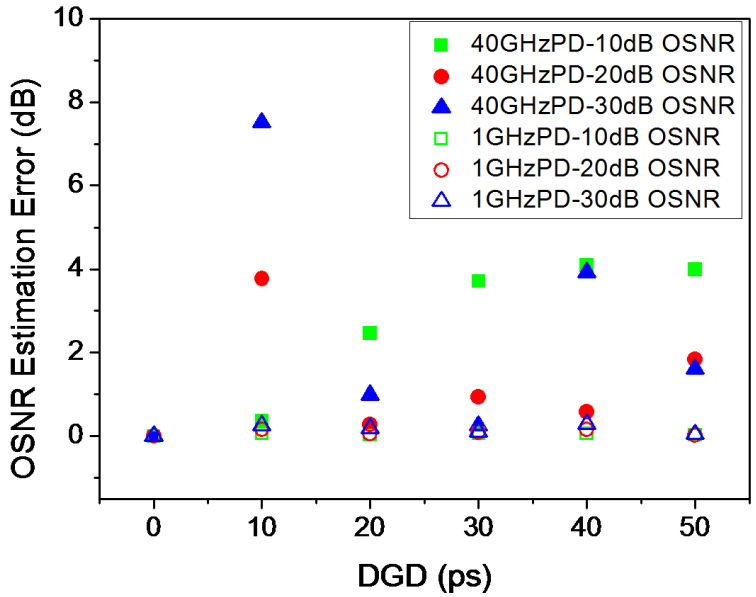


Figure 3.28: Simulation results of 1st order PMD versus OSNR monitoring error in 40-Gb/s NRZ-OOK system for difference receiver schemes. OTF: 50 GHz; OBPF: 25 GHz.

## 3.3 Conclusion

In this chapter, a OSNR monitoring method was proposed and demonstrated by using uncorrelated signal power. The generation of the uncorrelated signal was demonstrated by balanced subtraction or optical interference. For the OSNR monitoring method using the uncorrelated signal power generated by balanced subtraction, it has been experimentally demonstrated in both single and dual polarization systems. Moreover, by using low bandwidth receivers, both CD and PMD induced monitoring errors are minimized, while the tolerance of the time mismatch of balanced receiver is increased. More importantly, the low bandwidth receiver scheme reduces the cost of monitoring module. This method has shown its advantages of dispersion sensitivity, simple and low cost system setup, polarization independence, and integrability. Thus, it is possible to fabricate a portable OSNR monitoring device which is implemented in the receiver end, switching center, and fiber link.

For the OSNR monitoring method using the uncorrelated signal generated by optical interference, it is demonstrated by simulation work. The proposed scheme generates novel band-stop filtering effect to derive uncorrelated signal power for OSNR monitoring, which shows a larger monitoring dynamic range than that of the OSNR monitoring method using ODI. Since this method is based on optical interference that is sensitive to polarization rotation, it is difficult to experimentally demonstrate this method by using the discrete devices, which are connected by fiber patch cords. Thus, the monitoring setup needs to be integrated into a waveguide based photonic device for further demonstration.

# Chapter 4

# Optical Signal to Noise Ratio and Chromatic Dispersion Monitoring Based on Single Channel Sampling Technique

In the previous chapter, the OSNR monitoring method based on filtering effect is discussed, which is a cost effective method of single optical impairment monitoring in optical fiber transmission systems. However, the monitoring accuracy depends on the stable working performance of the optical devices, including working wavelength, attention, polarization, optical gain, and etc. The precise control of the optical devices increases the complexity of OPM system, which is an important factor for the monitoring system design. Compared with the OPM method using analog signal processing, the monitoring method based on digital signal processing (DSP) shows its advantages of simple setup and easy maintenance, which employs a limited number of devices.

Since the optical impairments cause the received signal waveform distortion in

different forms and degree, it is an effective way to monitor the optical impairments through the analysis on the received waveform. 2-dimension (2-D) phase portrait is an alternative expression of electrical waveform. Thus, the method using the 2-D phase portrait is a good approach for multiple optical impairments monitoring. By using the statistical analysis on the 2-D phase portrait, the OSNR monitoring and CD monitoring parameters can be derived by simple pattern recognition [75–77]. However, for the 2-D phase portrait generation, high bandwidth samplers are necessary to display the waveform distortion induced by optical impairments, so that the two samplers are the major cost of the monitoring setup. Thus, we propose to derive the X-Y pairs by using single-channel-sampling (SCS) technique, which could reduce the monitoring setup cost significantly. Moreover, as discussed in [66], for OSNR monitoring, the monitoring system noise should be much smaller than the monitored signal noise, which means that larger optical input power is preferred for the monitoring system. Since the SCS method samples the received signal directly without a 3-dB split, it can save 3-dB power budget for the monitored signal, compared with the two-channel-sampling (TCS) method.

In this chapter, the generation of the 2-D phase portrait using SCS method is proposed and demonstrated in both NRZ and RZ systems. Additionally, statistical pattern recognition is used to derive the monitoring parameters.

## 4.1 Operation Principle and Experimental Setup

### 4.1.1 Working Principle of Single Channel Sampling Scheme

The schematic diagrams of the TCS method and the SCS method are shown in Fig. 4.1. For the TCS method setup, the two samplers are the major part of the monitoring system, which convert analog signal into digital sequence. The sampled data is processed

by digital signal processing (DSP) successively. The whole monitoring system setup is much simple, which is easy to be maintained. The SCS method saves one sampler cost, while the abandon of the time delay line enables the further simplification of the monitoring system.

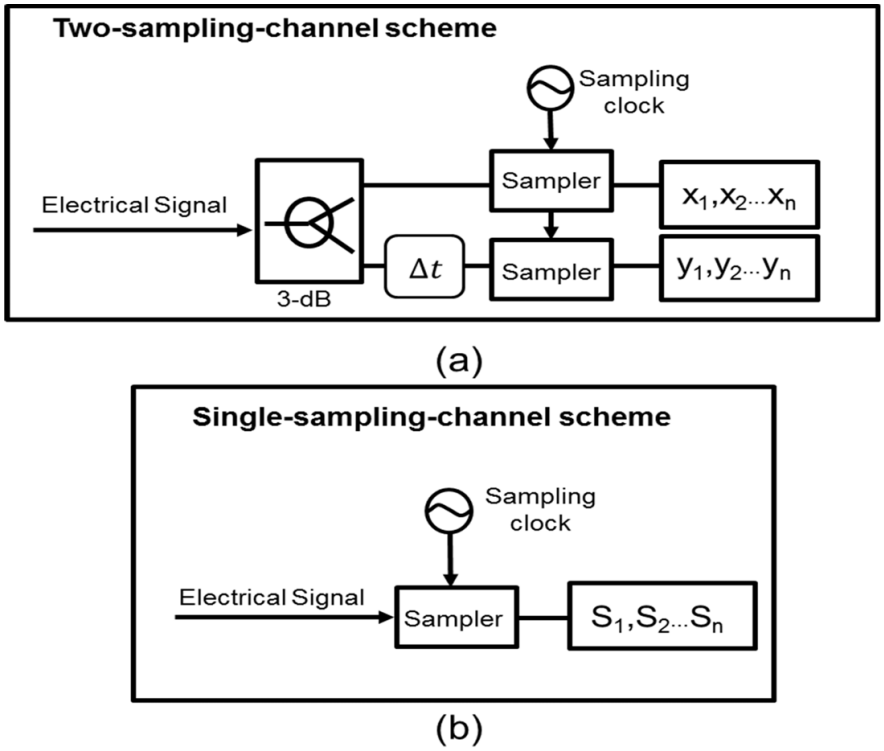


Figure 4.1: Schematic diagram of the two sampling schemes: (a) two-channel-sampling method, (b) single-channel-sampling method.

The X-Y pair derivation procedures of these two methods are shown and compared in Fig. 4.2. In the TCS method, the two samples (x and y) are obtained by the two sampling channels separately with short and fixed time delay ($\Delta t$) as a X-Y pair. Typically, the time delay ($\Delta t$) is less than one symbol duration. In the SCS method, since a single sampler continuously samples electrical signal with relatively slower frequency ($f_s$), the time interval between the continuous two samples, $S_1$ and $S_2$, can be expressed as $1/f_s$, which can also be described as $n \times T + \tau$ ($n$ is an integer number; $T$

is one symbol duration; $\tau$ is the remaining time that is less than one symbol duration). Once the data rate and the sampling rate are known, $\tau$ can be obtained.

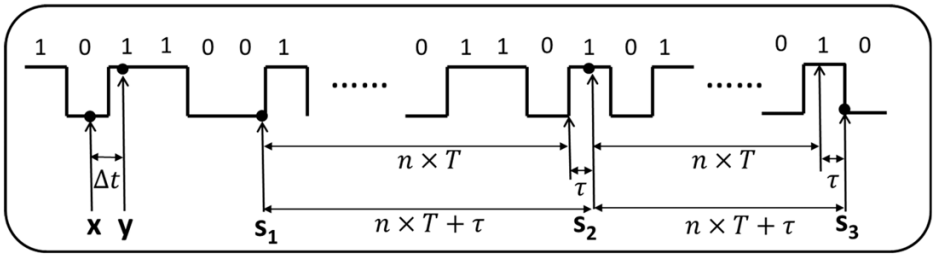


Figure 4.2: Working principle of these two methods.

### 4.1.2 X-Y Pairs Generation by Self-delay Scheme

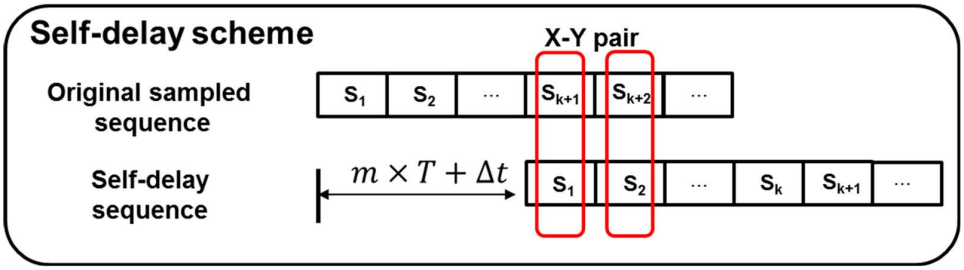


Figure 4.3: Schematic diagram for the self-delay method.

By using the SCS method, we can obtain the discrete sample sequence $(S_1 ... S_n)$ with a known sampling interval, which is shown in Fig. 4.3. There exists a sample $(S_{k+1})$ that has the time interval $(k \cdot n \times T + k \times \tau)$ between $S_1$ and $S_{k+1}$, which can also be expressed as $m \times T + \Delta t$ (m is an integer number, $\Delta t$ is the same as TCS method). The original sequence makes self-delay by k samples, so that $S_{k+1}$ and $S_1$ are composed of a new X-Y pair with large time delay $m \times T + \Delta t$. The following sample pairs between the two sequences, such as $S_{k+2}$ and $S_2$, $S_{k+3}$ and $S_3$, and so on, have same time delay. Thus, the following sample pairs between these two sequences are selected to form the X-Y pairs, which are depicted in a 2-D coordinate system successively.

The accumulated X-Y pairs depict a particular pattern in the 2-D coordinate system, which delivers the relative intensity between the two addresses on waveform, who are with a fixed phase difference ($2\pi \cdot \Delta t/T$). It is an equivalent phase portrait of the phase portrait generated by using TCS method. In the experimental demonstration of the proposed SCS method, a single channel of sampling oscilloscope is used to derive the discrete waveform serial. A sampling clock, whose frequency is $f_d/256$ ($f_d$ =data rate), is employed to obtain the accurate and known sampling time interval for the SCS method demonstration.

### 4.1.3 Experimental Setup

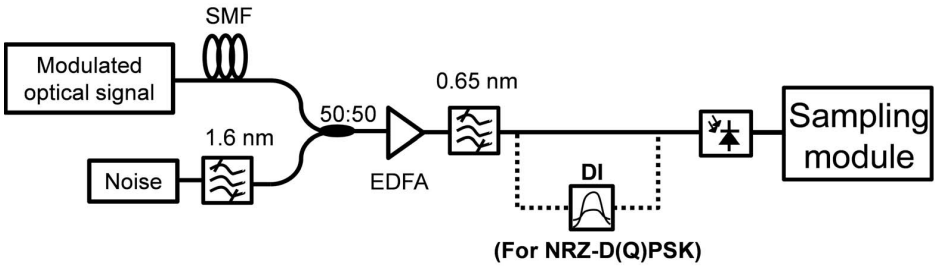


Figure 4.4: Experimental demonstration setup of our proposed method. DI: delay interferometer.

The experimental demonstration setup of our proposed SCS method is shown in Fig. 4.4. 10-Gb/s NRZ-OOK and NRZ-DPSK are modulated by a Mach-Zehnder modulator with different bias voltage respectively, while 20-Gb/s NRZ-DQPSK and 50-Gb/s RZ-DQPSK are modulated by an I/Q modulator separately. After optical fiber transmission, the optical signal is coupled with a 1.6-nm bandwidth noise source. An EDFA is used to compensate the power loss in the fiber transmission. Before photo detection, another 0.65-nm optical band pass filter (OBPF) is used to remove the redundant noise. For the NRZ-OOK and RZ-DQPSK systems, we employ a single photo detector (42

GHz) to detect the optical signal directly, and then, use a single channel of sampling oscilloscope (20 GHz) to sample the detected electrical signal. For the NRZ-DPSK and NRZ-DQPSK signals, a delay interferometer (DI) is used to demodulate the phase modulated signals before the photo detector. Since ASE noise induces significant mark level variation, the phase demodulation can emphasize the ASE noise induced signal variation. The input power of the photo detector is kept at -3 dBm. In this chapter, we demonstrate the OSNR monitoring from 10 dB to 30 dB. At the same time, the residual CD is introduced by the optical fibers with different distances, in order to investigate the OSNR monitoring performance under residual CD impairment. For the CD monitoring demonstration, the residual CD is changed from 0 ps/nm to 425 ps/nm.

## 4.2 OSNR Monitoring Based on 2-D Phase Portrait

### 4.2.1 2-D Phase Portrait

**Simulation Study of Different Phase Difference Phase Portraits**

In order to make a systematic study of the 2-D phase portrait, the simulation study is carried out in this part. The received electrical waveform of the tested modulation formats can be divided into three types, as shown in Fig. 4.5. As the eye diagrams show, the three types of waveform have two-level features. The eye diagram of the NRZ-OOK signal is from the direct photo detection of the optical signal. For NRZ-DPSK signal, the phase modulated optical signal has almost constant intensity, which is not preferred for signal quality monitoring. Thus, the demonstrated DPSK signal is phase-demodulated by an optical delay interferometer (DI). However, for $50\%$ RZ-DQPSK signal, the direct detection obtains the sinusoid pulse carver waveform that has two levels. For OSNR monitoring, the efficient way is to investigate the significant variation of the mark level, which is induced by ASE noise. In the conventional delay-tap

sampling method, the tenth symbol or half symbol delay phase portrait is employed for OSNR monitoring. For single channel sampling technique, the time delay between the two samples is much larger than one symbol duration, so that the pattern of the phase portrait is different to that of the two-channel scheme.

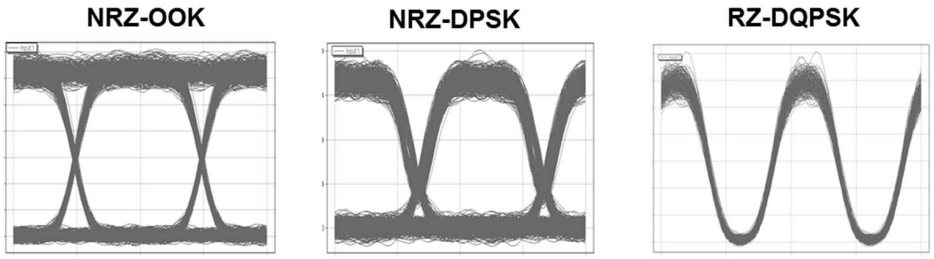


Figure 4.5: Eye diagrams of the three types of electrical waveform, including 10-Gb/s NRZ-OOK, 10-Gb/s NRZ-DPSK, and 20-Gb/s RZ-DQPSK.

Firstly, the phase portraits generated by using different time delay are studied and compared by simulation software. In Fig. 4.6, the generated phase portraits of 10-Gb/s NRZ-OOK signal are shown, which are formed by using different time delay. The tested time delay values are $0.1 \times T_s$, $1.1 \times T_s$, $2.1 \times T_s$, $10.1 \times T_s$, $0.5 \times T_s$, $1.5 \times T_s$, $2.5 \times T_s$, and $10.5 \times T_s$ respectively. Although the time delay values are different, the phase differences between the two samples, whose time delay values are $0.1 \times T_s$, $1.1 \times T_s$, $2.1 \times T_s$, $10.1 \times T_s$ respectively, are same, and the phase differences between the sample pairs, whose time delay values are $0.5 \times T_s$, $1.5 \times T_s$, $2.5 \times T_s$, and $10.5 \times T_s$, are same. The phase differences of these two groups of phase portraits are tenth symbol duration ($\pi/5$) and half symbol duration ($\pi$) separately. For the tenth symbol phase difference phase portraits, the patterns are different from that of the portraits generated by less than two symbol duration time delay. When the time delay is larger than two, the tenth symbol phase difference phase portraits have same pattern. For OSNR monitoring, a simple approach is to derive the mark level and space level

variations from the diagonal direction of the phase portrait. Thus, in single channel sampling technique, the larger time delay between the sample pairs leads to that the tenth symbol phase difference phase portrait is not suitable for OSNR monitoring. However, for the half symbol phase difference phase portraits, the patterns are almost same in the different time delay cases, as shown in the second row of Fig. 4.6. More importantly, the representations of the mark level and the space level of the waveform are separated along the diagonal direction of the half symbol phase difference phase portrait, which is suitable for the OSNR monitoring parameter derivation. Thus, for NRZ-OOK signal, the half symbol phase difference phase portrait is used for OSNR monitoring.

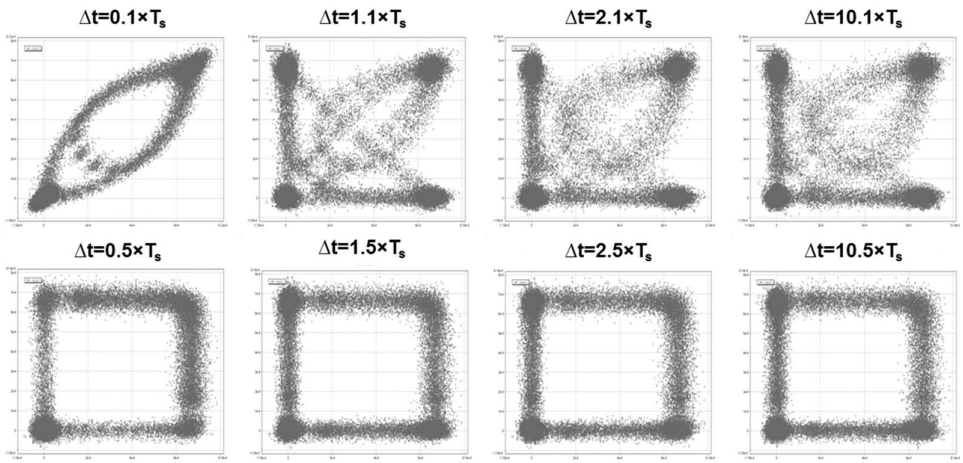


Figure 4.6: 10-Gb/s NRZ-OOK phase portraits generated by using different time delay.

For NRZ-DPSK signal, the tenth symbol phase difference phase portraits generated by using different time delay are also different, as exhibited in Fig. 4.7. The time delay values are as $0.1 \times T_s$, $1.1 \times T_s$, $2.1 \times T_s$, $10.1 \times T_s$, $0.5 \times T_s$, $1.5 \times T_s$, $2.5 \times T_s$, and $10.5 \times T_s$ separately. As similar as NRZ-OOK signal, the tenth symbol phase difference phase portraits have same pattern when the time delay is larger than two symbol duration. For SCS technique, it is not straight to derive the OSNR monitoring information from the tenth symbol phase difference phase portrait generated by larger

time delay. However, for the half symbol phase difference phase portrait, the patterns are almost same for the portraits using different time delay, which separate the mark level and the space level. Thus, in NRZ-DPSK system, the half symbol phase difference phase portrait is adopted for the OSNR monitoring parameter derivation.

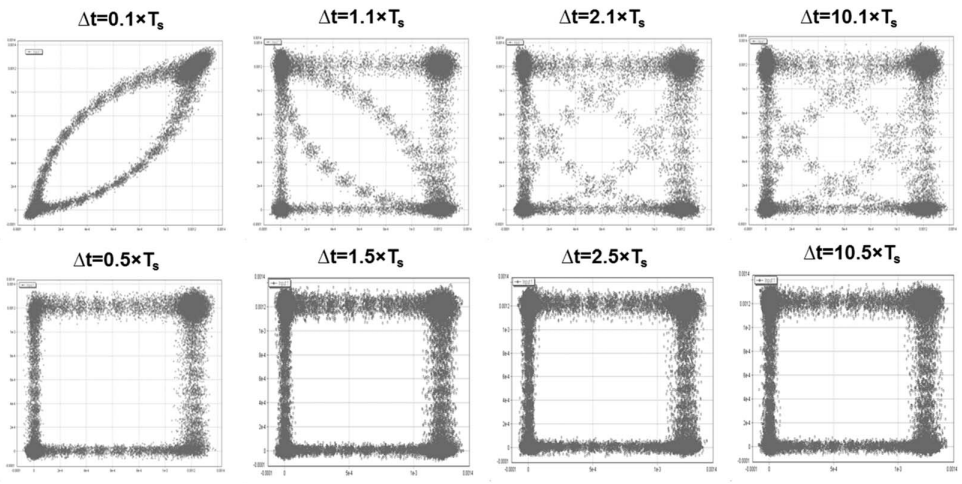


Figure 4.7: 10-Gb/s NRZ-DPSK phase portraits generated by using different time delay.

The third case of the investigated phase portraits is RZ-DQPSK signal. For the RZ phase modulation format, including RZ-DPSK, RZ-DQPSK, and RZ-8PSK, the direct detection of the optical signal generates the periodic pulse carver waveform. In this chapter, RZ-DQPSK signal is employed for the demonstration. Due to the periodic waveform feature, the phase difference phase portraits generated by using same phase difference have same pattern, as shown in Fig. 4.8. For the tenth symbol phase difference phase portrait, the mark level and space level of the signal are split into the two ends of the elliptical pattern. By using half symbol phase different, there generates the phase portrait with a line pattern, as shown in Fig. 4.8. The two ends of the line pattern represent the peak to valley variation of the periodic waveform, which can be used for OSNR monitoring [76]. Moreover, in the low OSNR cases, it is easier to derive OSNR

monitoring parameter from the line pattern, compared with the tenth symbol phase difference phase portrait. Thus, for RZ phase modulation format, the half symbol phase difference phase portrait is used for OSNR monitoring in this work.

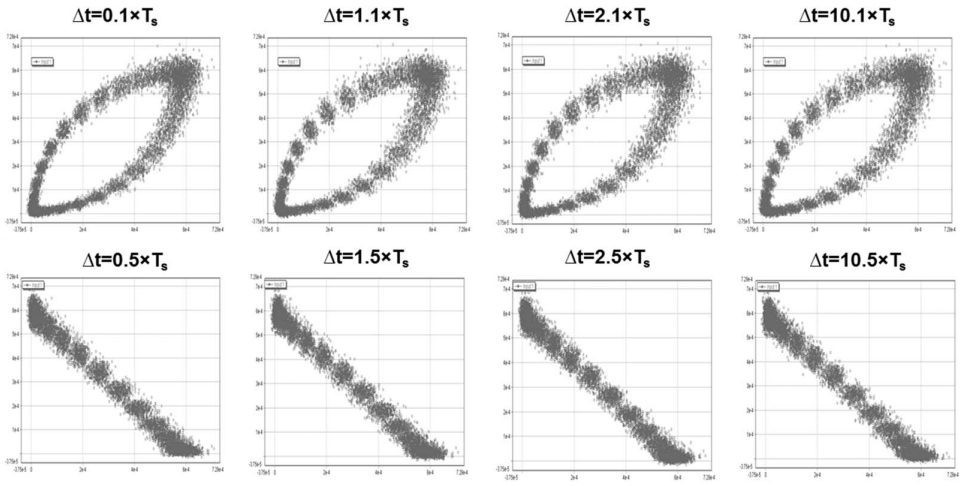


Figure 4.8: 20-Gb/s RZ-DQPSK phase portraits generated by using different time delay.

**Experiment Demonstrated 2-D Phase Portrait**

By using single channel sampling technique, the generated phase portraits of the tested signals are shown in Fig. 4.9. The tenth symbol phase difference and the half symbol phase difference are used to generate the 2-D phase portrait. The experimental demonstrated phase portraits have same pattern as that of the simulation demonstration. For the NRZ signals, the half symbol phase difference phase portrait separates the mark level and the space level along the diagonal direction of the portrait, which is more effective for OSNR monitoring parameter derivation. For the RZ signal, the monitoring system noise fills the open area of the tenth symbol phase difference phase portrait, which leads to the difficulty of the monitoring parameter derivation. However, the influence of the monitoring system noise does not affect the noise parameter derivation from the line pattern portrait. Thus, for the all investigated signals, the half

symbol phase difference phase portrait is adopted for OSNR monitoring.

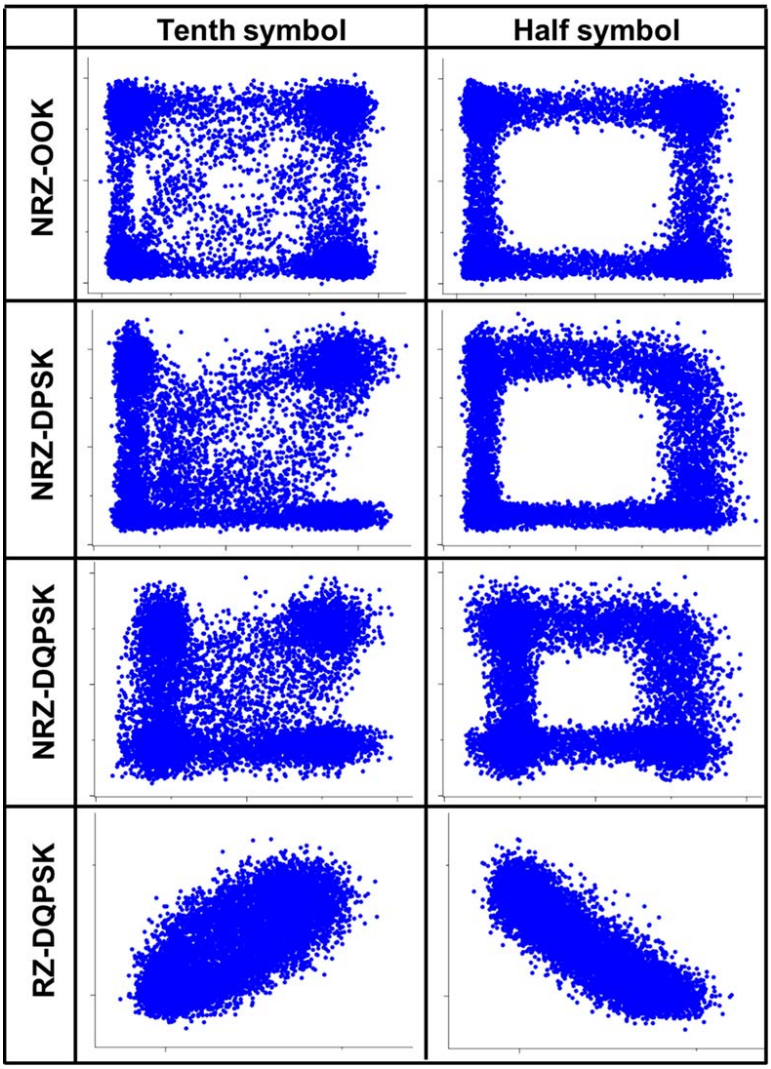


Figure 4.9: In the case of 30-dB OSNR, tenth symbol phase difference phase portrait and half symbol phase difference phase portrait of 10-Gb/s NRZ-OOK, 10-Gb/s NRZ-DPSK, 20-Gb/s NRZ-DQPSK, and 50-Gb/s RZ-DQPSK.

In 10-Gb/s NRZ-OOK system, the half symbol phase difference phase portraits of different OSNR are shown in Fig. 4.10. The points along the diagonal direction represent the waveform intensity of the mark level and space level. As the OSNR

varies from 10 dB to 30 dB, the pattern line becomes thicker and more noisy, especially the part that represents the mark level intensity. Thus, the point distribution along the diagonal direction can be derived for OSNR estimation. For the CD induced pattern evolution, when signal OSNR is 30 dB, the half symbol phase difference phase portraits of 10-Gb/s NRZ-OOK signal with different residual CD are demonstrated in Fig. 4.11. In the demonstrated residual CD range (from 0 to 425 $ps/nm$), the pattern has a limited change as the residual CD value increases.

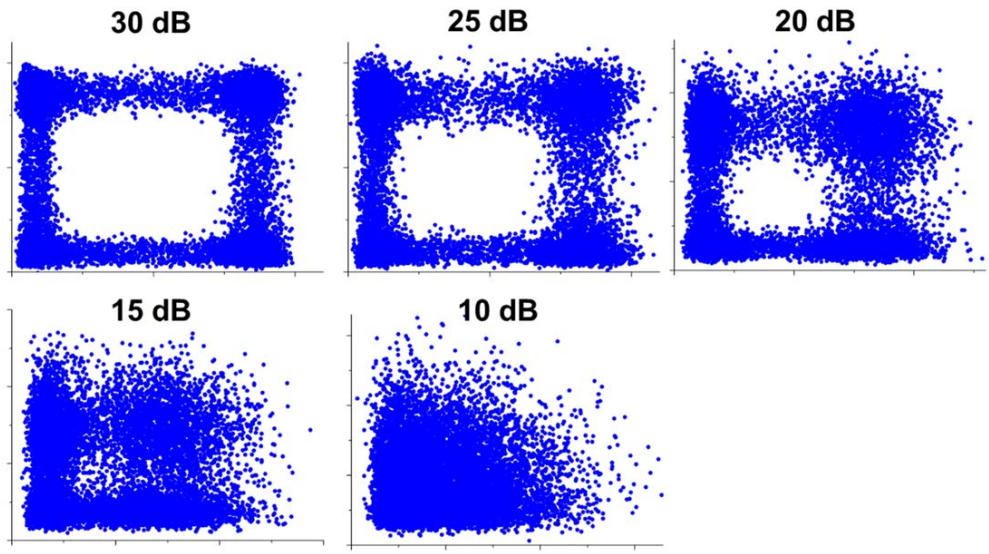


Figure 4.10: 10-Gb/s NRZ-OOK half symbol phase difference phase portraits generated by using SCS method in different OSNR.

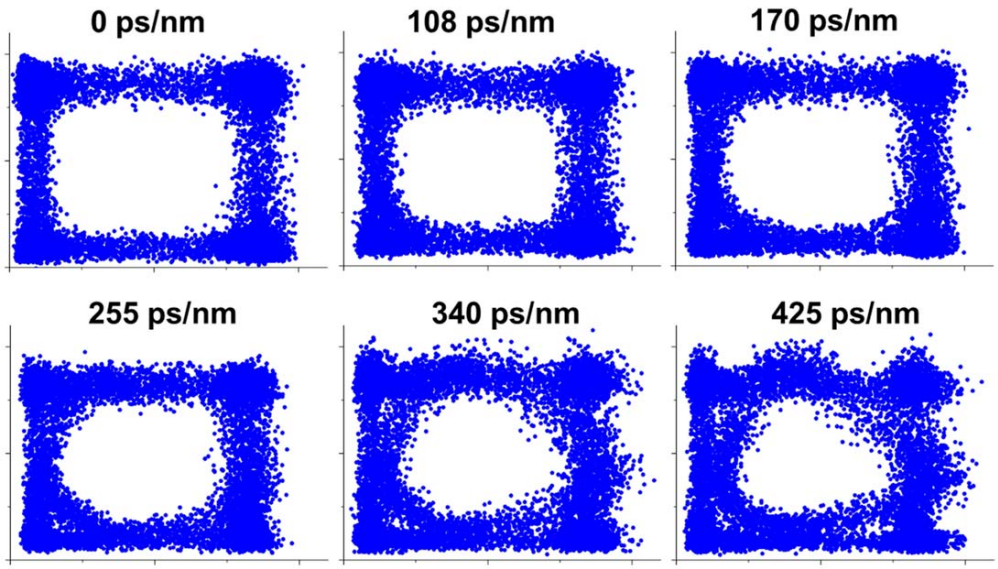


Figure 4.11: 10-Gb/s NRZ-OOK half symbol phase difference phase portraits generated by using SCS method in 30-dB OSNR with different CD.

In Fig. 4.12, the 10-Gb/s NRZ-DPSK half symbol phase difference phase portraits with difference OSNR are exhibited. As the OSNR is changed from 10 dB to 30 dB, the "grid" pattern is coarsened by the increase of ASE noise power, which is similar to the phase portrait of NRZ-OOK signal. However, in the presence of CD effect, residual CD induces an obvious pattern evolution, as shown in Fig. 4.13. Since CD effect affects the pulse width, the pattern of the half symbol phase difference phase portrait of NRZ-DPSK signal is changed. The pattern width of the diagonal direction is reduced as the CD value increases. However, for NRZ-OOK signal, the presence of its continuous mark level contributes the robustness of CD effect for the half symbol phase difference phase portraits.

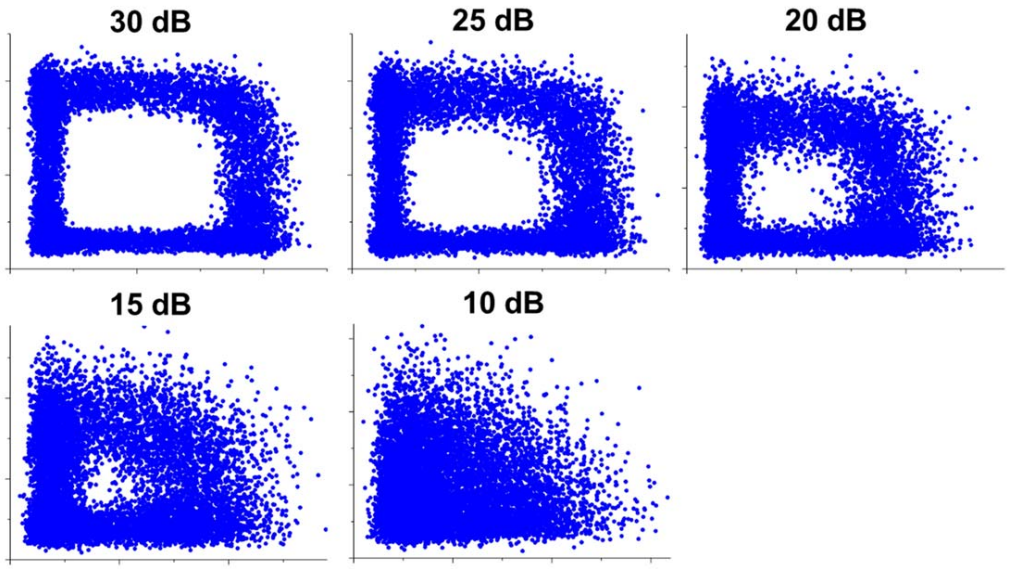


Figure 4.12: 10-Gb/s NRZ-DPSK half symbol phase difference phase portraits generated by using SCS method in different OSNR.

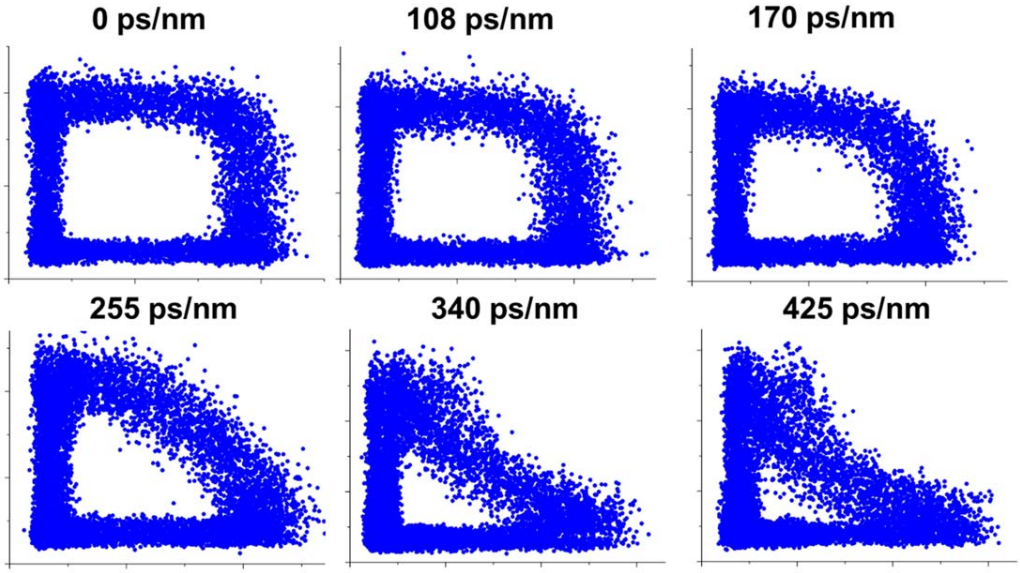


Figure 4.13: 10-Gb/s NRZ-DPSK half symbol phase difference phase portraits generated by using SCS method with different CD, when the OSNR is at 30 dB.

In Fig. 4.14, the 50-Gb/s RZ-DQPSK half symbol phase difference phase por-

traits with different OSNR are exhibited. For the RZ-DQPSK line-pattern plot, the line pattern becomes broader, and evolves to the triangle pattern, as the signal OSNR increases. In the presence of CD effect, the pattern is also broaden, due to the CD induced pulse width change, as shown in Fig. 4.15.

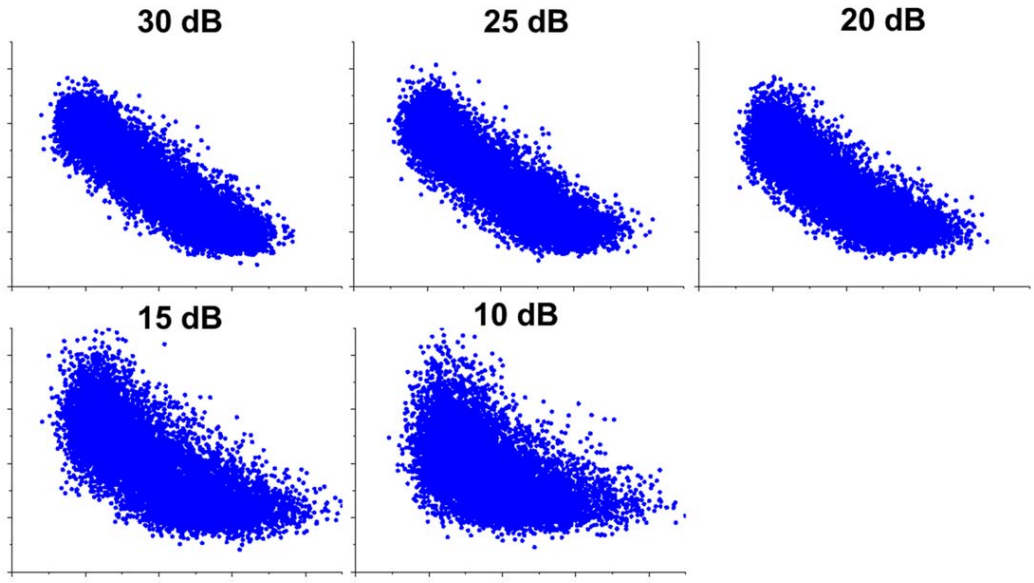


Figure 4.14: 50-Gb/s RZ-DQPSK half symbol phase difference phase portraits generated by using SCS method in different OSNR.

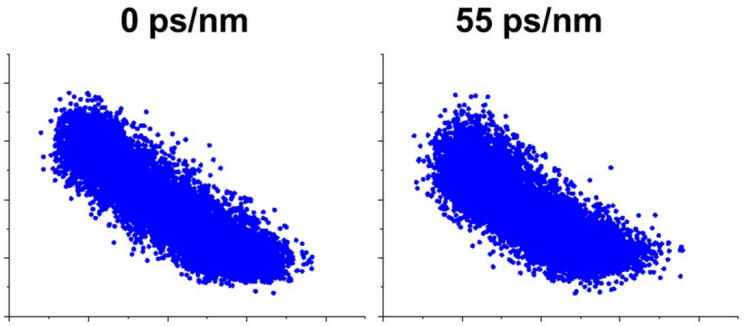


Figure 4.15: 50-Gb/s RZ-DQPSK half symbol phase difference phase portraits generated by using SCS method in 30-dB OSNR with different CD.

### 4.2.2 OSNR Monitoring Parameter Derivation

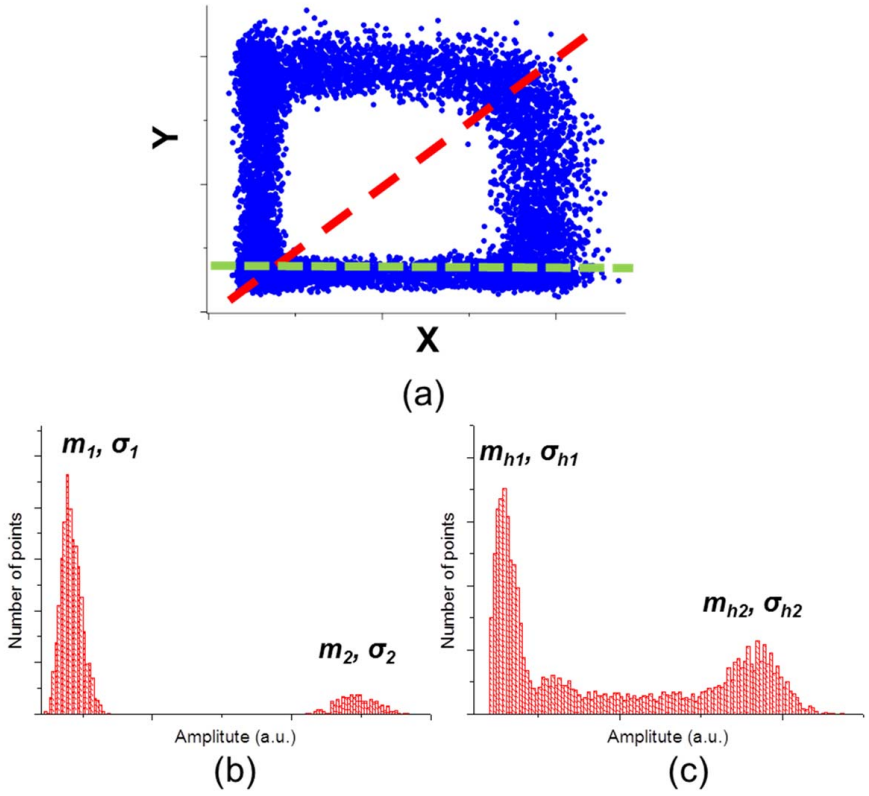


Figure 4.16: NRZ-DPSK half symbol phase difference phase portrait, (a) the points on the diagonal and horizontal directions are derived, (b) bimodal distribution along the diagonal direction, (c) bimodal distribution along the horizontal direction.

According to the different patterns of the NRZ and RZ signals, the OSNR monitoring parameter derivation algorithms are divided into two groups. For the "grid" pattern of the NRZ signals (including NRZ-OOK, NRZ-D(Q)PSK), the points along the diagonal and horizontal directions of the pattern are acquired to calculate the bimodal distribution coefficients, including the mean values ($m$) and the standard deviations ($\sigma$), as shown in Figs. 4.16. In [75, 77], authors proposed that OSNR is estimated by using their defined factor $F$ based on the bimodal distribution along the diagonal direction. Since the bimodal distance at the diagonal direction in NRZ-DPSK and NRZ-DQPSK

systems varies with CD, we propose to involve the bimodal distance ($m_{h2} - m_{h1}$) on the horizontal direction to represent the signal power, which is not sensitive to CD variation. Moreover, the bimodal variation along the diagonal direction is used to convey the ASE noise induced two-level variation, so that the OSNR monitoring factor is defined by Eq. 4.1 for the NRZ systems. The exact OSNR value can be calculated by using data fitting.

$$F_{NRZ(dB)} = 10 \cdot log_{10}(\frac{m_{h2} - m_{h1}}{\sigma_2 + \sigma_1}) \tag{4.1}$$

For RZ-DQPSK system, the two ends of the line pattern deliver the waveform peak to valley variation, which is influenced by ASE noise. Thus, the points below the highlighted line are extracted to calculate the uni-modal distribution on the horizontal direction, including the mean value ($m_u$) and the standard deviation ($\sigma_u$), as shown in Fig. 4.17. Thus, the OSNR monitoring factor of RZ-DQPSK system is defined as Eq. 4.2, which is proposed in [76].

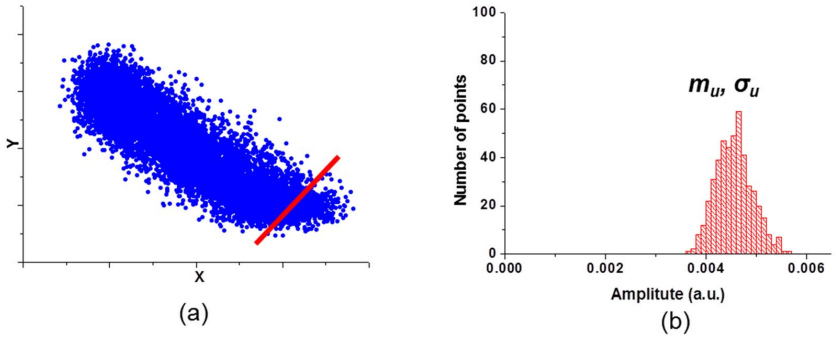


Figure 4.17: RZ-DQPSK half symbol phase difference phase portrait, (a) the points below the red line are derived; (b) uni-modal distribution of the selected points on horizontal direction

$$F_{NRZ(dB)} = 10 \cdot log_{10}(\frac{m_u}{\sigma_u}) \tag{4.2}$$

### 4.2.3 Experiment Results and Discussions

In Fig. 4.18, the experimental results show that the phase portrait derived by our proposed SCS method can successfully be used to monitor OSNR in NRZ-OOK system. The calculated OSNR monitoring factor has been converted to the corresponding OSNR value by using polynomial fitting. Additionally, each single estimated value is an average value of ten times estimation, where 20,000 X-Y pairs are used to calculate the monitoring parameter each time. More importantly, in Fig 4.18, the proposed OSNR monitoring method exhibits its certain tolerance to CD effect. The OSNR estimation errors vary within $\pm 1$ dB for the OSNR monitoring from 10 dB to 25 dB, when the CD is below 340 ps/nm.

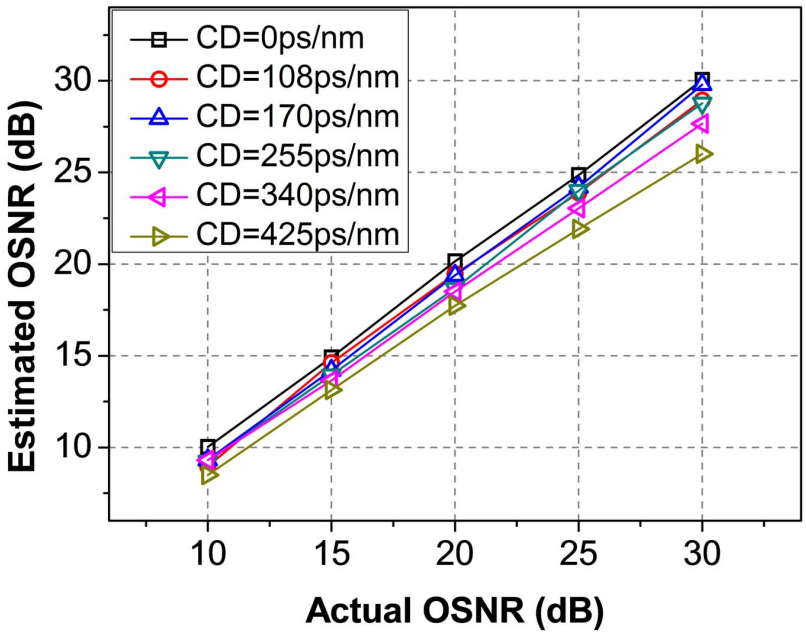


Figure 4.18: OSNR monitoring of 10-Gb/s NRZ-OOK signal in the presence of CD

In Fig. 4.19, the experimental results show the OSNR monitoring performance of 10-Gb/s NRZ-DPSK system in the presence of CD effect. The OSNR monitoring errors can be kept within 1-dB monitoring from 15-dB to 25-dB OSNR monitoring at

the demonstrated CD range. It is significant to obtain an accurate OSNR monitoring performance from 15 dB to 25 dB. As the CD increases, the pattern width on the diagonal direction becomes narrow, which refers to Fig. 4.13, so that the points from the two clusters on the diagonal direction are overlapped in the lower OSNR case. Thus, it is difficult to derive accurate bimodal statistical parameters, which reduces OSNR monitoring dynamic range and increases monitoring errors. When the OSNR is high, large CD induces a strong waveform distortion that overrides the OSNR induced variation, which also causes OSNR monitoring errors.

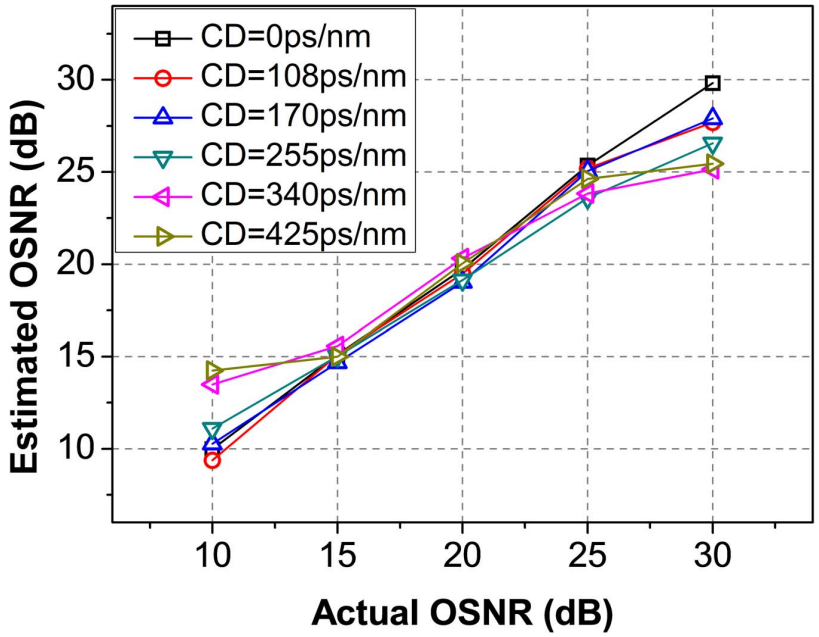


Figure 4.19: OSNR monitoring of 10-Gb/s NRZ-DPSK signal in the present of CD

Fig. 4.20 shows the experimental results of 20-Gb/s NRZ-DQPSK system OSNR monitoring in the presence of CD effect. The OSNR monitoring performance of 20-Gb/s NRZ-DQPSK is more sensitive than the one in 10-Gb/s NRZ-DPSK. The OSNR monitoring accuracy can be kept within 1-dB error from 15 dB to 25 dB, when the CD is below 255 ps/nm. As same as NRZ-DPSK signal, CD effect reduces the pattern width of NRZ-DQPSK signal, which starts to cause OSNR monitoring errors as CD

increases to a certain value.

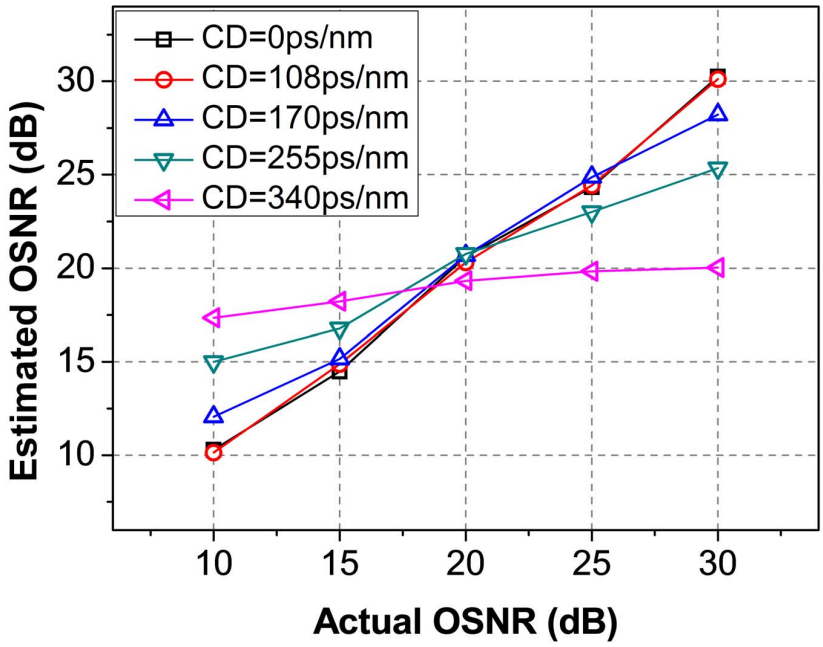


Figure 4.20: OSNR monitoring of 20-Gb/s NRZ-DQPSK signal in the present of CD

In Fig. 4.21, the experimental results demonstrate the OSNR monitoring of 50-Gb/s RZ-DQPSK signal. The signal OSNR is successfully derived by using the proposed method. However, as the data rate increases to 50 Gb/s, CD effect significantly influences the OSNR monitoring accuracy, due to the narrower pulse width of the transmitted signal. When the CD is at 55 ps/nm and the OSNR varies from 10 dB to 20 dB, the OSNR monitoring errors reach 2 dB. Additionally, the monitoring dynamic range is also decreased.

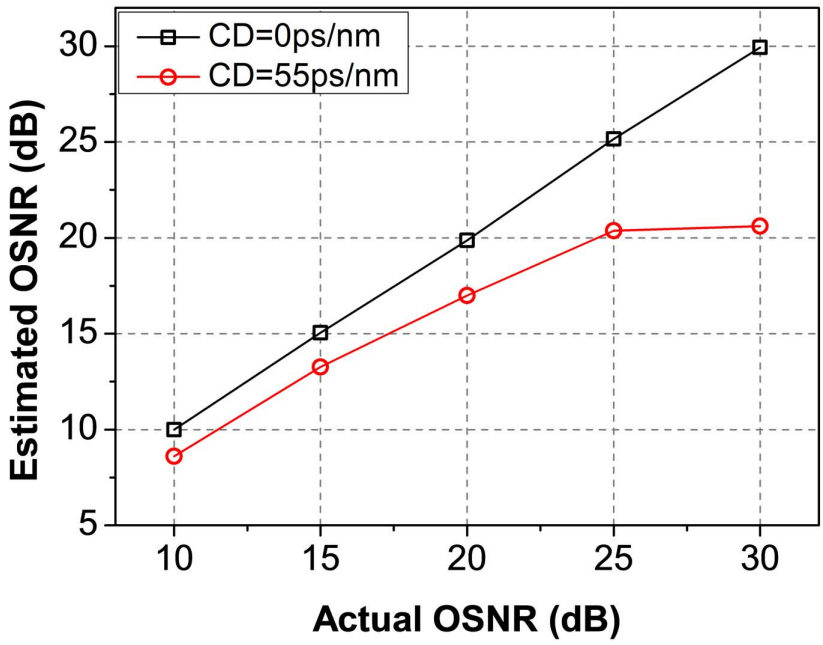


Figure 4.21: OSNR monitoring of 50-Gb/s RZ-DQPSK signal in the presence of CD

By using the statistical analysis on the monitoring parameter derivation, the sample size used for the statistical calculation is an important factor that determines the accuracy and efficiency of monitoring system. As the results in Fig. 4.22 show, when the sample point size used for the phase portrait depiction and monitoring parameter calculation reaches 10,000, the standard deviation of the estimated OSNR value can be kept below 0.5 dB (the exhibited signal is 15-dB 50-Gb/s RZ-DQPSK). As the sample size increases, the monitoring performance becomes more stable and accurate. However, there is a tradeoff between the monitoring accuracy and the total monitoring cost. Firstly, in this work, one of the merits is using the low-speed sampling component to reduce the monitoring setup cost. The case using larger sample size requires the sampler with faster sampling speed to keep the original sampling time. In addition, the computational cost is increased by the larger amount of sample pairs, which includes the electrical energy consumption and the cost of high-performance computer. Thus, the tradeoff between the monitoring accuracy and the total cost is important for the real

system design. Since the sampling rate can be at dozens of MHz, the derivation time of single phase portrait can be less than one micro-second.

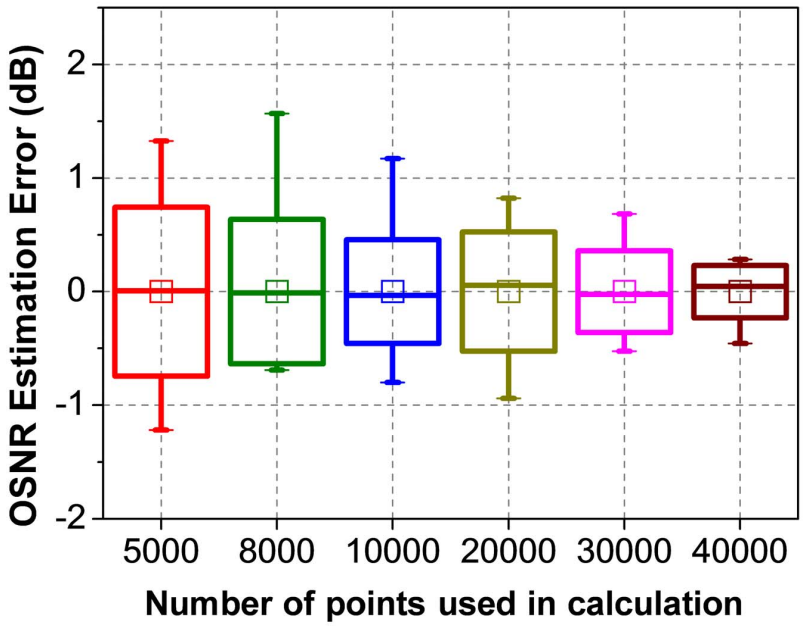


Figure 4.22: OSNR monitoring accuracy versus sample size used for portrait depiction and monitoring parameter calculation.

## 4.3 CD Monitoring of NRZ Phase Modulated Signal

### 4.3.1 Working Principle of CD Monitoring

As discussed in the last section, CD reduces the pattern width of the phase portrait at the diagonal direction, which can be the basis of CD monitoring. However, the pattern width is also related to the received signal power. Thus, the distance ratio between the diagonal direction and horizontal direction of the pattern is proposed for CD monitoring, since the pattern width at the horizontal direction is mainly determined by the received signal power. For the CD monitoring of NRZ-DPSK and NRZ-DQPSK

signals, the statistical coefficients in the horizontal and diagonal directions are derived by using the same approach as the OSNR monitoring parameter derivation, as Fig. 4.16 shows. The mean values ($m$) and the standard deviations ($\sigma$) are derived from the bimodal distributions on the two directions of the portrait. The distance of the two directions are represented by Eq. 4.3 and Eq. 4.4. Thus, the distance ratio, as expressed in Eq. 4.5, is proposed to estimate CD.

$$D_d = m_2 - m_1 + \sigma_1 + \sigma_2 \tag{4.3}$$

$$D_d = m_{h2} - m_{h1} + \sigma_{h1} + \sigma_{h2} \tag{4.4}$$

$$DR = \frac{D_d}{D_h} = \frac{m_2 - m_1 + \sigma_1 + \sigma_2}{m_{h2} - m_{h1} + \sigma_{h1} + \sigma_{h2}} \tag{4.5}$$

### 4.3.2 Experimental Results of CD Monitoring

In Fig. 4.23, the CD monitoring of 10-Gb/s NRZ-DPSK signal is demonstrated by using the proposed distance ratio between the two directions of the portrait. The demonstrated CD monitoring range is from 0 ps/nm to 425 ps/nm. The linear performance of the CD monitoring is from 150 ps/nm to 425 ps/nm. Moreover, when the OSNR varies from 15 dB to 30 dB, the CD monitoring is not sensitive to the OSNR variation. However, as the OSNR falls below 15 dB, the CD monitoring performance has an offset to the larger OSNR cases.

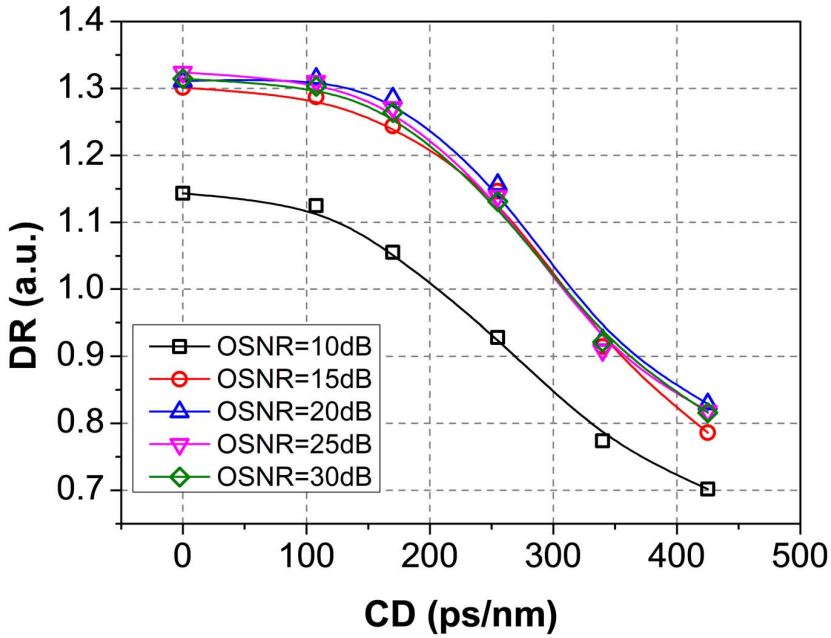


Figure 4.23: CD monitoring of 10-Gb/s NRZ-DPSK signal in the presence of OSNR variation.

As the experimental results show in Fig. 4.24, the proposed distance ratio is a function of residual CD in 20-Gb/s NRZ-DQPSK system. The linear performance of the CD monitoring is from 150 ps/nm to 425 ps/nm. In DQPSK systems, when the OSNR is above 20 dB, the CD monitoring performance is insensitive to the OSNR variation. When the OSNR is below 20 dB, the CD monitoring performance degrades seriously. In the demonstrated NRZ-DPSK and DQPSK systems, the CD monitoring has poor performance on the small CD value measurement, since the half symbol delay phase portrait derived from the relatively large duty ratio waveform is insensitive to the slight distortion.

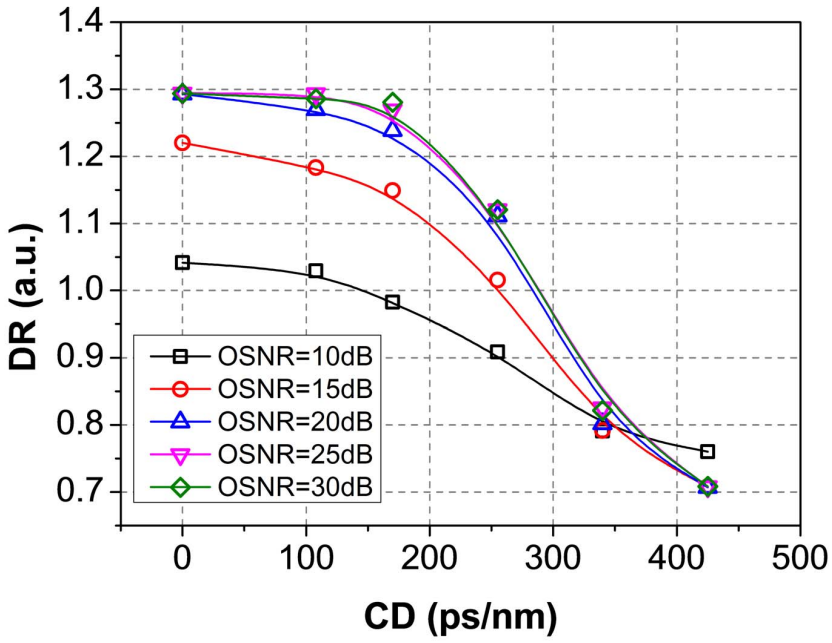


Figure 4.24: CD monitoring of 20-Gb/s NRZ-DQPSK signal in the presence of OSNR variation.

## 4.4 Conclusion

In this chapter, we have proposed and experimentally demonstrated the 2-D phase portrait depicted by using our proposed single channel sampling technique. By employing corresponding statistical pattern recognition on the 2-D phase portraits, OSNR monitoring and CD monitoring are demonstrated in both RZ and NRZ systems successfully. Moreover, the SCS scheme saves monitoring setup cost and 3-dB monitored signal power budget. More importantly, the monitoring setup is simplified in large degree, which reduces the system management complexity. Based on the self-delay method, it is flexible to generate the phase portraits with different phase differences, which enlarges its application area. Additionally, the phase portrait generated by our proposed method has potential for multiple optical impairments monitoring. However,

this method employs a high bandwidth sampling channel and data processing, which is high energy consuming. Thus, it is preferred to be implemented in the receiver end or the switching center, where the monitoring device can use a continuous power supplier.

# Chapter 5

# Optical Signal to Noise Ratio Monitoring Based on Software Synchronized Sampling Technique

In chapter 4, single channel sampling technique was proposed to generate 2-D phase portrait for OSNR monitoring and CD monitoring. In order to obtain an accurate sampling interval, the related sampling frequency is used to trigger sampler, which limits the application scope of the monitoring system, since the sampling frequency is synchronized with the monitored signal. The un-related sampling frequency can break this restriction, which is not related to the data rate of the monitored signal. However, this scheme requires additional synchronization on the sampling sequence.

In [104, 105], the software based synchronization technique was proposed to synchronize the sample sequence for eye diagram reconstruction. The aliasing frequency in the un-related low-speed sampling scheme is estimated by using fast Fourier transform (FFT) and phase reference detection method, which is the key step of the software synchronization technique. Then, the eye diagram is reconstructed after software synchronization, which is used to monitor the signal quality by the analysis of the signal

amplitude distribution at the symbol center. However, this method requires the highly accurate estimation of the aliasing frequency. The estimated aliasing frequency offset (FO) would lead to re-timing shift for the re-construction of eye diagram, which seriously affects the monitoring accuracy, as the recovered eye diagrams generated by using this method shows in Fig. 5.1. When the estimated aliasing frequency offset is up to 500 Hz, the eye diagram formed by ten thousands of samples suffers the re-timing error, which causes the half eye being closed. As the offset increases, the recovered eye is almost closed.

In this chapter, we propose to use the low-speed un-related sampling scheme with the software based synchronization technique to depict the 2-D phase portrait for OSNR monitoring, which has a certain tolerance to the aliasing frequency estimation offset. Moreover, in order to increase the tolerance to the aliasing frequency estimation offset, the tolerated phase difference is proposed for the phase portrait generation. In the experimental demonstration, OSNR monitoring is successfully performed by using the proposed method in different modulation formats in the presence of a certain amount of chromatic dispersion (CD).

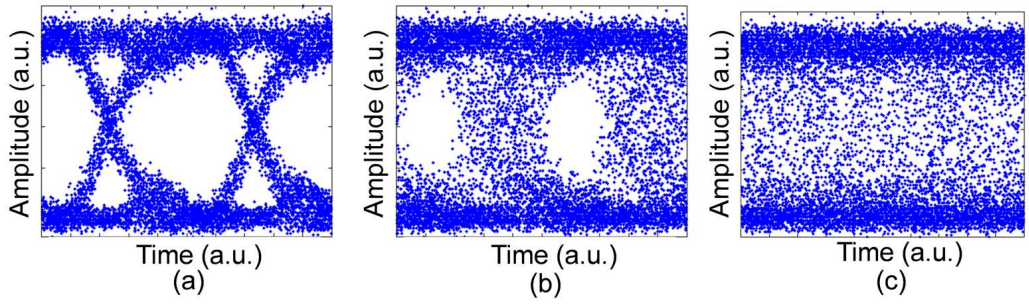


Figure 5.1: NRZ-OOK signal eye diagrams that are reconstructed under different aliasing clock frequency estimation offset. (a) FO=0 Hz, (b) FO=500 Hz, (c) FO=1000 Hz.

## 5.1 Working Principle and Experimental Setup

The experimental setup of the proposed software synchronized single channel sampling method is shown in Fig. 5.2. The modulated signal is coupled with a 0.8-nm noise source after a certain period of standard single mode fiber (SSMF) transmission. In this chapter, 10.7-Gb/s NRZ-OOK, NRZ-DPSK and RZ-DPSK signals are tested. The OSNR value of the monitored signal is tuned by changing the output power of the noise source, while the different values of residual CD are introduced by using different lengths of SSMF. Then, an erbium-doped fiber amplifier (EDFA) is used to compensate the power loss during fiber transmission. Before the receiver, the redundant noise is removed by a 0.65-nm optical band pass filter (BPF).

In this work, the receiver of NRZ-OOK and RZ-DPSK signals is composed of a single photo detector and a linear electrical amplifier, while an optical delay interferometer (DI) is employed before the photo detector to demodulate NRZ-DPSK signal. By using this approach, the ASE noise induced significant waveform peak variation can be obtained. In the experimental demonstration, a single 16-GHz bandwidth sampling channel of real-time oscilloscope is triggered by un-related low sampling frequency ($\sim$9.77 MHz), as an analog to digital converter (ADC), which derives the discrete waveform sequence. The rest part of this OSNR monitoring setup is signal processing, which includes sampling sequence synchronization and monitoring parameter derivation.

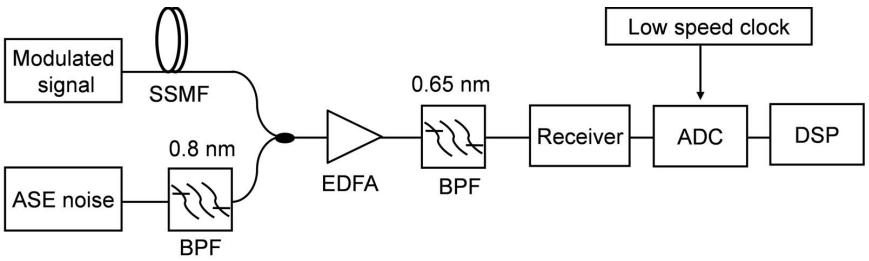


Figure 5.2: The experimental setup of the proposed OSNR monitoring method.

## 5.2 Working Principle of Software Synchronization Technique

Since the sampler is triggered by the un-related low speed sampling frequency ($f_s$), it generates the aliasing frequency ($f_a$), as shown in Fig. 5.3. The sampling interval can be expressed by $n \times T + \tau$ ($n$ is an integer number; $T$ is one symbol duration; $\tau$ is within one symbol time shift between neighbor samples). There is a particular relationship between the aliasing frequency and the sampling frequency as expressed in Eq. 5.1 [104].

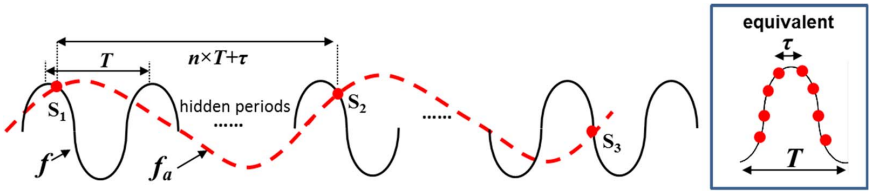


Figure 5.3: Un-related low speed sampling scheme.

$$\frac{f_a}{f_s} = \frac{\tau}{T} \tag{5.1}$$

After the aliasing frequency is estimated, the phase difference ($\tau$/T) between adjacent samples can be obtained by Eq. 5.1. Moreover, the accumulated phase difference of the whole sample sequence can be obtained, as Fig. 5.4 shows.

| Intensity | S1 | S2 | S3 | ... | $S_k$ | $S_{k+1}$ | ... |
|---|---|---|---|---|---|---|---|
| Phase difference | $\frac{\tau}{T}$ | $\frac{2*\tau}{T}$ | $\frac{3*\tau}{T}$ | ... | $\frac{k*\tau}{T}$ | $\frac{(k+1)*\tau}{T}$ | ... |

Figure 5.4: Synchronized sample sequence with known phase difference.

Thus, the aliasing frequency estimation is the core part of the software synchronization. In this chapter, the aliasing frequency estimation is based on the FFT based reference phase detection method [104], which is originally used for eye diagram reconstruction. Firstly, the sample sequence is transformed into frequency domain by FFT, whose power spectrum is shown in Fig. 5.5. Due to the limited resolution of FFT, the rough aliasing frequency ($f_e$) is obtained by searching the peak of the power spectrum. The FFT resolution leads to a frequency estimation offset between the rough aliasing frequency and the true aliasing one. Thus, the reference phase detection is used to further estimate the aliasing frequency ($f_a$), as shown in Fig. 5.6.

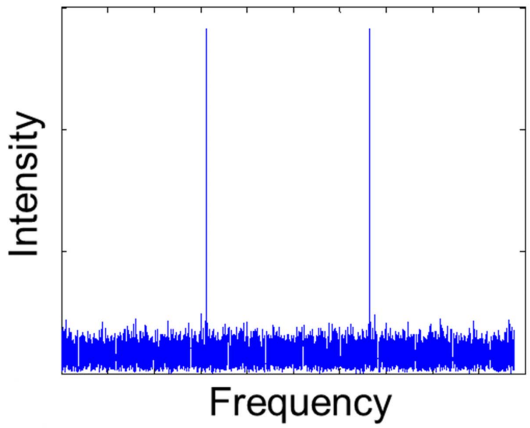


Figure 5.5: 10.7-Gb/s NRZ-DPSK signal power spectrum generated by FFT.

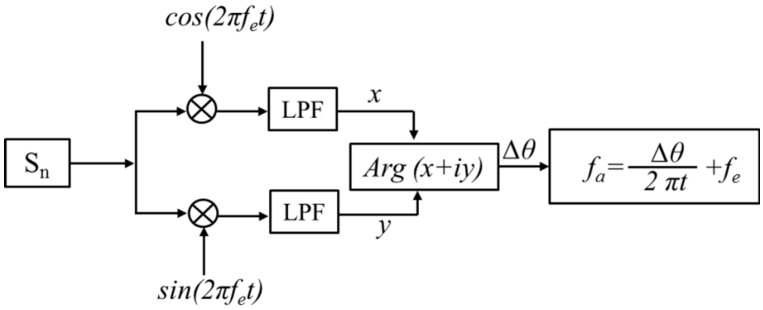


Figure 5.6: Reference phase detection method.

# 5.3 OSNR Monitoring Using Fixed Phase Difference Phase Portrait

## 5.3.1 Phase Portrait Generation and Monitoring Parameter Derivation

For the typical delay-tap sampling plot, the time delay or the phase difference between the X-Y pair is a fixed value. In the chapter 4, the fixed half symbol phase difference is used to generate the 2-D phase portrait for OSNR monitoring and CD monitoring, which is applicable to the software synchronized single channel sampling method.

For the X-Y pair generation using software synchronized single channel sampling method, the nearest sample pairs, whose phase difference is equal to half symbol period, are selected from the software synchronized sample sequence as X-Y pairs. Then, the selected X-Y pairs are depicted in a 2-D coordinate system, as shown in Fig. 5.7.

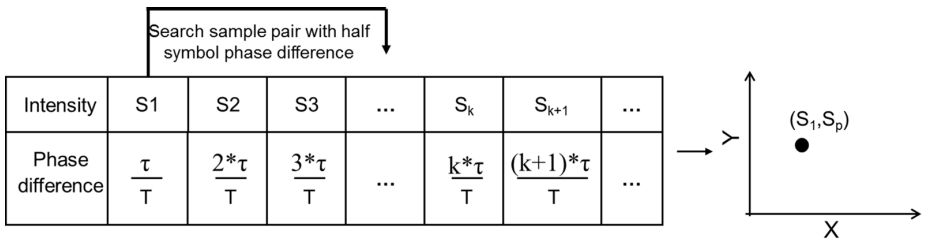


Figure 5.7: X-Y pairs generation for 2-D phase portrait depiction.

The generated half symbol phase difference phase portraits of 10.7-Gb/s NRZ-OOK, NRZ-DPSK and RZ-DPSK signals are shown in Fig. 5.8. They have similar patterns as the phase portraits generated by the method using related sampling frequency. The pattern of 10.7-Gb/s NRZ-OOK is not standard “grid” pattern, due to the low pass filtering effect of the 16-GHz sampling channel.

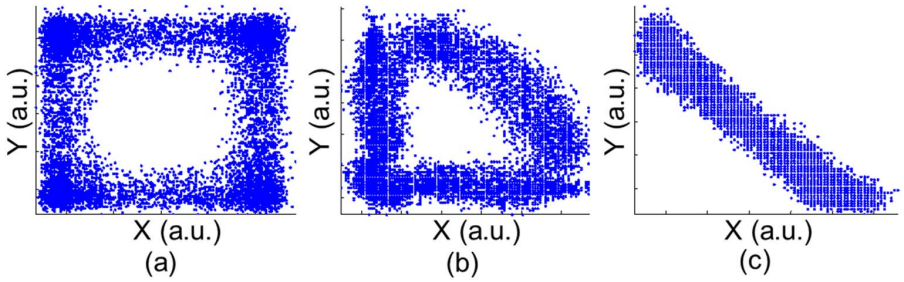


Figure 5.8: The generated 2-D phase portrait of (a) NRZ-OOK, (b) NRZ-DPSK, (c) RZ-DPSK.

Since the patterns are different in the three tested systems, the derivation approaches of the monitoring parameter are diverse in different systems. For the NRZ-OOK and NRZ-DPSK signals, the points along the diagonal direction of the phase portrait are derived, which follow bimodal distribution, as shown in Fig. 5.9 (a). The bimodal points represent the mark level and space level of the signal separately. The bimodal statistical parameters, including the mean values ($m_1$, $m_2$) and the standard deviations ($\sigma_1$, $\sigma_2$), are calculated. The summation of the bimodal variances is used to represent the noise power variation, while the input monitored signal power ($P_{in}$) is used to express the signal power. Accordingly, the OSNR monitoring parameter of NRZ signals is expressed in Eq. 5.2.

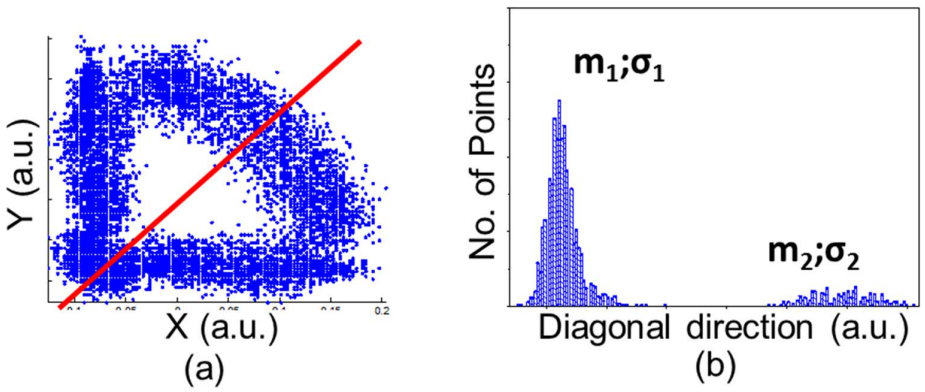


Figure 5.9: (a) Statistical information acquisition for the NRZ signals. (b) Bimodal distritbution of the point along diagonal direction of the phase portrait.

$$F_{NRZ} = \frac{P_{in}}{\sigma_1^2 + \sigma_2^2} \tag{5.2}$$

For the half symbol phase portrait of RZ-DPSK signal, the points at the two ends of the line pattern convey the waveform peak to valley variation. For these sample pairs, when one is located at waveform peak, the other is from waveform valley. In this work, as shown in Fig. 5.10 (a), the points at the one end are derived to calculate its distribution information in the horizontal direction, which can express the ASE noise induced waveform peak-to-valley variation. Then, the OSNR monitoring parameter can be calculated by using the derived variance of the uni-modal distribution and the monitored optical signal power, as expressed by Eq. 5.3.

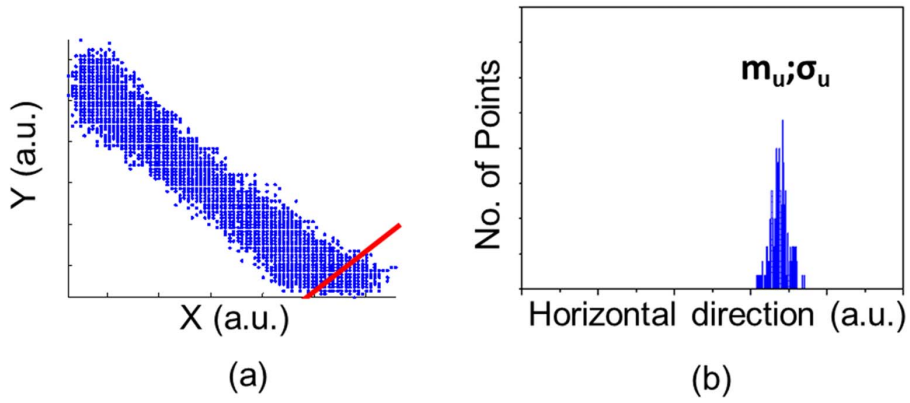


Figure 5.10: Statistical information acquisition for the RZ signals. (b) Uni-modal distritbution of the points at the one end of the phase portrait.

$$F_{RZ} = \frac{P_{in}}{\sigma_u^2} \tag{5.3}$$

### 5.3.2 Experimental Results

In Fig. 5.11, the experimental results show the propose OSNR monitoring performance of 10.7-Gb/s NRZ-OOK signal in the presence of CD effect. The demonstrated OSNR monitoring range is from 10 dB to 30 dB, while the CD is changed from 0 ps/nm to 595 ps/nm. As the residual CD increases, the OSNR monitoring accuracy degrades gradually. For the higher OSNR cases (larger than 25 dB), the OSNR monitoring accuracy is significantly influenced by serious CD effect, because the CD induced waveform distortion becomes dominant. For OSNR monitoring, the more meaningful monitoring range is from 10 dB to 25 dB. In this range, the total OSNR monitoring variation range is within $\pm 1$ dB, when the CD is less than 510 ps/nm.

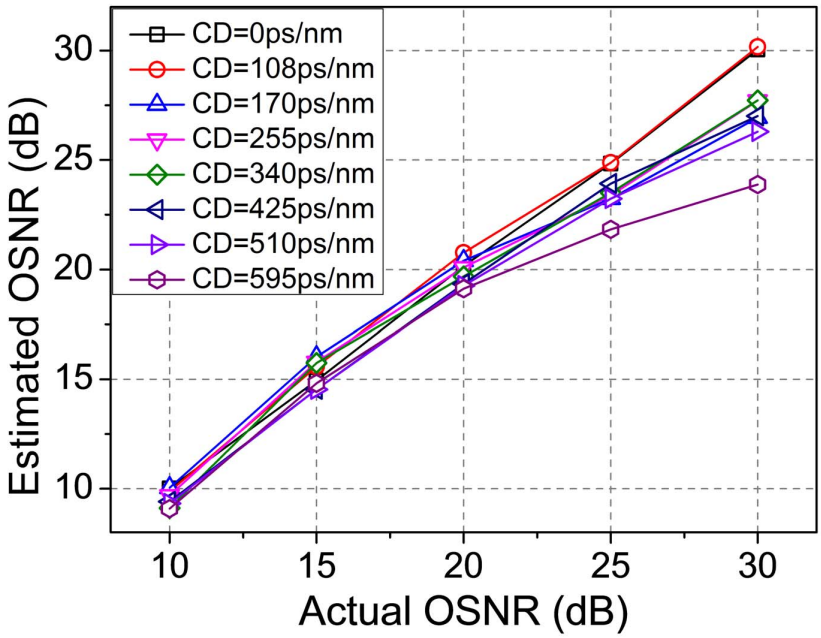


Figure 5.11: Experimental results of OSNR monitoring in the present of CD effect in 10.7-Gb/s NRZ-OOK system.

In Fig. 5.12, the experimental results show the proposed OSNR monitoring performance in 10.7-Gb/s NRZ-DPSK system, which undertakes CD effect simultaneously. The demonstrated OSNR monitoring range is from 10 dB to 30 dB, while the residual CD is changed from 0 ps/nm to 595 ps/nm. When the CD is less than 510 ps/nm, for the OSNR monitoring from 10 dB to 25 dB, the OSNR monitoring variation range is within $\pm 1$ dB. When the CD is larger than 510 ps/nm, serious CD effect reduces the phase portrait pattern width to a quite narrow level, where it is difficult to derive an accurate OSNR monitoring parameter.

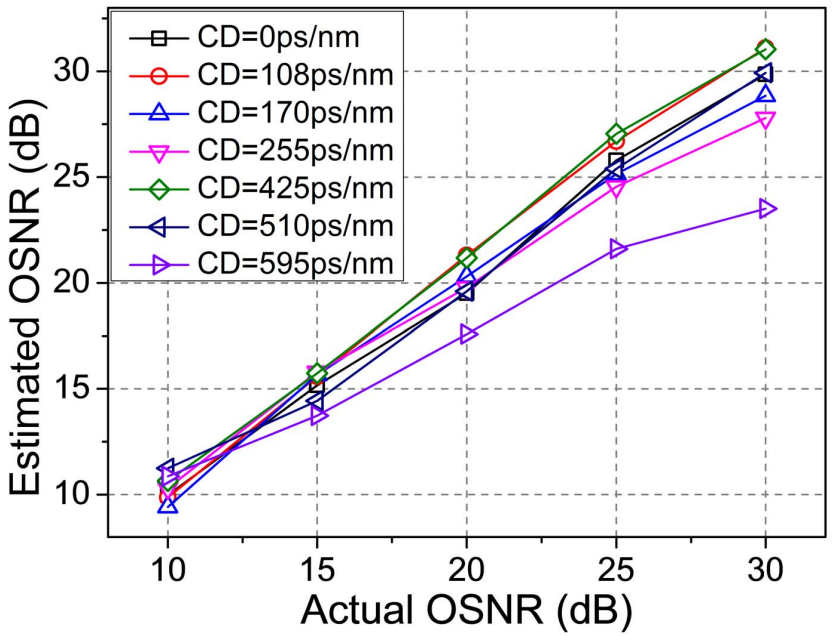


Figure 5.12: Experimental results of OSNR monitoring in the present of CD effect in 10.7-Gb/s NRZ-DPSK system.

In Fig. 5.13, the experimental results show the proposed OSNR monitoring performance for 10.7-Gb/s RZ-DPSK signal in the presence of CD effect simultaneously. The demonstrated OSNR monitoring range is from 10 dB to 30 dB, while the residual CD is changed from 0 ps/nm to 595 ps/nm. Signal OSNR is successfully estimated by using the proposed method. At the same time, the OSNR monitoring method has a certain tolerance to CD effect. When the CD is not larger than 425 ps/nm, the OSNR monitoring variation range can be kept within $\pm 1$ dB.

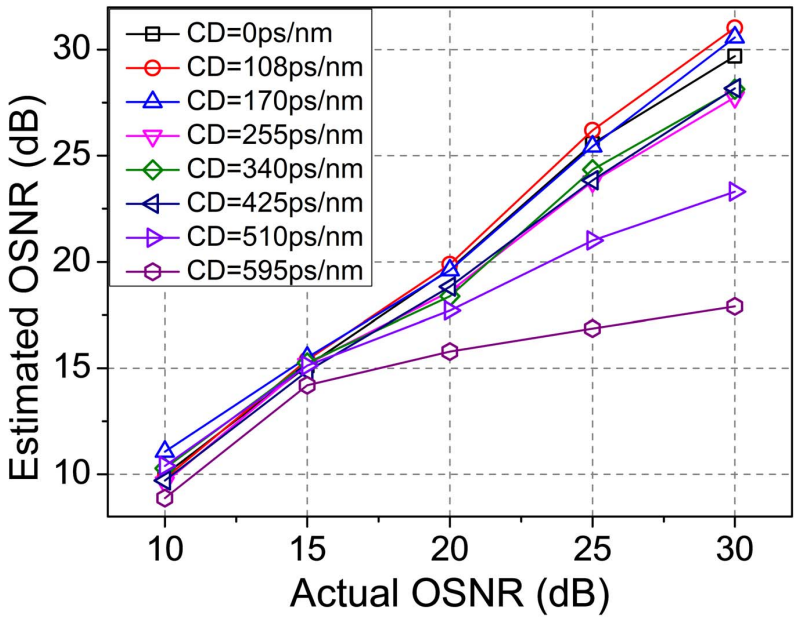


Figure 5.13: Experimental results of OSNR monitoring in the presence of CD effect in 10.7-Gb/s RZ-DPSK system.

In Fig. 5.14, the experimental results show the OSNR monitoring accuracy versus the estimated aliasing frequency offset. When it is within 500 Hz, the OSNR monitoring errors of all the demonstrated formats are within 1 dB. However, as the frequency offset keeps increasing, the OSNR monitoring accuracy of the NRZ-DPSK and RZ-DPSK systems is seriously degraded for the higher OSNR value estimation, while the OSNR monitoring performance of the NRZ-OOK system is more robust. It is due to that NRZ-OOK signal has continuous mark level, it still can derive waveform peak to peak variation for large frequency drift.

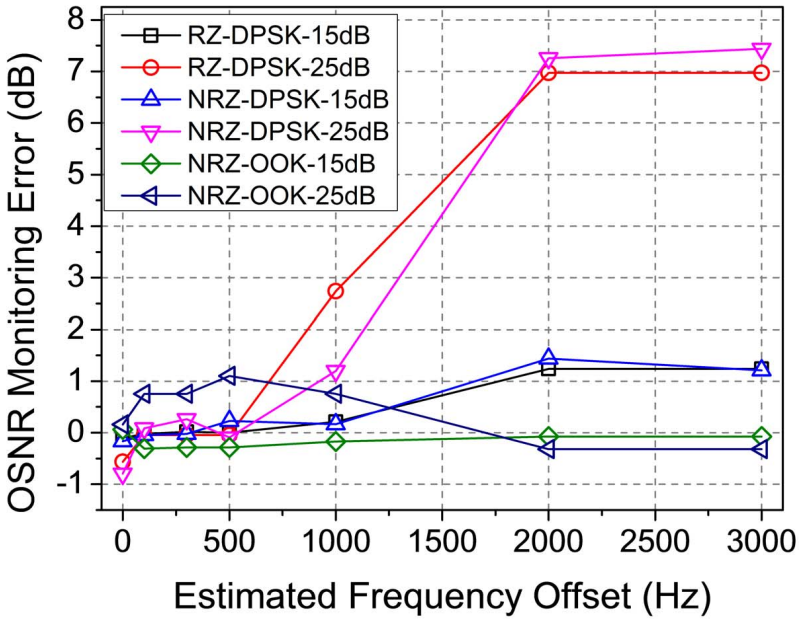


Figure 5.14: Estimated aliasing frequency offset versus OSNR monitoring error in the three tested systems.

## 5.4 OSNR Monitoring Using Tolerated Phase Difference Phase Portrait

### 5.4.1 Working Principle of Tolerated Phase Difference Phase Portrait

$$\frac{f_a + f_0}{f_s} = \frac{\tau + \Delta\tau}{T} \tag{5.4}$$

As discussed in the previous part, the core part of the software synchronization is the aliasing frequency estimation, which is in charged by the FFT based reference phase detection. However, when the aliasing frequency has a certain estimation offset ($f_o$), it generates the drift phase ($\Delta\tau/T$) in the obtained phase difference between samples, as expressed in Eq. 5.4. More seriously, the drift phase is accumulated in the sample

sequence, which destroys the recovered eye diagrams. As shown in Fig. 5.15(a) and (b), for 500-Hz aliasing FO, the recovered eye of 10.7-Gb/s NRZ-DPSK signal suffers the re-timing error (phase drift), which would be worse as the frequency offset keeps increasing.

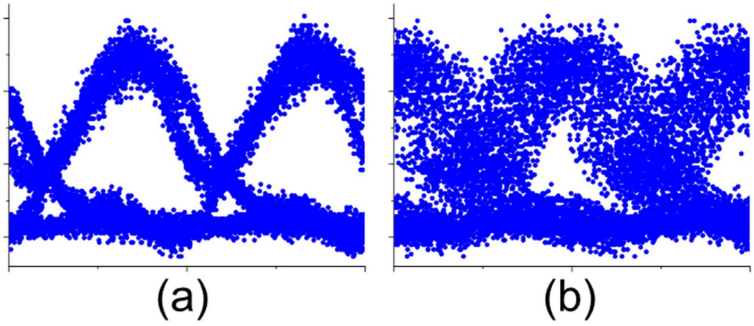


Figure 5.15: Eye diagrams of NRZ-DPSK signal with 30-dB OSNR, which is recovered under different aliasing FO: (a) 0 Hz, (b) 500 Hz.

Since the interval between the X-Y pair is several samples apart, the 500-Hz aliasing FO induced accumulated drift phase between samples pair leaves limited influence on the phase portrait pattern, as shown in Fig. 5.16(a) and (b). However, as the aliasing FO continuously increases to 10 kHz, the plot pattern is changed by the fault phase difference between the sample pairs, as shown in Fig. 5.16(c).

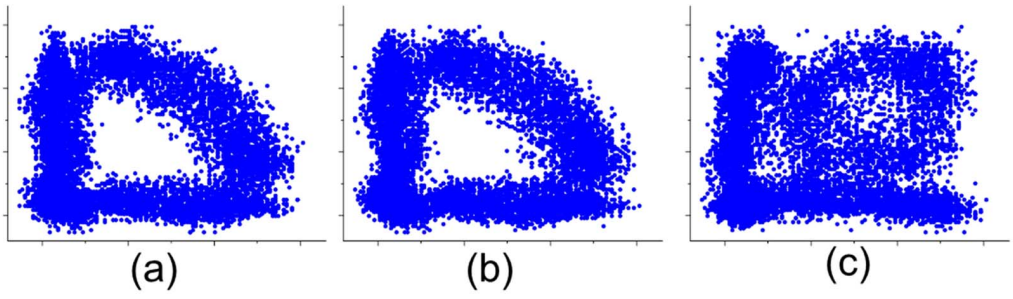


Figure 5.16: Half symbol delay phase portrait of NRZ-DPSK with 30-dB OSNR, which is generated under different aliasing FO: (a) 0 Hz, (b) 500 Hz, (c) 10 kHz.

For the conventional 2-D phase portrait, the time delay or the phase difference between the sample pair is a fixed value, such as tenth symbol or half symbol duration [72, 75, 77]. The pattern of the tenth symbol phase difference phase portrait is totally different from that of the half symbol phase difference phase portrait. However, a slight deviation of the phase difference does not change the patterns of the portraits significantly. As the plots in Fig. 5.17 show, the phase portraits are generated by using different equivalent phase differences ($\Delta\tau/T$). The patterns generated by using 0.5 times symbol phase difference are similar to that generated by 0.47 times symbol phase difference in all the three tested modulation formats. Thus, the OSNR monitoring relying on these two different phase portraits would have similar monitoring performance. However, as the phase difference deviation increases, the pattern changes gradually.

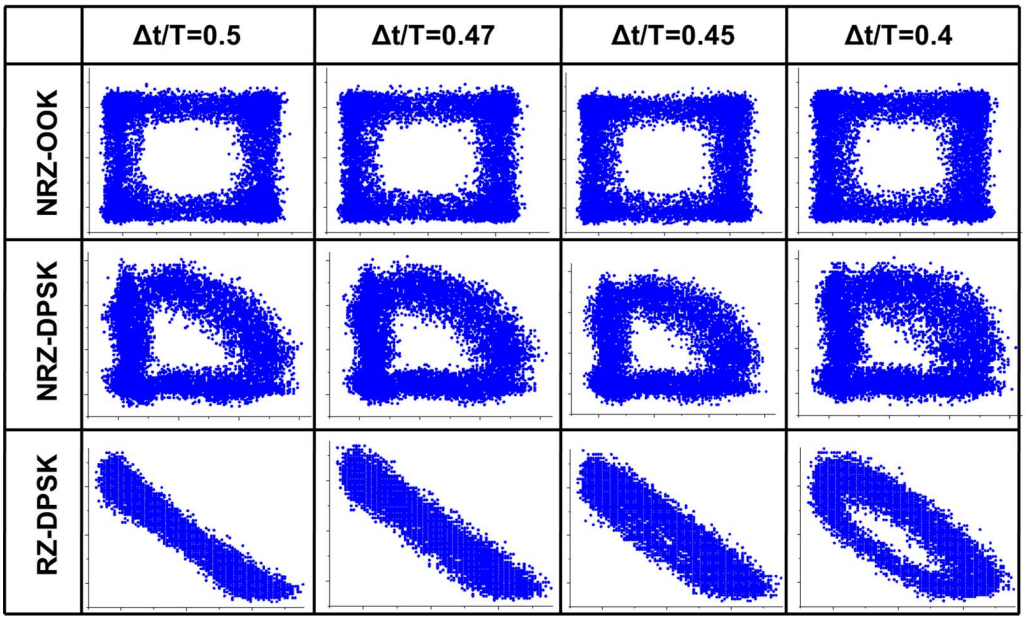


Figure 5.17: Phase portrait generated by using different equivalent time delay in different modulation systems.

Since the patterns of the phase portraits with slightly different phase differences are similar, the sample pairs, whose phase difference is within the tolerated range ($2 \cdot$

$t_o/T$), are selected from the sample sequence to depict a phase portrait, as shown in Fig. 5.18(a). For example, the phase difference between the sample $S_1$ and its partner $S_p$ is in the range from $(\Delta t - t_o)/T$ to $(\Delta t + t_o)/T$, so that the sample pairs that satisfy the phase difference would be easier to be found during the X-Y pairs generation. The time interval between the sample pairs would be reduced, which increases the tolerance to the drift phase induced by the aliasing frequency estimation offset. As the tolerated half symbol phase difference phase portrait generated under 10-kHz aliasing frequency offset in Fig. 5.18(b) shows, the tolerated phase difference ($t_o/T = 0.003$) scheme is more robust to the aliasing frequency estimation offset.

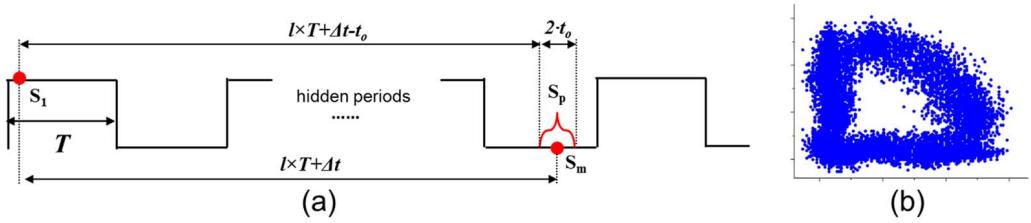


Figure 5.18: (a) Schematic diagram of tolerated phase difference phase portrait generation. (b) NRZ-DPSK signal phase portrait generated by tolerated phase difference.

In Fig. 5.19, the phase portraits in both the fixed and tolerated phase difference schemes are compared in the case that the estimated aliasing frequency offset is 10 kHz. It is noted that the patterns of the tolerated phase difference plot do not change under 10-kHz aliasing frequency estimation offset. For the fixed phase difference, since the aliasing frequency offset leads to a certain amount of drift phase, the true phase difference is changed.

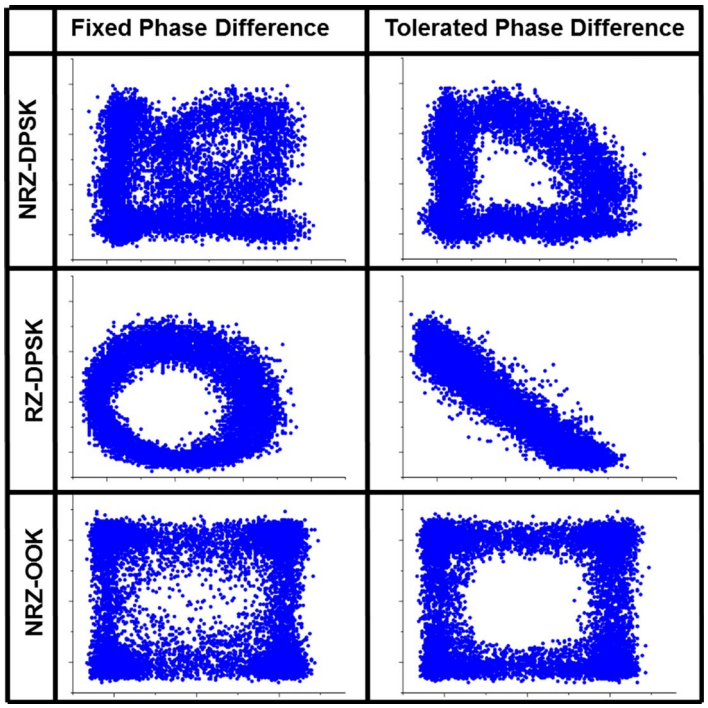


Figure 5.19: Phase portrait comparison between the fixed phase difference scheme and the tolerated phase difference scheme in the three tested formats, when the aliasing frequency offset is 10 kHz.

### 5.4.2 Experimental Results and Discussions

The tolerated phase difference scheme is a method that overlaps the phase portraits generated by using slight different phase differences. Firstly, the OSNR monitoring performance based on the phase portraits with different phase differences are investigated. As the experimental results shown in Fig. 5.20, when the phase difference deviates from half symbol duration, the OSNR monitoring errors increase in the NRZ-DPSK and RZ-DPSK systems. In the high OSNR cases, the OSNR monitoring is more sensitive to the phase difference deviation. When the deviation is less than 0.03/T, the OSNR monitoring error can almost be kept in an acceptable range. However, for NRZ-OOK signal, the OSNR monitoring error is almost within 1 dB, since its continuous

mark level signal feature leads to the similar pattern in the demonstrated phase difference range, which can also be referred to the phase portraits in Fig. 5.17. Thus, the tolerated phase difference, which is 0.03/T, is adopted to generate the phase portrait for OSNR monitoring.

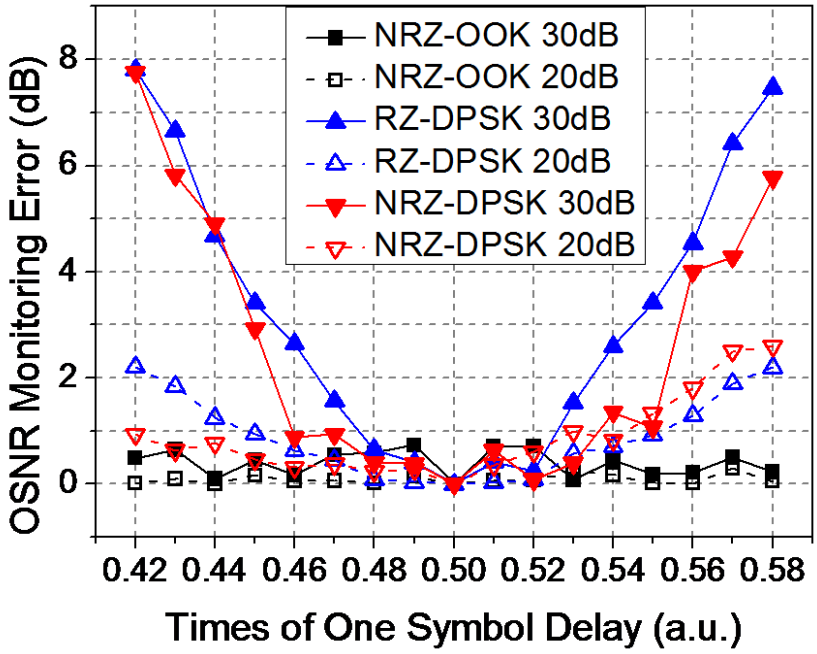


Figure 5.20: OSNR monitoring accuracy versus the phase difference deviation of the sample pairs .

In Fig. 5.21, the experimental results show the OSNR monitoring error of the proposed tolerated phase portrait scheme versus the aliasing frequency offset in 10.7-Gb/s NRZ-DPSK system. The signal OSNR is tested from 10 dB to 30 dB. The OSNR monitoring errors can almost be kept below 1 dB as the aliasing frequency estimation offset increases up to 10 kHz for the demonstrated OSNR value. Compared with the fixed phase difference phase portrait scheme, the tolerated phase difference scheme is more robust to the aliasing frequency estimation.

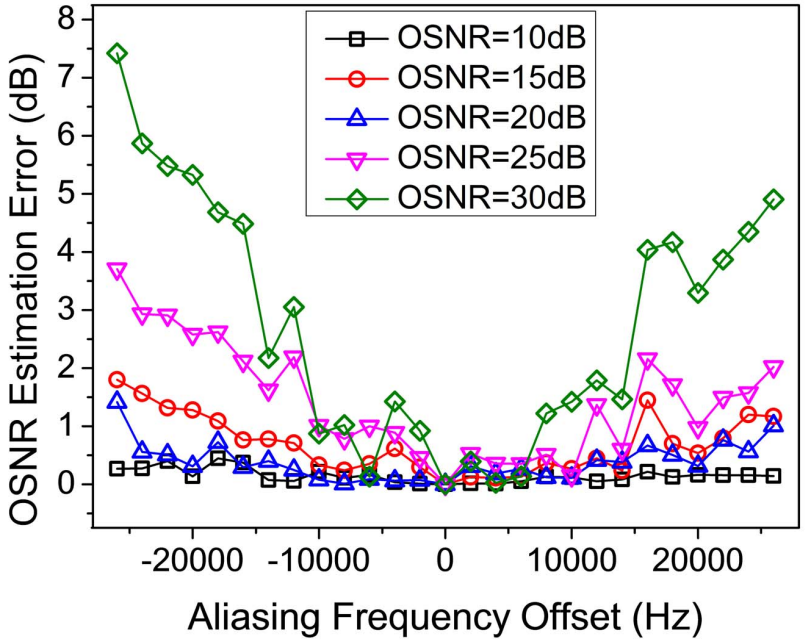


Figure 5.21: OSNR monitoring error versus aliasing frequency offset in 10.7-Gb/s NRZ-DPSK system for the tolerated phase difference phase portrait scheme.

In Fig. 5.22, the experimental results show the OSNR monitoring error of the proposed tolerated phase portrait scheme versus the aliasing frequency offset in 10.7-Gb/s RZ-DPSK system. The signal OSNR is tested from 10 dB to 30 dB. The 1-dB OSNR monitoring tolerance to the aliasing frequency offset can reach 10 kHz in the demonstrated OSNR value.

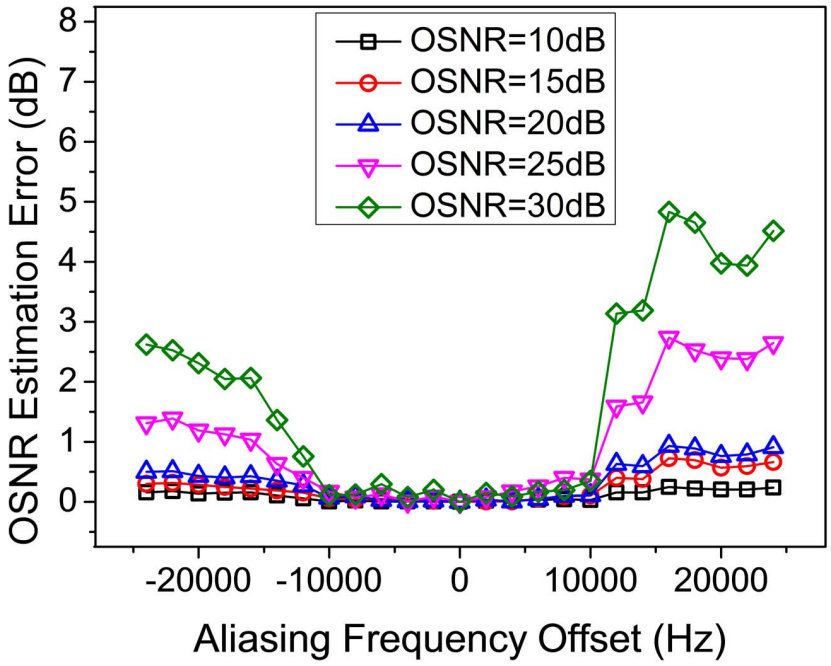


Figure 5.22: OSNR monitoring error versus aliasing frequency offset in 10.7-Gb/s RZ-DPSK system for the tolerated phase difference phase portrait scheme.

In Fig. 5.23, the experimental results show the OSNR monitoring error of the proposed tolerated phase portrait scheme versus the aliasing frequency offset in 10.7-Gb/s NRZ-OOK system. The signal OSNR is tested from 10 dB to 30 dB. For the NRZ-OOK format, due to its continuous mark level, its half symbol phase portrait is more robust to the aliasing frequency estimation offset. In the demonstrated frequency offset range from -26 kHz to 26 kHz, the OSNR monitoring error can almost be kept within 1 dB.

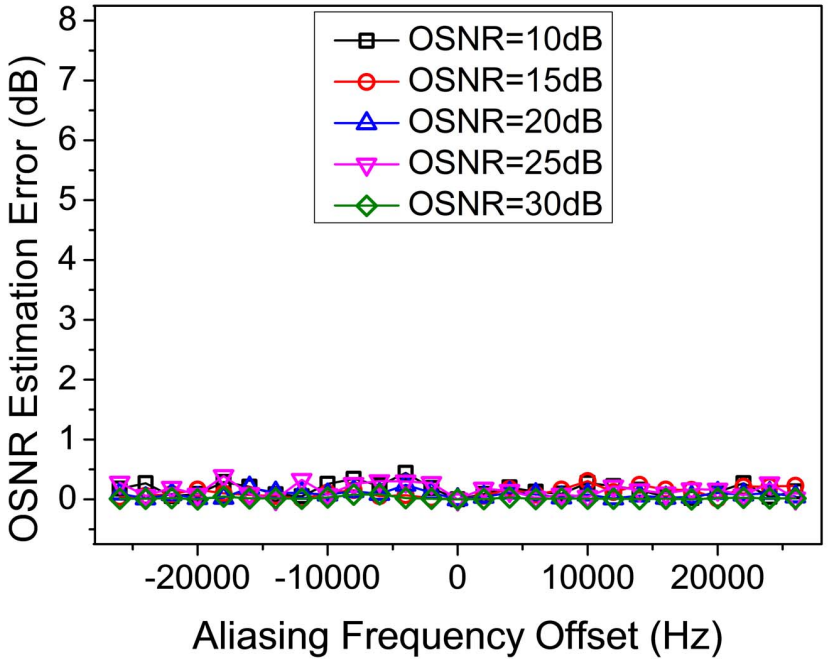


Figure 5.23: OSNR monitoring error versus aliasing frequency offset in 10.7-Gb/s RZ-DPSK system for the tolerated phase difference phase portrait scheme.

In Fig. 5.24, the experimental results exhibit the OSNR monitoring performance in the presence of both aliasing frequency offset and CD effect in 10.7-Gb/s NRZ-DPSK system. The signal OSNR is tested from 10 dB to 30 dB. At the same time, the aliasing frequency estimation offset varies from 0 Hz to 10 kHz, while the CD is changed from 0 ps/nm to 425 ps/nm. When the two factors co-exist in the monitoring system, the proposed OSNR monitoring method can keep a good monitoring accuracy from 10 dB to 25 dB. Beyond 25 dB, the OSNR monitoring accuracy is poor, since it is more sensitive to the CD induced pattern distortion.

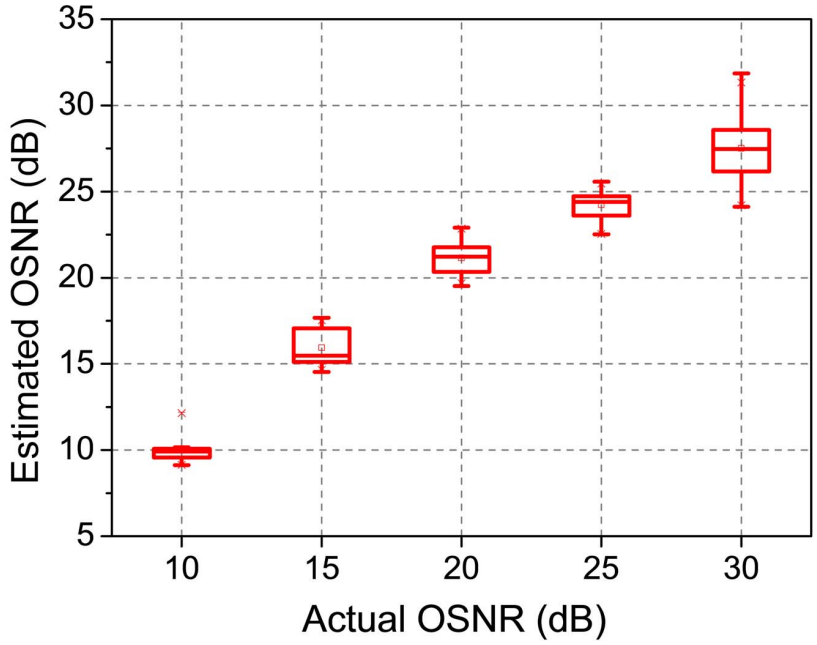


Figure 5.24: Experimental results of OSNR monitoring by using tolerated phase difference phase portrait in the present of CD effect in 10.7-Gb/s NRZ-DPSK system.

In Fig. 5.25, the experimental results show the OSNR monitoring performance in the presence of both aliasing frequency offset and CD effect in 10.7-Gb/s RZ-DPSK system. The signal OSNR is tested from 10 dB to 30 dB. At the same time, the aliasing frequency estimation offset varies from 0 Hz to 10 kHz, while the residual CD is changed from 0 ps/nm to 425 ps/nm. In the presence of the variation of these two factors, the proposed OSNR monitoring performs with good accuracy from 10 dB to 25 dB. For the larger than 25-dB OSNR case, the monitoring accuracy reduces significantly, because CD induces more obvious pattern distortion.

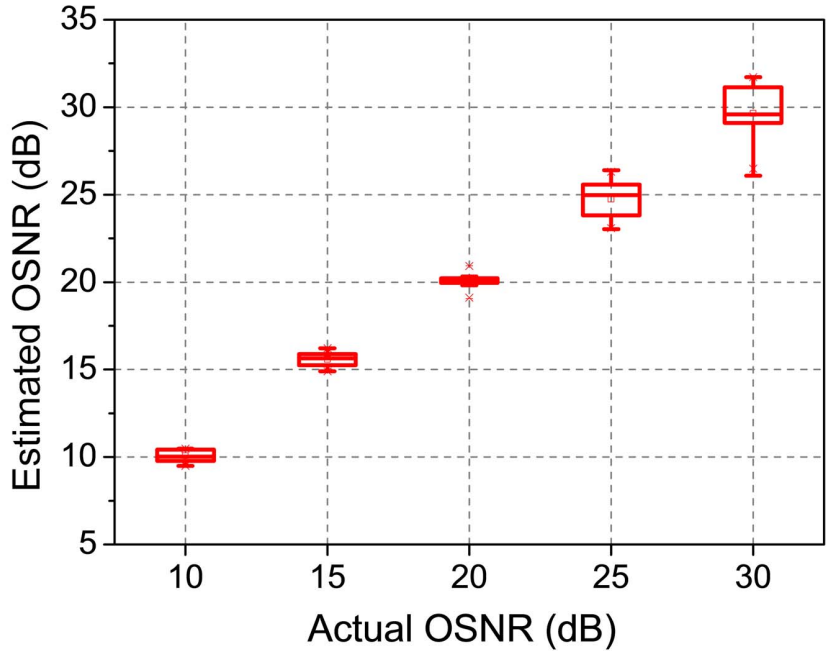


Figure 5.25: Experimental results of OSNR monitoring using tolerated phase difference phase portrait in the presence of CD effect in 10.7-Gb/s RZ-DPSK system.

In Fig. 5.26, the experimental results show the OSNR monitoring performance in the presence of both aliasing frequency offset and CD effect in 10.7-Gb/s NRZ-OOK system. The signal OSNR is tested from 10 dB to 30 dB. In the meanwhile, the aliasing frequency estimation offset varies from 0 Hz to 10 kHz, while the CD is changed from 0 ps/nm to 425 ps/nm. In the demonstrated CD and aliasing frequency offset variation ranges, the proposed OSNR monitoring method can keep accurate performance in the demonstrated OSNR range.

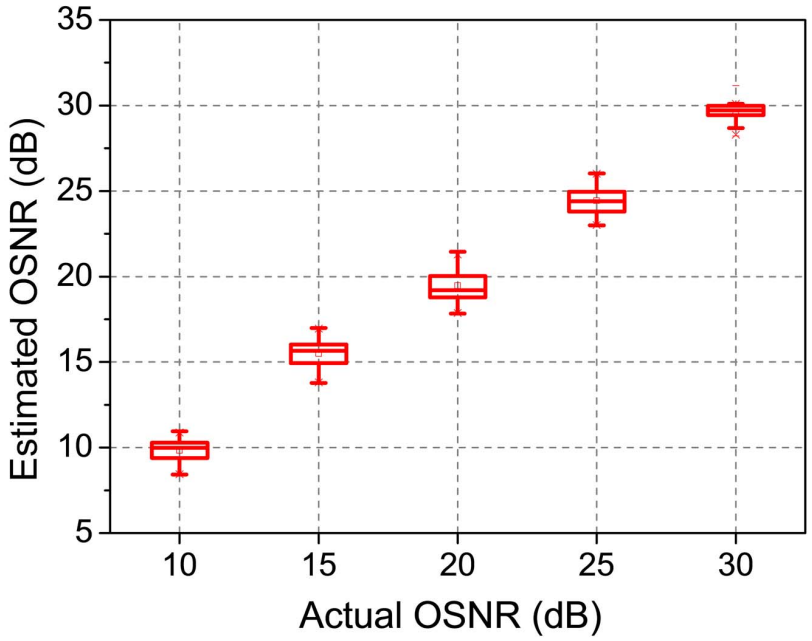


Figure 5.26: Experimental results of OSNR monitoring using tolerated phase difference phase portrait in the presence of CD effect in 10.7-Gb/s NRZ-OOK system.

## 5.5 Conclusion

In this chapter, the OSNR monitoring method using single channel sampling with software synchronization technique was proposed and successfully demonstrated in 10.7-Gb/s NRZ-OOK, NRZ-DPSK, and RZ-DPSK systems. More importantly, by using the proposed tolerated phase difference phase portrait, the tolerance to the aliasing frequency estimation offset of the software synchronization is significantly improved, which reduces the accuracy requirement of the software synchronization technique. This method employs the software based algorithm to synchronize the sampling sequence that is sampled by un-related sampling frequency, so that the system setup complexity is further simplified. This method has the simplest OSNR monitoring setup, to the best of our knowledge. In addition, the un-related sampling frequency extends its

application scope. However, the software synchronization increases the computation loading in some degree, so the monitoring speed is reduced. Thus, there is a tradeoff between the application scope and the monitoring speed.

# Chapter 6

# Time Alignment Monitoring Using Electrical Sampling Technique

In this chapter, RZ pulse carver alignment and I/Q branch alignment monitoring of RZ phase modulation systems are investigated. So far, there are some RZ pulse carver alignment monitoring methods that have been proposed for RZ signals [19,84,86,106]. These methods are based on the fact that the time misalignment induces optical or RF spectrum evolution. However, it is difficult to identify the sign of the time misalignment from frequency domain of the signal. Thus, during system calibration, the monitoring system needs to keep testing the signal till the calibration is finished, which is not efficient.

For the time alignment monitoring, the sign of the time mis-alignment can be observed from time domain of the signal [87]. In this chapter, we propose and demonstrate a novel method to monitor RZ pulse carver alignment of RZ-DPSK and RZ-DQPSK systems by using electrical sampling technique with cooperation of simple pattern recognition. The proposed method is demonstrated by using both simulation and experimental demonstration. More importantly, the proposed method is demonstrated by using software synchronized single channel sampling technique being dis-

cussed in chapter 5. The sign and degree of the time mis-alignment can be estimated by investigating the pattern evolution. Moreover, the I/Q alignment of RZ-DQPSK signal can also be monitored by using our proposed method. More importantly, the proposed method is convenient to be operated and maintained, since digital signal processing (DSP) is in charge of the core part of the monitoring system.

## 6.1 Pulse Carver Alignment Monitoring

### 6.1.1 Working Principle of Pulse Carver Alignment Monitoring

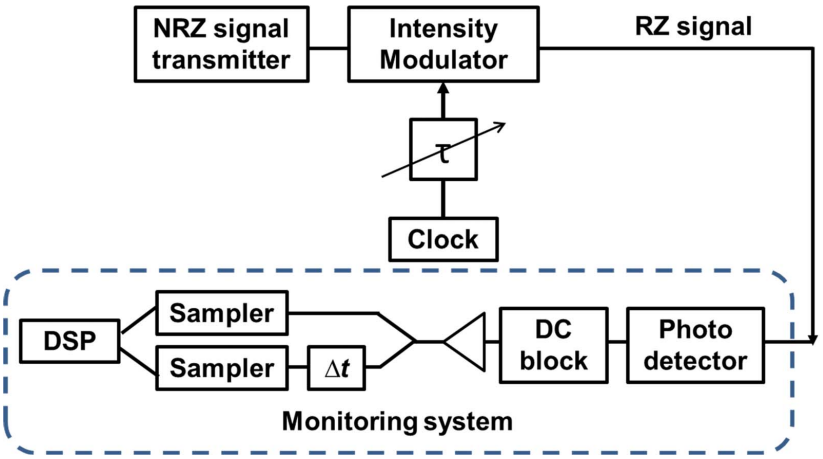


Figure 6.1: Schematic diagram of the proposed pulse carver alignment monitoring system setup.

In the simulation work, delay-tap sampling method is used to investigate the time alignment monitoring performance, where different time delay phase portraits with same phase difference are investigated. The simulation setup of our proposed RZ pulse carver alignment monitoring system is shown in Fig. 6.1. The integrated optical transmitters generate NRZ-DPSK and NRZ-DQPSK signals separately in the two tested systems. An optical intensity modulator works as a RZ pulse carver to generate RZ

pulse, which is driven by clock signal. The pulse carver employs a tuneable delay line to synchronize the pulse carver and the modulated data. In order to reduce the cost and complexity of the monitoring setup, we propose to monitor the time alignment by analysis on the pulse carvers waveform, so that a single photo detector is used to transform the time mis-aligned optical signal into electrical signal. After a DC block and an electrical amplifier, a power divider splits the electrical signal into two branches. An electrical delay line is placed in one branch, which emulates an internal delay ($\Delta t$) between the two samplers. The bandwidth of the sampling channel is 10 GHz for 10-Gb/s RZ-DPSK signal, while it is 25 GHz for 50-Gb/s RZ-DQPSK signal.

In this work, we propose to monitor the time alignment by using the tenth symbol phase difference phase portrait. In the simulation work, the tenth symbol difference phase portraits generated by using within one symbol delay and larger than one symbol delay are investigated in the alignment monitoring performance. The larger time delay values ($1.1 * T_s$, $10.1 * T_s$, $30.1 * T_s$ and $50.1 * T_s$, $T_s$: one symbol duration) are used to generate phase portraits separately, whose phase differences are tenth symbol duration. Thus, they are named as equivalent tenth symbol phase difference phase portrait.

For the synchronized RZ pulse carver, the waveform peak of the pulse carver is aligned with the bit center, while the waveform valley is placed at the phase transition center. In Fig. 6.2(a), the diagram shows the generation of RZ-DPSK. NRZ-DPSK signal has almost a constant light intensity except that at the phase transition. In the bit transition period, the phase change of the neighbour bits causes a slight optical intensity dip, while the transitions of the continuous same phase keep almost constant intensity. Thus, there are two types of light intensities during bit transition. For the well aligned case, the pulse carver suppresses the two types into one. The intensity of the RZ-DPSK signal has a sinusoid-like profile. However, when there is a certain number of time mis-alignment between the pulse carver and the modulated light, the intensity profile of RZ-DPSK signal is distorted, as shown in Fig. 6.2(b). The intensity

dip of the NRZ-DPSK signal shifts to one edge of the pulse carver, which leads to the edge distortion of the combined RZ-DPSK signal. At the meantime, the mis-alignment does not influence the waveform at the no-dip transition, which means that the pulse carver waveform is not changed in this case. Thus, these two cases cause the two edges in one side, as the eye diagram of mis-aligned RZ-DPSK signal shows in Fig. 6.2. The sign of the time mis-alignment decides which side the double edge appears.

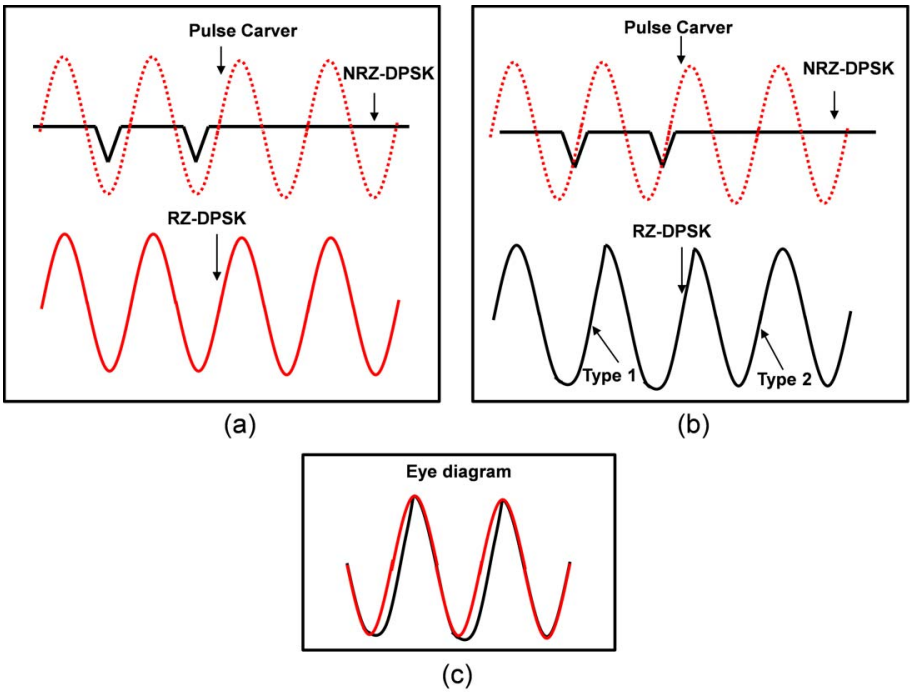


Figure 6.2: Illustration of RZ pulse carver alignment (a) synchronized RZ-DPSK signal generation, (b) mis-aligned RZ-DPSK signal generation, (c) eye diagram of mis-aligned RZ-DPSK signal.

In Fig. 6.3, the eye diagrams and phase portraits of 10-Gb/s RZ-DPSK signal generated by simulation demonstrate the waveform and pattern evolutions as the time mis-alignment varies. As the eye diagrams show in the first column of Fig. 6.3, the received pulse carver waveform appears the double edge, whose gap increases as the time mis-alignment increases. The sign of the time mis-alignment can be observed

from the eye diagrams.

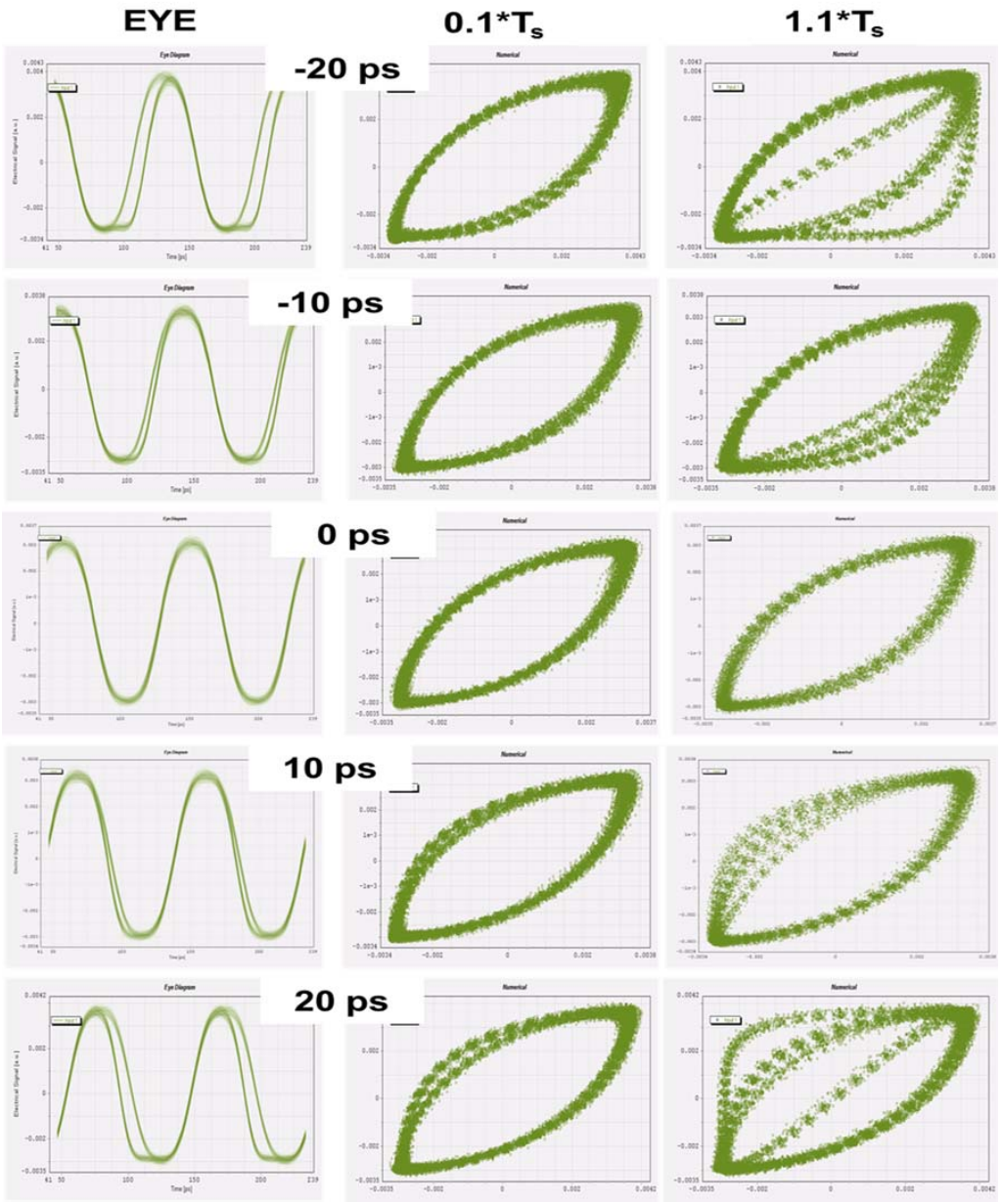


Figure 6.3: The evolution of eye diagram, tenth symbol delay phase portrait, and one and tenth symbol delay phase portrait of 10-Gb/s RZ-DPSK signal as the pulse carver mis-alignment varies. The demonstrated time mis-alignment is -20 ps, -10 ps, 0 ps, 10 ps and 20 ps

After the electrical signal waveform is transformed into the tenth symbol delay phase portrait ($\Delta t = 0.1 * T_s$), the pattern evolves as the time mis-alignment changes, as shown in the second column of Fig. 6.3. It can be noticed that the tenth symbol delay phase portrait is extended at the diagonal direction as the time mis-alignment increases, but the one and tenth symbol delay phase portraits ($\Delta t = 1.1 * T_s$) show more obvious pattern distortion, even if these two types of phase portraits show the similar pattern of the synchronized signal, as exhibited in the third column of Fig. 6.3. For the case using tenth symbol delay, the sample pairs are from same transition edge, while the sample pairs with one and tenth symbol delay are from either of these two edges, which cause a different phase portrait in the large time mis-alignment case. As the -20-ps mis-alignment phase portrait in the third column of Fig. 6.3 shows, the curve pattern at right bottom of the portrait is formed by the X-Y pairs from different types of edges, which lead to a significant pattern evolution as the time mis-alignment increases.

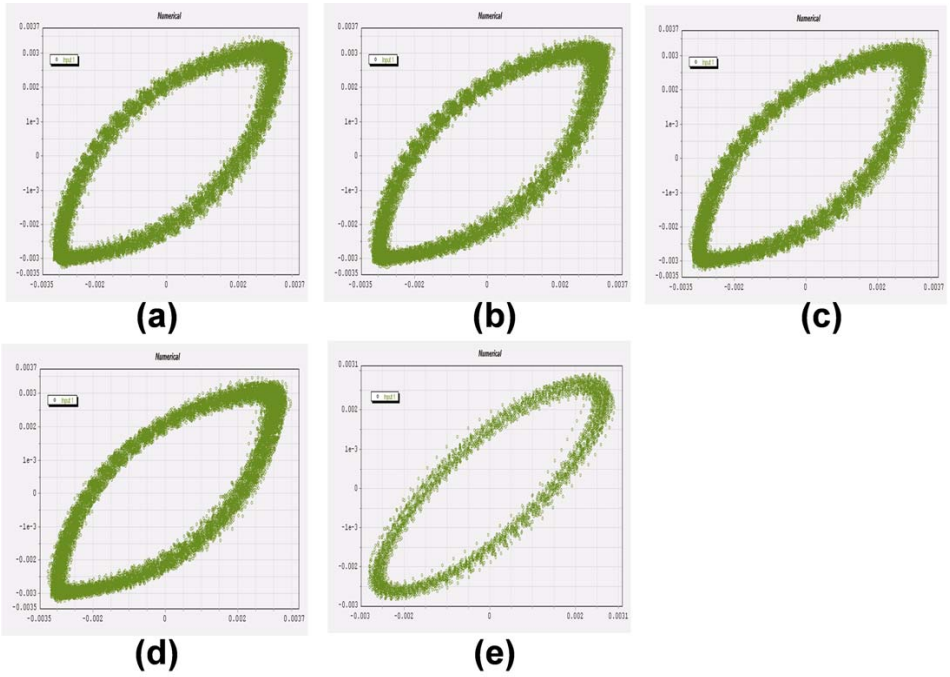


Figure 6.4: Phase portrait of 10-Gb/s RZ-DPSK signal generated by using different time delay: (a) $1.1 * T_s$, (b) $10.1 * T_s$, (c) $30.1 * T_s$, (d) $50.1 * T_s$; (e) phase portrait of 50-Gb/s RZ-DQPSK signal generated by using $50.1 * T_s$ time delay.

In Fig. 6.4(a)-(d), the 10-Gb/s RZ-DPSK equivalent tenth symbol phase difference phase portraits generated by using different time delay are demonstrated. It can be noted that the tenth symbol phase difference phase portraits generated by using different time delay have same pattern. Moreover, for the 50-Gb/s RZ-DQPSK signal, the tenth symbol phase difference phase portrait generated by using large time delay has a similar elliptical pattern as the RZ-DPSK signal tenth symbol phase difference phase portrait, due to their similar received pulse carver waveform, as Fig. 6.4(e) shows.

### 6.1.2 Monitoring Parameter Derivation

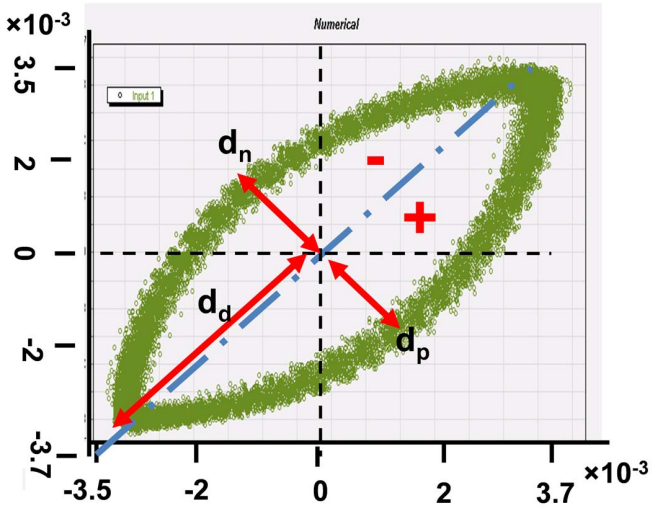


Figure 6.5: Equivalent tenth symbol difference phase portrait of 10-Gb/s RZ-DPSK signal and schematic diagram of pattern recognition.

According to the pattern evolution as the time mis-alignment varies, we propose to use the ratio of the pattern widths to monitor pulse caver alignment. As the schematic diagram shows in Fig. 6.5, initially, the pattern is divided into two areas at the diagonal direction of the 2-D coordinate system. One area is defined as the positive region, the other is the negative one. Then, the pattern widths of these two areas are measured as $d_n$ and $d_p$, while the pattern length along the diagonal direction at the third quadrant of the original coordinate system is measured as $d_d$. The pattern widths are obtained by calculating the distance of the points to the diagonal lines. The three width parameters are the average values of several longest distances in each case. Thirdly, by comparing the pattern widths in the two areas, the region sign of the wider one determines the sign of the distance ratio ($DR$) as expressed by Eq. 6.1. The normalized parameter ($DR_0$) is the distance ratio of the synchronized signal, as expressed by Eq. 6.2, where the three distances ($d_{n0}$, $d_{p0}$, $d_{d0}$) are measured from the synchronized signal. We propose to monitor RZ pulse carver alignment by using Eq. 6.1, which can determine the sign

of the time mis-alignment.

$$DR = (\pm)(\frac{d_n + d_p}{d_d} - DR_0) \tag{6.1}$$

$$DR_0 = \frac{d_{n0} + d_{p0}}{d_{d0}} \tag{6.2}$$

### 6.1.3 Simulation Results of RZ Pulse Carver Alignment Monitoring

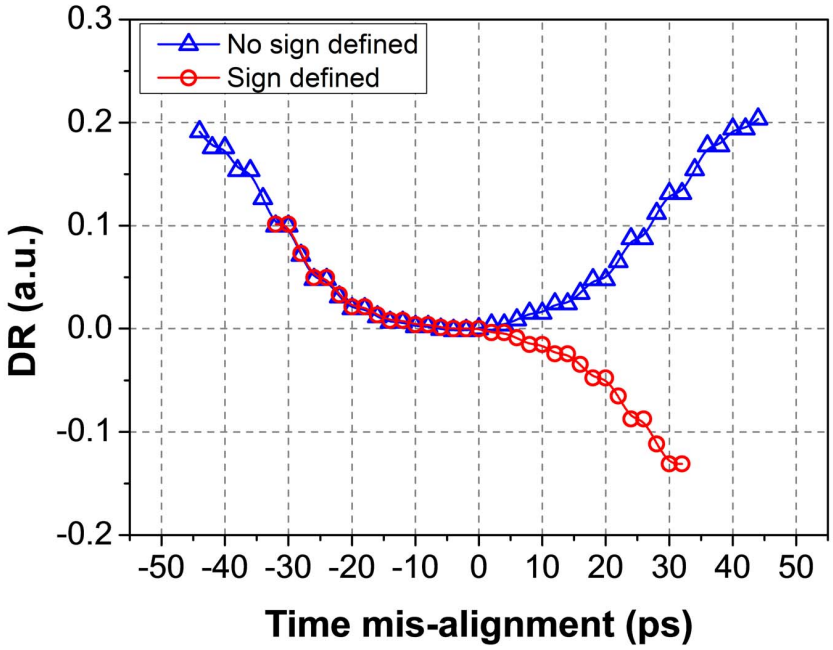


Figure 6.6: Simulation results of the proposed pulse carver alignment monitoring using tenth symbol delay phase portrait in 10-Gb/s RZ-DPSK system.

In Fig. 6.6, the simulation results show the proposed distance ratio of the tenth symbol delay ($\Delta t/T = 0.1$) phase portrait as a function of the time mis-alignment in 10-Gb/s RZ-DPSK signal. By comparing the pattern width of the phase portrait in the two regions, the sign of the time mis-alignment can be identified. Otherwise, it can only estimate the absolute value of the time mis-alignment, as the no-sign-defined curve

shows in Fig. 6.6. The no-sign-defined scheme does not distinguish the pattern widths of the two region. Although the sign can be determined, the monitored range is reduced by 10 ps, which is from -30 ps to 30 ps. Beyond this range, the two area widths of the pattern are comparable, so that it is difficult to determine the accurate sign of the time mis-alignment. Thus, the effective monitoring range of the sign defined scheme is reduced.

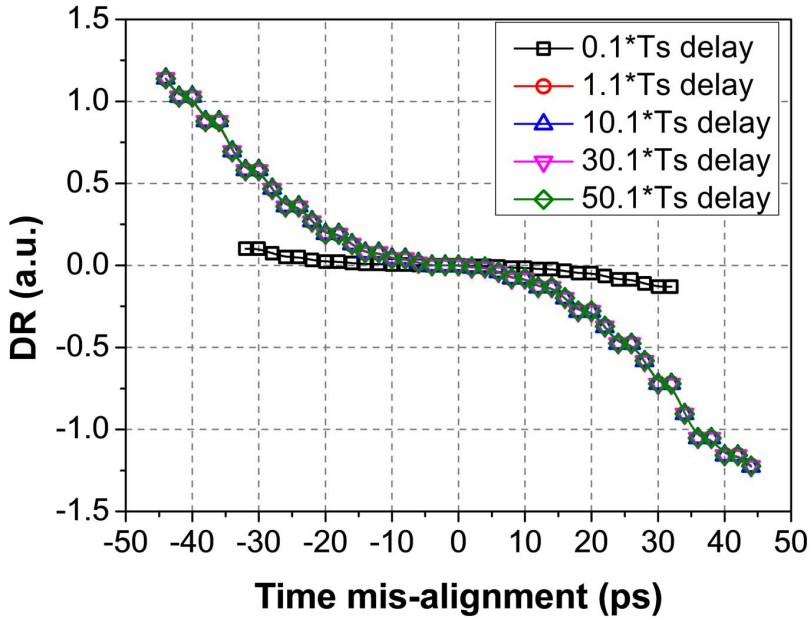


Figure 6.7: Simulation results of the proposed pulse carver alignment monitoring using equivalent tenth symbol delay phase portrait in 10-Gb/s RZ-DPSK system. Ts: one symbol duration.

More importantly, by using the equivalent tenth symbol phase difference phase portrait, the monitoring dynamic range is significantly improved, as Fig. 6.8 shows. It shows that the equivalent tenth symbol phase difference phase portraits have same monitoring performance, whose time delay values are $1.1 * T_s, 10.1 * T_s, 30.1 * T_s$ and $50.1 * T_s$, since these phase portraits have same patterns and evolution trend. Additionally, the pulse carver alignment monitoring range regains 12 ps.

The proposed pattern recognition algorithm is also applied for RZ pulse carver alignment of RZ-DQPSK signal. In Fig. 6.8, the simulation results show the distance ratio versus the time mis-alignment of 50-Gb/s RZ-DQPSK signal, which uses the tenth symbol phase difference phase portraits generated by using different time delay. The equivalent tenth symbol phase difference phase portraits are more sensitive to the time mis-alignment than the tenth symbol delay phase portrait, which shows a larger monitoring range and monitoring dynamic range. Thus, it can be concluded that the equivalent tenth symbol phase difference phase portrait is a better candidate for pulse carver alignment monitoring in RZ-DPSK and RZ-DQPSK systems.

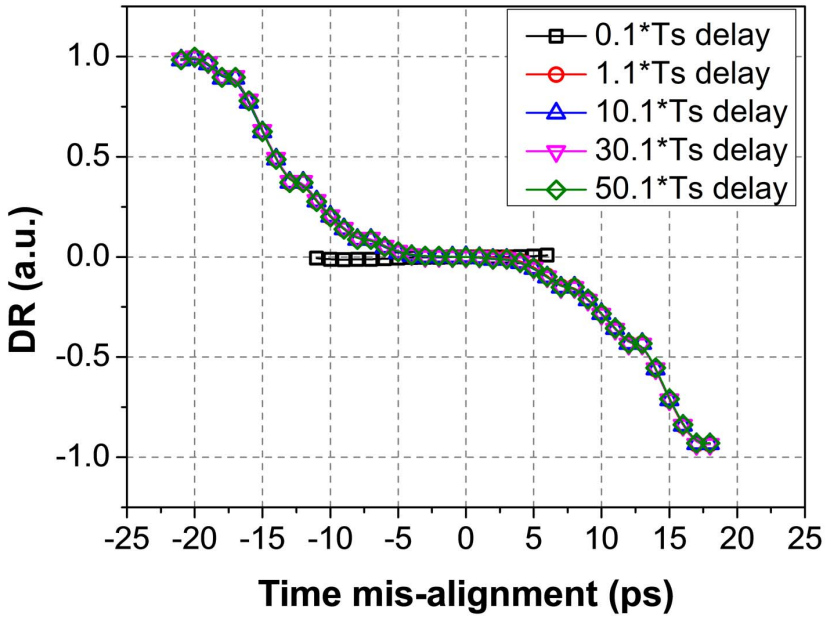


Figure 6.8: Simulation results of the proposed pulse carver alignment monitoring by using equivalent tenth symbol phase difference phase portrait in 50-Gb/s RZ-DQPSK system. Ts: one symbol duration.

### 6.1.4 Experimental Demonstration of RZ Pulse Alignment Monitoring

As the simulation results exhibit, the phase difference phase portraits using larger time delay are more sensitive to pulse carver alignment monitoring. Additionally, the sign monitored range is extended. Thus, the proposed phase portrait generated by using single channel sampling method is a good solution for pulse carver alignment monitoring, which generates the X-Y pairs with large time delay. In Fig. 6.9, the experimental setup of the proposed pulse carver monitoring method is exhibited. Firstly, the light generated by an external cavity laser (ECL) laser is modulated by the transmitted data. Then, the modulated light is modulated by clock signal, which works as a pulse carver. The tuneable delay line is used to synchronize the pulse carver to the modulated data. In this work, 10-Gb/s RZ-DPSK and 20-Gb/s RZ-DQPSK signals are tested. For the generation of 10-Gb/s RZ-DPSK signal, the first optical modulator is an MZM that is biased at the nulling point for NRZ-DPSK signal generation, while an I/Q modulator is used as the data modulator for 20-Gb/s NRZ-DQPSK signal generation. The pulse carver is modulated by a 10-Gb/s clock signal to generate $50\%$ RZ pulse carver. The obtained RZ signal is directly sent into the monitoring module for testing. For the monitoring module setup, a single photo detector transforms the optical signal into the electrical waveform. Then, an electrical amplifier increases the electrical signal power after the DC component is removed. A single sampling channel of real-time oscilloscope samples the electrical signal by using un-related sampling frequency. Finally, the sample sequence is processed by off-line software. Since this method employs the SCS method with un-related sampling frequency, the 2-D phase portrait generation procedure is the same as the method in chapter 5. At first, the sample sequence is synchronized by software algorithm. Then, the 2-D phase portrait is generated by searching the nearest sample pairs that are with certain phase difference.

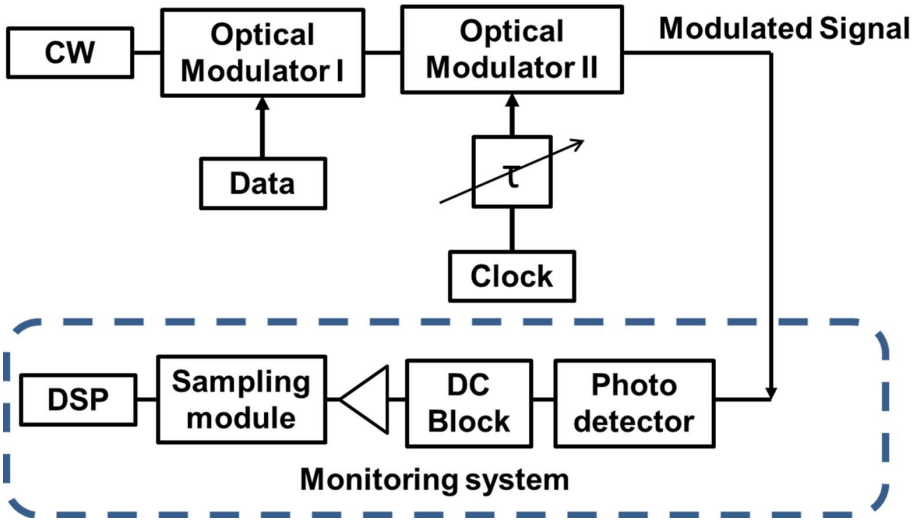


Figure 6.9: Experimental setup of RZ pulse carver alignment monitoring

### 6.1.5 Generated 2-D Phase Portrait

The generated tenth symbol phase difference phase portraits and eye diagrams of 10-Gb/s RZ-DPSK signal with different degree of RZ pulse carver time mis-alignment are exhibited in Fig. 6.10. From the eye diagrams, it can be observed that the received pulse carver waveform is distorted by the time mis-alignment, and the sign of the time mis-alignment can be distinguished from the eye diagrams by identifying the dual edge appearance direction. The generated phase portraits display the pattern evolution induced by the RZ pulse carver mis-alignment, which is the same as the simulated plots in section 6.1.1. The sign of the time mis-alignment can be distinguished by identifying the pattern width in the two regions. For the quantization of the time mis-alignment, the alignment monitoring parameter is calculated by using the proposed algorithm in section 6.1.2.

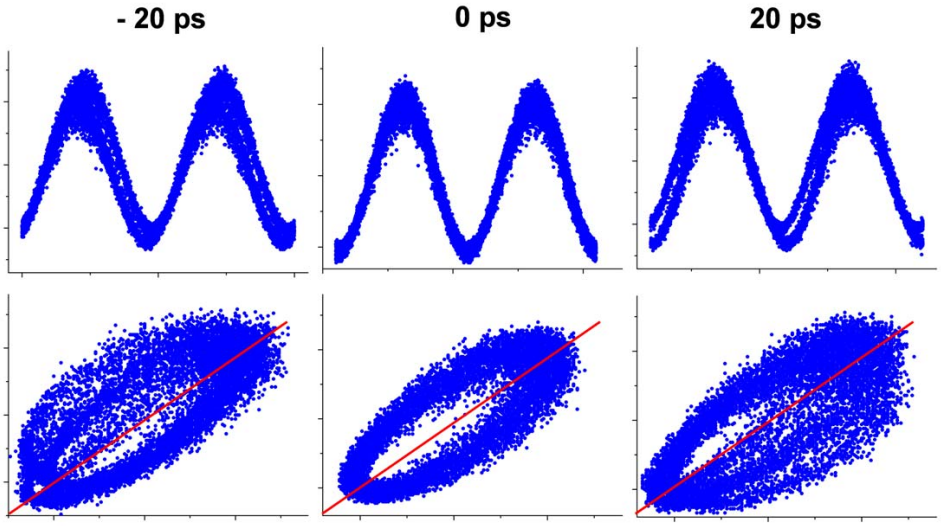


Figure 6.10: Eye diagrams and tenth symbol phase difference phase portraits of 10-Gb/s RZ-DPSK signal with different degree of pulse carver mis-alignment (-20 ps, 0ps, and 20 ps).

Moreover, in this work, 20-Gb/s RZ-DQPSK signal is also investigated and demonstrated. The generated RZ-DQPSK signal eye diagrams and tenth symbol phase difference phase portraits with different degree of the time mis-alignment are shown in Fig. 6.11. For the 10-Gsymbol signal, its pulse carver frequency is the same as 10-Gb/s RZ-DPSK, but the two transition levels of RZ-DQPSK signal cause slightly different pattern from that of RZ-DPSK signal. However, the pattern distortion trends of these two signals are similar. Thus, they can use the same algorithm to calculate the RZ pulse carver monitoring parameter.

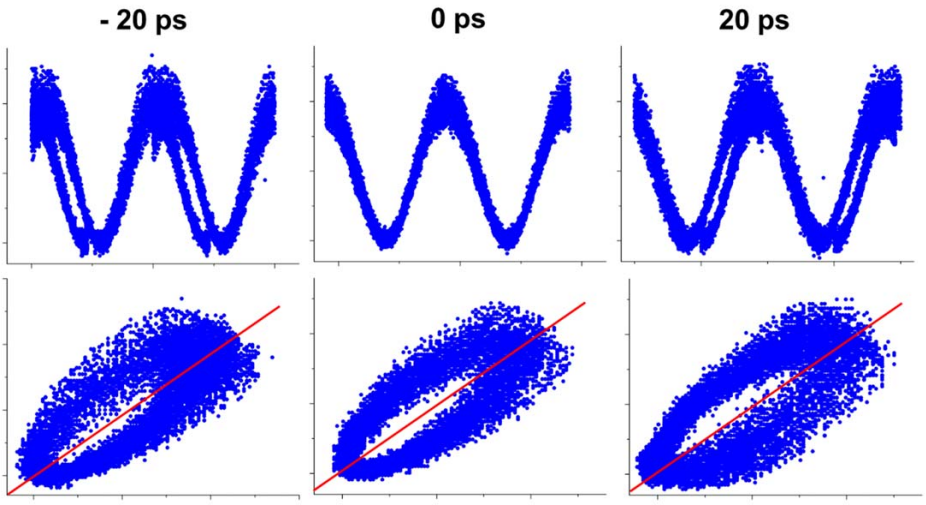


Figure 6.11: Eye diagrams and tenth symbol phase difference phase portraits of 20-Gb/s RZ-DQPSK signal with different degree of pulse carver mis-alignment (-20 ps, 0ps, and 20 ps).

### 6.1.6 Experimental Results and Discussions

In Fig. 6.12, the experimental results show that the proposed distance ratio of the phase portrait is a function of the RZ pulse carver mis-alignment in 10-Gb/s RZ-DPSK system. By comparing the pattern widths in two regions, the sign of the time mis-alignment can be distinguished, as the sign defined line shows in Fig. 6.12. Otherwise, it can only estimate the absolute value of the time mis-alignment, which does not define the sign of Eq. 6.1. In the demonstrated 10-Gb/s RZ-DPSK system, the sign defined time mis-alignment is from -45 ps to 45 ps. Beyond this range, the sign decision accuracy is quite poor.

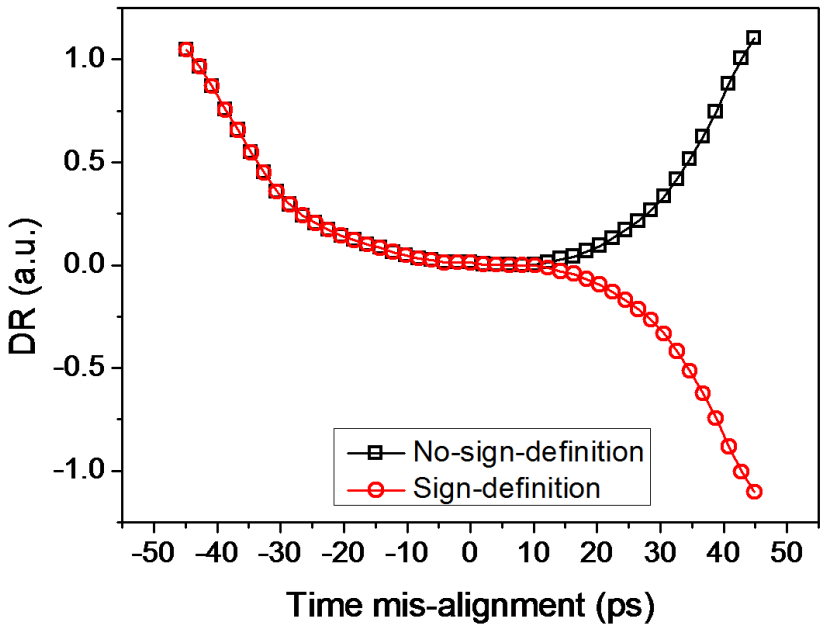


Figure 6.12: Experimental results of 10-Gb/s RZ-DPSK pulse carver alignment monitoring by using tenth symbol phase difference phase portrait.

For 20-Gb/s RZ-DQPSK signal, the time mis-alignment of RZ pulse carver can be estimated with sign by using the proposed distance ratio, as the experimental results demonstrate in Fig. 6.13. For the sign defined monitoring method, the RZ pulse carver alignment of 20-Gb/s RZ-DQPSK signal can be monitored from -45 ps to 45 ps. Otherwise, the absolute value of the time mis-alignment is obtained, as the no-sign-definition scheme shows.

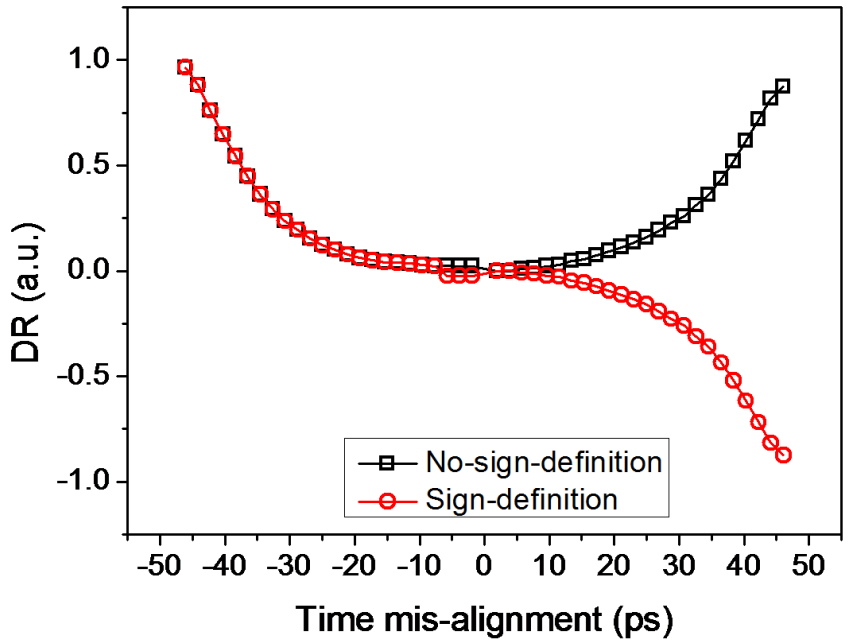


Figure 6.13: Experimental results of 20-Gb/s RZ-DQPSK pulse carver alignment monitoring by using tenth symbol phase difference phase portrait

## 6.2 I/Q Alignment Monitoring in RZ-DQPSK system

### 6.2.1 Working Principle and Simulation Setup

For RZ-DQPSK signal, the I/Q branch alignment is another critical issue. In this work, the 2-D phase portrait is also proposed to monitor the I/Q branch alignment of RZ-DQPSK signal. The simulation setup of the I/Q branch alignment monitoring of RZ-DQPSK signal is demonstrated in Fig. 6.14. In the transmitter part, the I/Q modulator is drived by the I and Q branches of the modulated data. An electrical tuneable delay line is inserted into the Q branch to manipulate the time mis-alignement between the I and Q branches. Then, the generated 20-Gb/s NRZ-DQPSK signal is modulated by a RZ pulse carver, which is realized by an optical intensity modulator driven by clock signal. The generated RZ-DQPSK signal is sent into the monitoring system di-

rectly. In order to reduce the monitoring system setup cost, the direct detection of the RZ-DQPSK signal is used, which obtains RZ pulse carver waveform. After the DC current is removed by a DC block, the received signal is processed by delay-tap sampling scheme. The generated 2-D phase portrait is processed by DSP for monitoring parameter derivation.

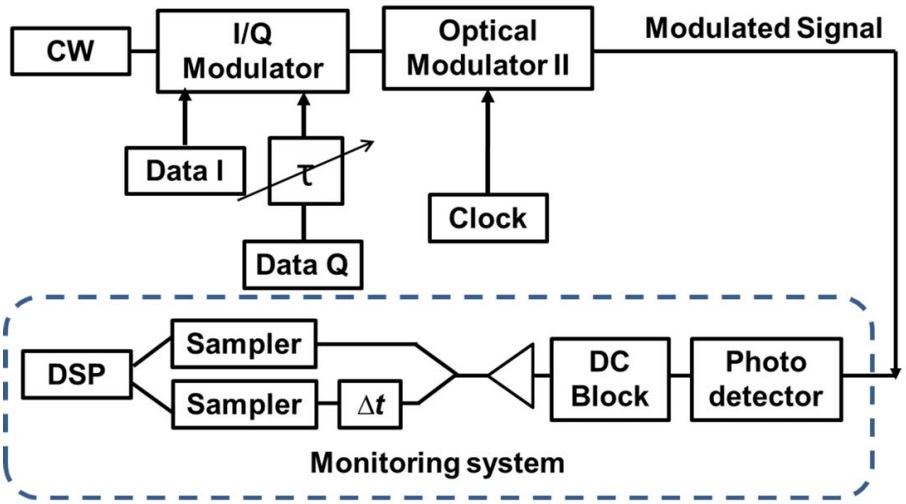


Figure 6.14: Simulation setup of I/Q alignment monitoring in RZ-DQPSK system.

### 6.2.2 2-D Phase Portrait

In Fig. 6.15, the simulated eye diagrams and phase portraits of 20-Gb/s RZ-DQPSK signal demonstrate the waveform and pattern evolutions as the time mis-alignment varies respectively. Since the intensity dip of NRZ-DQPSK signal has two levels, the eye diagram of the received pulse carver waveform appears triple edge feature, whose gap increases as the time mis-alignment increases, as shown in the first column of Fig. 6.15. The sign of the time mis-alignment can be observed from the eye diagrams by identifying the appearance direction of the triple edge.

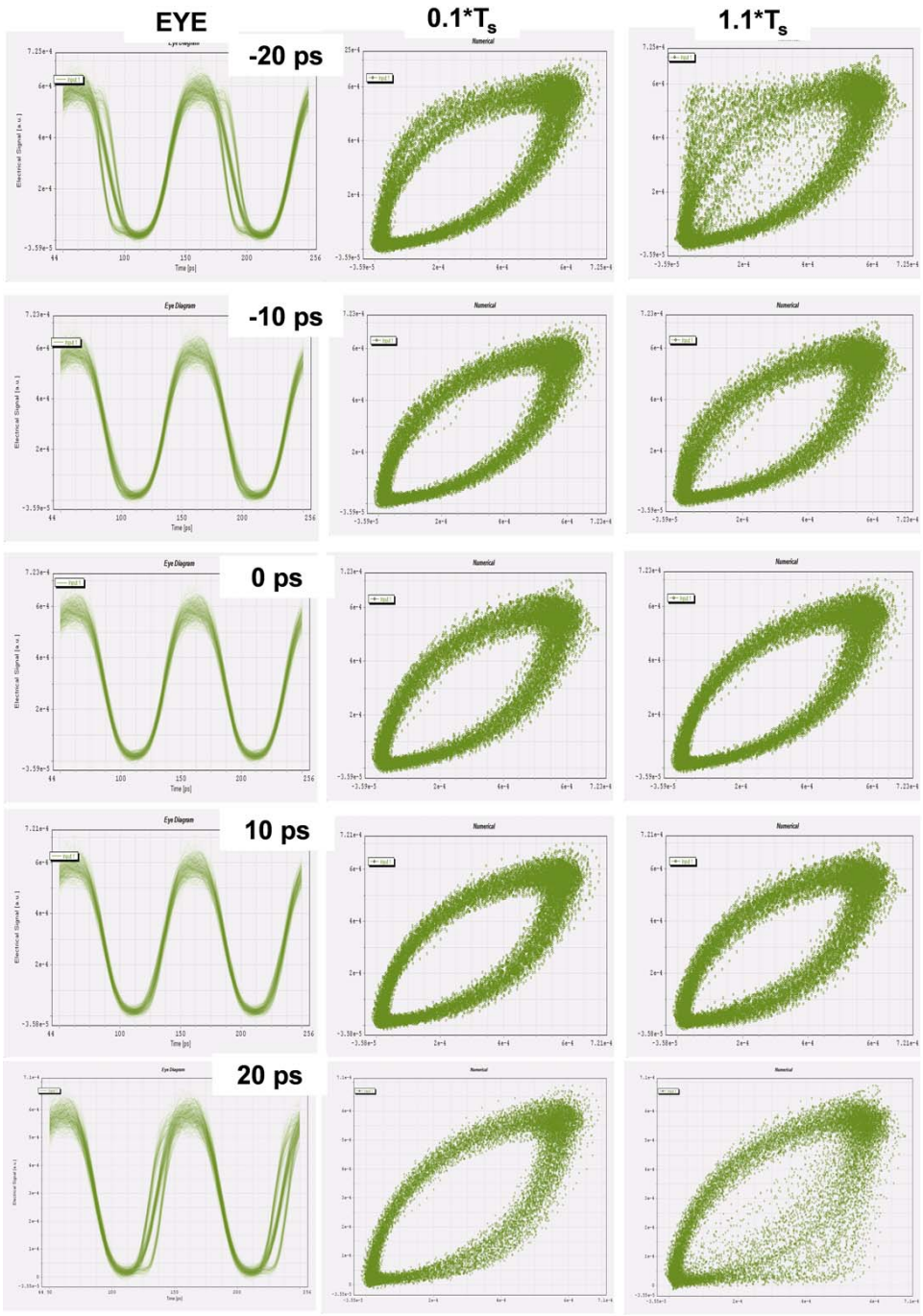


Figure 6.15: The evolution of eye diagram, tenth symbol delay phase portrait, and one and tenth symbol delay phase portrait of 20-Gb/s RZ-DQPSK signal. The demonstrated time mis-alignment is -20 ps, -10 ps, 0 ps, 10 ps and 20 ps.

As shown in the second column of Fig. 6.15, the generated tenth symbol delay

phase portrait ($\Delta t = 0.1 * T_s$) pattern evolves as the time mis-alignment changes. It can be observed that the tenth symbol delay portrait is extended at the diagonal direction as the time mis-alignment increases. In the third column of Fig. 6.15, the one and tenth symbol delay phase portraits ($\Delta t = 1.1 * T_s$) exhibit the distinguished pattern distortions, even if these two types of phase portraits have similar pattern in the synchronized case. For the case using the tenth symbol delay, the sample pairs are from same transition edge, while the sample pairs with one and tenth symbol delay are from any edge of the three levels, which is more sensitive to the time mis-alignment. More importantly, for the different sign of the time mis-alignment, the distortion direction of the phase portrait is different. Since the pattern evolution of the I/Q branch mis-alignment is similar to the one of RZ pulse carver mis-alignment, the I/Q branch mis-alignment monitoring is proposed to use the same pattern recognition algorithm as discussed in section 6.1.2. The I/Q branch mis-alignment monitoring parameter is referred to Eq. 6.1 and 6.2.

### 6.2.3 Simulation Results and Discussions

In the simulation work, the I/Q branch mis-alignment monitoring is investigated by using the tenth symbol phase difference phase portrait, which is generated by using different time delay. The time delay values are $0.1 * T_s, 1.1 * T_s, 10.1 * T_s, 30.1 * T_s$ and $50.1 * T_s$ separately. In Fig. 6.16, the simulation results show that 20-Gb/s RZ-DQPSK signal I/Q branch mis-alignment is a function of the proposed distance ratio, where the tenth symbol phase difference phase portraits are generated by using different time delay. It can be observed that the phase portrait formed by using larger time delay is more sensitive to the time mis-alignment. Thus, single channel sampling method discussed in chapter 4 and 5 can be used for the I/Q branch alignment monitoring.

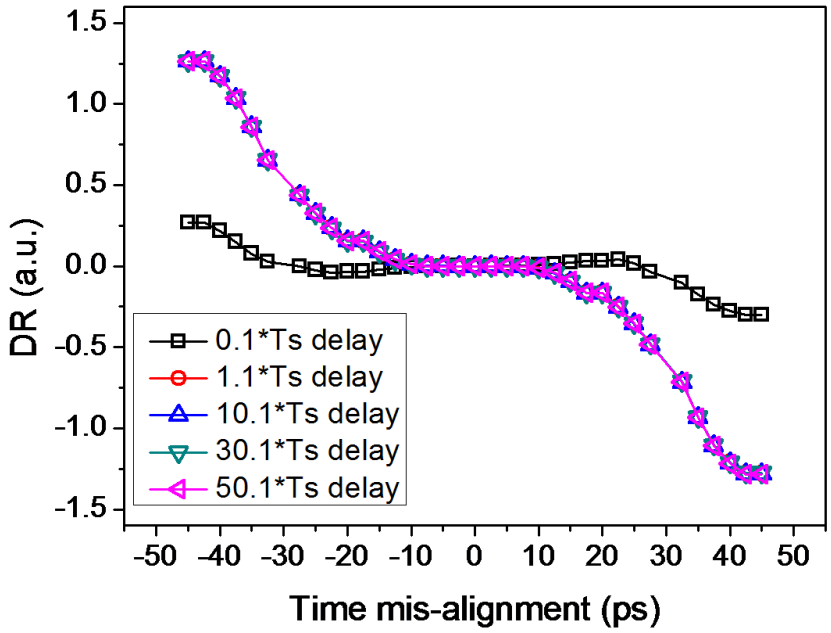


Figure 6.16: Simulation results of IQ alignment monitoring of 20-Gb/s RZ-DQPSK signal.

### 6.2.4 Experimental Setup

For the experimental demonstration, the un-related single channel sampling scheme is employed to generate 2-D phase portrait for I/Q branch mis-alignment monitoring. The experimental setup of the I/Q branch mis-alignment monitoring using un-related single channel sampling technique is demonstrated in Fig. 6.17. In the optical transmitter part, 20-Gb/s NRZ-DQPSK signal is generated by using an I/Q modulator. Then, an optical RZ pulse carver is applied to generate the RZ-DQPSK signal. In this work, the I branch is already aligned with the pulse carver, so a tuneable delay line is inserted to the Q branch to synchronize the I and Q branches. Moreover, the pulse carver is modulated by 10-Gb/s clock signal to generate $50\%$ RZ pulse carver. The RZ-DQPSK signal is directly sent into the monitoring module for testing. For the monitoring part, a single photo detector is used to obtain the pulse carver waveform. Then, an electrical

amplifier increases the electrical signal power without DC component. A single sampling channel of real-time oscilloscope samples the electrical signal with un-related sampling frequency. The sample sequence is processed by DSP. In the DSP part, the 2-D phase portrait generation procedure is the same as the method in chapter 5. The 2-D phase portrait is generated by searching the nearest sample pairs that are with tenth symbol phase difference after the sample sequence is synchronized.

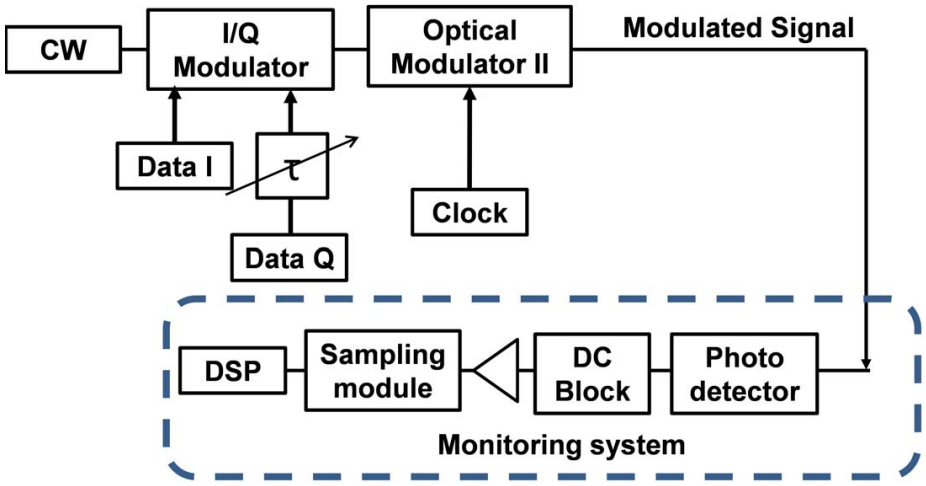


Figure 6.17: Experimental setup of I/Q branch alignment monitoring in 20-Gb/s RZ-DQPSK system.

### 6.2.5 Experimental Results and Discussions

In Fig. 6.18, the generated tenth symbol phase difference phase portrait with different degree of I/Q branch mis-alignment is demonstrated. The pattern width is extended as the I/Q mis-alignment increases. The sign of the mis-alignment can be observed by comparing the pattern widths between the two sides. Since the pattern evolution is similar to that of the pulse carver mis-alignment, the defined distance ratio of the pattern is also used for I/Q branch mis-alignment monitoring, as Eq. 6.1 expressed.

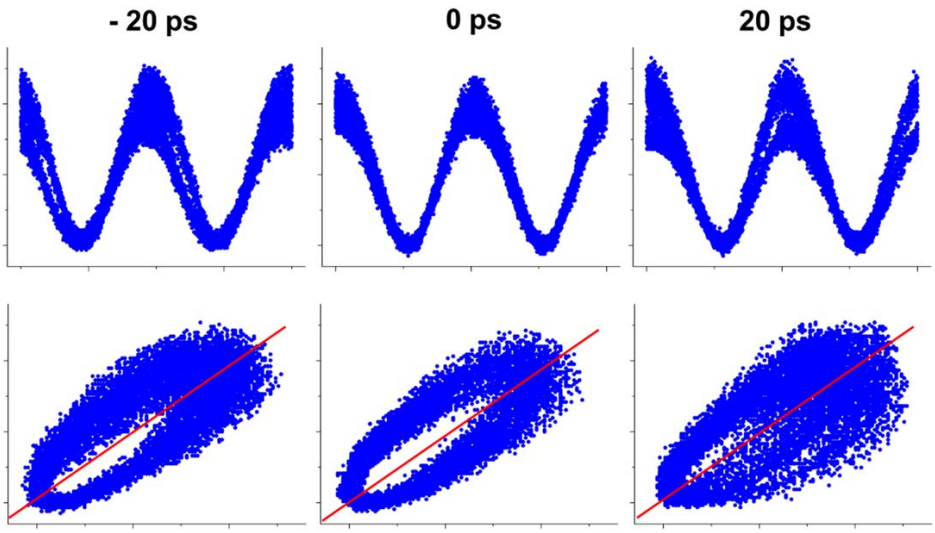


Figure 6.18: Eye diagrams and tenth symbol phase difference phase portraits of 20-Gb/s RZ-DQPSK signal at different I/Q mis-alignment (-40 ps, 0ps, and 40 ps).

In Fig. 6.19, the experimental results show the proposed distance ratio as a function of I/Q branch time mis-alignment in 20-Gb/s RZ-DQPSK system. The I/Q branch time alignment of 20-Gb/s RZ-DQPSK signal is demonstrated from -46 ps to 46 ps. When the I/Q branch mis-alignment is within 15 ps, the monitoring dynamic range is poor, since the pattern distortion induced by I/Q branch mis-alignment is not significant. More importantly, the sign of the time mis-alignment can be distinguished by using the proposed pattern width comparison.

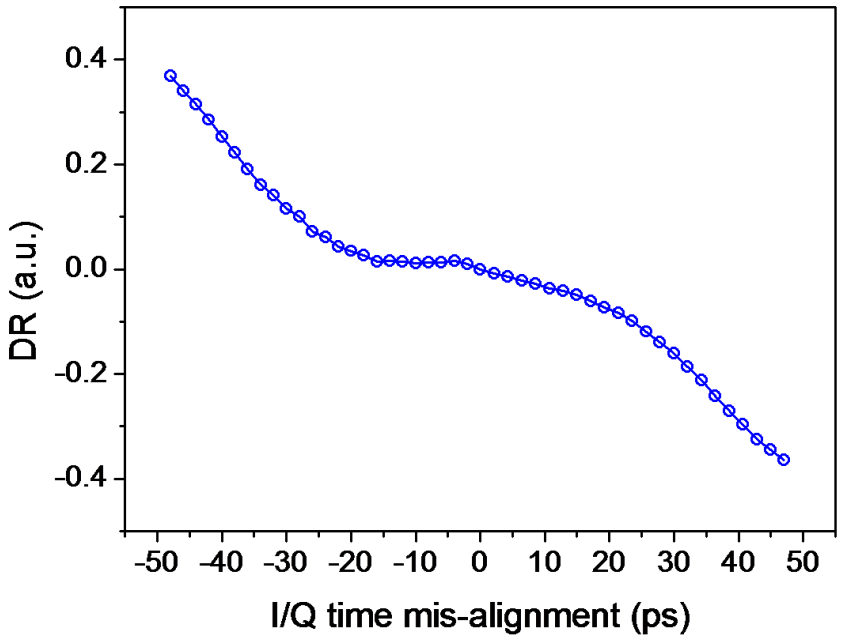


Figure 6.19: Experimental results of I/Q branch alignment monitoring of 20-Gb/s RZ-DQPSK signal.

## 6.3 Conclusions

In this chapter, the time alignment monitoring of the RZ pulse carver and the I/Q branch was proposed and demonstrated in RZ phase modulation systems. The sign and degree of the time mis-alignment are identified and quantified by the proposed pattern recognition method. From the simulation results, it is found that the method using larger time delay phase portrait has larger monitoring dynamic range. Thus, this method is able to be applied with single channel sampling technique, which generates the phase portrait with large time delay. In the experimental demonstration part, the time mis-alignment monitoring is successfully demonstrated by using the 2-D phase portrait, which is generated by using software synchronized single channel sampling technique. Thus, the proposed time alignment monitoring method is not only a sign de-

fined monitoring method, but also extends the application scope of our proposed single channel sampling technique. The time alignment monitoring of optical transmitter can share the same monitoring setup with other optical impairments monitoring scheme, which is located at transceiver end.

# Chapter 7

# Conclusions and Future Works

Optical fiber transmission system is the backbone of modern telecommunication networks, in which there are various optical impairments degrading the system performance. For future reconfigurable optical networks, optical performance monitoring (OPM) can offer great assistance for intelligent system management of dynamic optical networks. In this thesis, OSNR monitoring and CD monitoring were investigated by using different techniques. Moreover, time alignment monitoring in RZ phase modulation system was discussed. In this chapter, the main contributions of this thesis are summarized, and the future works are pointed out.

## 7.1 Conclusions

In this thesis, the discussed OPM methods can be divided into two types. One is based on analog signal processing, while the other relies on digital signal processing. These two types of methods have their particular merits and drawbacks in different applications. Their common merit is that the system setup cost is reduced, compared with the same type of methods. Generally speaking, the OPM methods using analog signal processing have fast monitoring speed, while the methods employing digital signal

processing have simple monitoring system setups that are easy to be operated. The detailed discuss of the particular method is stated in the following paragraphs.

In chapter 3, the OSNR monitoring method based on filtering effect was discussed. By using balanced subtraction or optical interference, the uncorrelated signal is generated, whose power is sensitive to noise power variation. Thus, the power ratio between the uncorrelated signal and the correlated signal was proposed to monitor signal OSNR. Moreover, by using low bandwidth receiver, the proposed OSNR monitoring method is insensitive to dispersion effect. More importantly, the usage of low bandwidth receiver reduces the cost of the OSNR monitoring system setup. Thus, for the OSNR monitoring method using filtering effect, it is a simple and cost effective method for single OSNR parameter monitoring. Moreover, the monitoring system setup is able to be integrated into a single photonic device, due to the usage of low bandwidth optical and electrical devices. Additionally, the energy consumption of this method is low, so the monitoring system is portable to be implemented at any place of the network for long time monitoring or temporary diagnosis.

The rest part of this thesis discussed the OPM methods based on electrical sampling technique. For the conventional OPM method based on electrical sampling technique, the two-sampling-channel scheme was used to generate the 2-D phase portrait, which was able to monitor multiple optical impairments. The classification and quantification of the optical impairments are based on the pattern recognition of the generated phase portrait. This method is simple to operate and maintain. However, the two expensive high bandwidth samplers in the monitoring system setup take the major cost. In order to reduce the monitoring system setup cost, the single channel sampling scheme was proposed to generate the 2-D phase portrait for OPM. In chapter 4, the single channel sampling method was demonstrated by using the related sampling scheme. The proposed method employs the self-delay scheme to generate the X-Y pairs from the sample sequence. By using statistical pattern recognition, OSNR monitoring and

CD monitoring are demonstrated in different modulation formats. The proposed SCS scheme saves both monitoring setup cost and 3-dB monitored signal power budget. However, the related sampling scheme has a limited application scope.

In chapter 5, in order to extend the application scope of the proposed single channel sampling technique, the un-related sampling scheme was proposed to generate the 2-D phase portrait. For the un-related sampling system, software synchronization technique is used to synchronize the sample sequence. The software synchronized sampling sequence is used to generate the 2-D phase portrait, which is demonstrated in OSNR monitoring. Moreover, in order to further improve the monitoring system tolerance to the software synchronization accuracy, the tolerated phase difference phase portrait was proposed. In the experimental demonstration, this method was successfully applied for OSNR monitoring. Thus, in this thesis, the proposed software synchronized single channel sampling technique achieves the simplest system setup for OPM, which reduces the monitoring system setup complexity in large degree. Compared with the monitoring system discussed in chapter 4, the un-related sampling scheme employs the software algorithm to synchronize the sampling sequence instead of the synchronized sampling frequency, which enlarges the application scope. However, the software synchronization increases the computational loading of the data processing, which further reduces the monitoring speed of the method using electrical sampling technique. Although the related sampling scheme requires the exact knowledge of the sampling rate and data rate, it can still be applied in the optical networks where these two parameters are fixed. Thus, the network manager can select the monitoring scheme, according to the particular network design.

In chapter 6, the pulse carver and I/Q branch alignment monitoring in RZ phase modulation systems were investigated. By using the proposed 2-D phase portrait, the time alignment of RZ phase modulation systems can be monitored with sign. From the simulation results, it is found that the monitoring scheme using the phase portrait with

large time delay has larger monitoring dynamic range, which shows its feasibility of using single channel sampling technique. In the experimental demonstration part, the time alignment monitoring is successfully demonstrated by using the proposed software synchronized single channel sampling technique. Thus, this method extends the application scope of the software synchronized single channel sampling technique.

In sum, the proposed single channel sampling technique is available to multiple optical impairments monitoring, which can monitor the optical impairment from channel and transmitter. Since this method has the simplest monitoring system setup, it is able to sweep different channels continuously or select the particular channel swiftly. Moreover, it can change its function from the received signal performance monitoring to the transmitted signal performance monitoring. Thus, this method has multiple functions, while the method using analog signal processing cannot achieve. Although the OSNR monitoring method discussed in chapter 3 is able to be integrated into a portable device for flexible usage, it has single function. However, we can not neglect its advantage of low cost. Thus, this method is still an effective solution for single OSNR monitoring.

## 7.2 Future Works

In this thesis, OSNR monitoring, CD monitoring, and time alignment monitoring have been studied, and some novel methods have been proposed and demonstrated. However, there are still several points worth further study, which have some gap between research and real application. Based on the current works, there are several valuable topics that need further investigation.

Firstly, for the OSNR monitoring method based on uncorrelated signal power, the uncorrelated signal generation is generated by using balanced subtraction or optical interference. In order to remove the high frequency signal power variation induced by

dispersion effect, low bandwidth receivers are used to remove the high frequency signal power. However, dispersion effect can be monitored by using the high frequency signal power [53]. Moreover, the differentiation of CD and PMD induced high frequency signal power is a key point of the dispersion monitoring [25, 107]. Thus, CD monitoring and PMD monitoring could be based on the high frequency power of the uncorrelated signal, such that the uncorrelated signal could be used for the three typical optical impairments monitoring.

Secondly, optical impairment monitoring has been demonstrated in this work by using the proposed single channel sampling method. This scheme has a quite simple system setup, which is convenient to operate in real system. By using simple statistical pattern recognition, the OSNR monitoring and CD monitoring parameters have been derived in several modulation formats. However, for the real transmission system, the optical impairments are not limited in ASE noise and CD. Thus, in the future work, the main challenge is to derive more optical impairments from the generated 2-D phase portrait with differentiation.

Finally, for the time alignment monitoring of the transmitter, RZ phase modulation format is demonstrated in this work. For the advanced modulation formats (e.g. 16QAM and 64QAM), the time alignment of the transmitter is a critical issue, which also needs a OPM scheme. For the multi-level advanced modulation format, the generated 2-D phase portrait has complicated pattern evolution. Thus, in future work, the advanced pattern recognition technique would be employed for the time alignment monitoring in the advanced modulation formats.

# Bibliography

[1] Z. Pan, C. Yu, and A. E. Willner, "Optical performance monitoring for the next generation optical communication networks," *Optical Fiber Technology*, vol. 16, no. 1, pp. 20–45, 2010.

[2] S. Bigo, Y. Frignac, G. Charlet, W. Idler, S. Borne, H. Gross, R. Dischler, W. Poehlmann, P. Tran, C. Simonneau *et al.*, "10.2 Tbit/s (256x42.7Gbit/s PDM/WDM) transmission over 100km Teralight fiber with 1.28 bit/s/Hz spectral efficiency," in *Optical Fiber Communication Conference*. Optical Society of America, 2001, p. PD25.

[3] A. H. Gnauck and P. J. Winzer, "Optical phase-shift-keyed transmission," *Journal of lightwave technology*, vol. 23, no. 1, pp. 115–130, 2005.

[4] P. Winzer, A. Gnauck, C. Doerr, M. Magarini, and L. Buhl, "Spectrally efficient long-haul optical networking using 112-Gb/s polarization-multiplexed 16-QAM," *Lightwave Technology, Journal of*, vol. 28, no. 4, pp. 547–556, 2010.

[5] A. H. Gnauck, P. J. Winzer, A. Konczykowska, F. Jorge, J.-Y. Dupuy, M. Riet, G. Charlet, B. Zhu, and D. W. Peckham, "Generation and transmission of 21.4-Gbaud PDM 64-QAM using a novel high-power DAC driving a single I/Q modulator," *Journal of Lightwave Technology*, vol. 30, no. 4, pp. 532–536, 2012.

[6] C. Davidson, C. Chen, M. Nissov, A. Pilipetskii, N. Ramanujam, H. Kidorf, B. Pedersen, M. Mills, C. Lin, M. Hayee *et al.*, "1800 Gb/s transmission of one hundred and eighty 10 gb/s WDM channels over 7,000 km using the full EDFA c-band," in *Optical Fiber Communication Conference*. Optical Society of America, 2000, p. PD25.

[7] E. Ip, A. P. T. Lau, D. J. Barros, and J. M. Kahn, "Coherent detection in optical fiber systems," *Optics Express*, vol. 16, no. 2, pp. 753–791, 2008.

[8] H. Bulow, F. Buchali, and A. Klekamp, "Electronic dispersion compensation," *Lightwave Technology, Journal of*, vol. 26, no. 1, pp. 158–167, 2008.

[9] C. R. Fludger, T. Duthel, D. Van den Borne, C. Schulien, E.-D. Schmidt, T. Wuth, J. Geyer, E. De Man, G.-D. Khoe, and H. De Waardt, "Coherent equalization and POLMUX-RZ-DQPSK for robust 100-GE transmission," *Lightwave Technology, Journal of*, vol. 26, no. 1, pp. 64–72, 2008.

[10] R. Varrazza, I. B. Djordjevic, and S. Yu, "Active vertical-coupler-based optical crosspoint switch matrix for optical packet-switching applications," *Journal of lightwave technology*, vol. 22, no. 9, pp. 2034–2042, 2004.

[11] Y. Liu, E. Tangdiongga, Z. Li, H. de Waardt, A. Koonen, G. Khoe, X. Shu, I. Bennion, and H. Dorren, "Error-free 320-Gb/s all-optical wavelength conversion using a single semiconductor optical amplifier," *Journal of Lightwave Technology*, vol. 25, no. 1, pp. 103–108, 2007.

[12] G. P. Agrawal, *Nonlinear fiber optics*. Springer, 2000.

[13] A. E. Willner and B. Hoanca, "Fixed and tunable management of fiber chromatic dispersion," *Optical Fiber Telecommunications IVB*, pp. 642–724, 2002.

[14] M. N. Petersen, Z. Pan, S. Lee, S. Havstad, and A. Willner, "Online chromatic dispersion monitoring and compensation using a single inband subcarrier tone," *Photonics Technology Letters, IEEE*, vol. 14, no. 4, pp. 570–572, 2002.

[15] W. Hatton and M. Nishimura, "Temperature dependence of chromatic dispersion in single mode fibers," *Lightwave Technology, Journal of*, vol. 4, no. 10, pp. 1552–1555, 1986.

[16] C. D. Poole, "Statistical treatment of polarization dispersion in single-mode fiber," *Optics Letters*, vol. 13, no. 8, pp. 687–689, 1988.

[17] G. P. Agrawal, *Fiber-optic communication systems*, 1997, vol. 1.

[18] J.-X. Cai, Y. Cai, C. R. Davidson, D. G. Foursa, A. Lucero, O. Sinkin, W. Patterson, A. Pilipetskii, G. Mohs, and N. S. Bergano, "Transmission of 96 100-Gb/s bandwidth-constrained PDM-RZ-QPSK channels with 300% spectral efficiency over 10610 km and 400% spectral efficiency over 4370 km," *Lightwave Technology, Journal of*, vol. 29, no. 4, pp. 491–498, 2011.

[19] H. Kim, C. Doerr, R. Pafchek, L. Stulz, and P. Bernasconi, "Alignment monitoring of the pulse carver and data modulator for RZ-DPSK systems," *Photonics Technology Letters, IEEE*, vol. 15, no. 11, pp. 1594–1596, 2003.

[20] X. Wu, L. Christen, B. Zhang, J.-Y. Yang, L. Zhang, S. R. Nuccio, A. E. Willner, and L. Paraschis, "Experimental synchronization monitoring of I/Q misalignment and pulse carving misalignment in 20-Gbit/s RZ-DQPSK data generation," *ECOC 2007*, 2007.

[21] A. A. Saleh and J. M. Simmons, "Evolution toward the next-generation core optical network," *Journal of lightwave Technology*, vol. 24, no. 9, pp. 3303–3321, 2006.

[22] C. C. Chan, *Optical performance monitoring: advanced techniques for next-generation photonic networks*. Academic Press, 2010.

[23] D. Kilper, R. Bach, D. Blumenthal, D. Einstein, T. Landolsi, L. Ostar, M. Preiss, and A. Willner, "Optical performance monitoring," *Journal of Lightwave Technology*, vol. 22, no. 1, pp. 294–304, 2004.

[24] J.-Y. Yang, L. Zhang, L. Christen, B. Zhang, S. Nuccio, X. Wu, L.-S. Yan, S. Yao, and A. Willner, "Polarization-mode-dispersion monitoring for phase-modulated signals using DGD-generated interferometric filter," *Photonics Technology Letters, IEEE*, vol. 20, no. 2, pp. 150–152, 2008.

[25] J. Yang, C. Yu, Y. Yang, L. Cheng, Z. Li, C. Lu, A. P. T. Lau, H.-y. Tam, and P. Wai, "PMD-insensitive CD monitoring based on RF clock power ratio measurement with optical notch filter," *Photonics Technology Letters, IEEE*, vol. 23, no. 21, pp. 1576–1578, 2011.

[26] G. Liu, S. Cao, Q. Xue, Y. Wei, S. Qiu, Z. Feng, Q. Xiong, and Z. Yu, "Iterative wiener deconvolution method for optical power monitoring," in *Optical Communications and Networks (ICOCN 2011), 10th International Conference on*. IET, 2011, pp. 1–2.

[27] H. Suzuki and N. Takachio, "Optical signal quality monitor built into WDM linear repeaters using semiconductor arrayed waveguide grating filter monolithically integrated with eight photodiodes," *Electronics Letters*, vol. 35, no. 10, pp. 836–837, 1999.

[28] G. Rossi, T. E. Dimmick, and D. J. Blumenthal, "Optical performance monitoring in reconfigurable WDM optical networks using subcarrier multiplexing," *Lightwave Technology, Journal of*, vol. 18, no. 12, pp. 1639–1648, 2000.

[29] D. Kilper and W. Weingartner, "Monitoring optical network performance degradation due to amplifier noise," *Journal of lightwave technology*, vol. 21, no. 5, pp. 1171–1178, 2003.

[30] J. Lee, O. Jung, C. Kim, and Y. Chung, "OSNR monitoring technique using polarization-nulling method," *Photonics Technology Letters, IEEE*, vol. 13, no. 1, pp. 88–90, 2001.

[31] J. Lee and Y. Chung, "Improved OSNR monitoring technique based on polarization-nulling method," *Electron. Lett*, vol. 37, no. 16, pp. 1032–1033, 2001.

[32] J. Lee, H. Choi, S. Shin, and Y. Chung, "A review of the polarization-nulling technique for monitoring optical-signal-to-noise ratio in dynamic WDM networks," *Journal of lightwave technology*, vol. 24, no. 11, pp. 4162–4171, 2006.

[33] X. Liu and Y.-H. Kao, "A simple OSNR monitoring technique independent of PMD and chromatic dispersion based on a 1-bit delay interferometer," in *Optical Communications, 2006. ECOC 2006. European Conference on*. IEEE, 2006, pp. 1–2.

[34] X. Liu, Y. Kao, S. Chandrasekhar, I. Kang, S. Cabot, and L. Buhl, "OSNR monitoring method for OOK and DPSK based on optical delay interferometer," *IEEE Photonics Technology Letters*, vol. 19, no. 13/16, pp. 1172–1174, 2007.

[35] Y. K. Lizé, J.-Y. Yang, L. C. Christen, X. Wu, S. Nuccio, T. Wu, A. E. Willner, R. Kashyap, and F. Séguin, "Simultaneous and independent monitoring of OSNR, chromatic and polarization mode dispersion for NRZ-OOK, DPSK and duobinary," in *Optical Fiber Communication Conference*. Optical Society of America, 2007, p. OThN2.

[36] Y. K. Lize, L. Christen, J.-Y. Yang, P. Saghari, S. Nuccio, A. E. Willner, and R. Kashyap, "Independent and simultaneous monitoring of chromatic and polarization-mode dispersion in OOK and DPSK transmission," *Photonics Technology Letters, IEEE*, vol. 19, no. 1, pp. 3–5, 2007.

[37] E. A. Flood, W. Guo, D. Reid, M. Lynch, A. Bradley, L. Barry, and J. Donegan, "Osnr monitoring using two fiber interferometers," in *Optical Fiber Communication Conference*. Optical Society of America, 2010, p. OWB3.

[38] E. Flood, W.-H. Guo, J. F. Smyth, M. Lynch, A. L. Bradley, L. P. Barry, and J. F. Donegan, "Dual polarization interferometric in-band OSNR measurement," *Photonics Technology Letters, IEEE*, vol. 24, no. 11, pp. 873–875, 2012.

[39] M. R. Chitgarha, S. Khaleghi, W. Daab, A. Almaiman, M. Ziyadi, A. Mohajerin-Ariaei, D. Rogawski, M. Tur, J. D. Touch, V. Vusirikala *et al.*, "Demonstration of in-service wavelength division multiplexing optical-signal-to-noise ratio performance monitoring and operating guidelines for coherent data channels with different modulation formats and various baud rates," *Optics Letters*, vol. 39, no. 6, pp. 1605–1608, 2014.

[40] M. R. Chitgarha, S. Khaleghi, W. Daab, M. Ziyadi, A. Mohajerin-Ariaei, D. Rogawski, M. Tur, V. Vusirikala, W. Zhao, J. Touch *et al.*, "Demonstration of WDM OSNR performance monitoring and operating guidelines for Pol-Muxed 200-Gbit/s 16-QAM and 100-gbit/s QPSK data channels," in *Optical Fiber Communication Conference*. Optical Society of America, 2013, pp. OTh3B–6.

[41] C. Courvoisier, J. Fatome, C. Finot *et al.*, "Measurement of residual chromatic dispersion or OSNR via nonlinear spectral evolution," *IEEE Photonics Technology Letters/IEEE Transactions Photonics Technol Lett*, vol. 23, no. 9, pp. 537–539, 2011.

[42] R. Adams, M. Rochette, T. T. Ng, and B. J. Eggleton, "All-optical in-band OSNR monitoring at 40 gb/s using a nonlinear optical loop mirror," *Photonics Technology Letters, IEEE*, vol. 18, no. 3, pp. 469–471, 2006.

[43] L. Li, J. Li, J. Qiu, Y. Li, W. Li, J. Wu, and J. Lin, "Investigation of in-band OSNR monitoring technique using power ratio," *Lightwave Technology, Journal of*, vol. 31, no. 1, pp. 118–124, 2013.

[44] T. Ng, J. Blows, and B. Eggleton, "In-band OSNR monitoring using fibre optical parametric amplifier," *Electronics Letters*, vol. 41, no. 6, pp. 352–353, 2005.

[45] T. T. Ng, J. L. Blows, J. T. Mok, R. W. McKerracher, and B. J. Eggleton, "Cascaded four-wave mixing in fiber optical parametric amplifiers: application to residual dispersion monitoring," *Journal of lightwave technology*, vol. 23, no. 2, pp. 818–826, 2005.

[46] J. Y. Huh and Y. C. Chung, "Simultaneous monitoring technique for OSNR and PMD based on four-wave mixing in SOA," in *Optical Fiber Communication Conference*. Optical Society of America, 2008, p. OThW1.

[47] Z. Chen, L. Yan, A. Yi, W. Pan, and B. Luo, "Simultaneous OSNR monitoring for two polarization tributaries of a PDM signal using a polarization-diversity nonlinear loop mirror based on FWM," *Journal of Lightwave Technology*, vol. 30, no. 14, pp. 2376–2381, 2012.

[48] A. Liu, G. Pendock, and R. S. Tucker, "Chromatic dispersion monitoring using time-multiplexed in-band RF tones," in *Optical Fiber Communication Conference*. Optical Society of America, 2005, p. OThH6.

[49] Y. Wang, Z. Pan, A. Sahin, L. Yan, C. Yu, and A. E. Willner, "In-line chromatic dispersion monitoring using optically-added phase-modulated in-band tones for

10 Gb/s system," in *Optical Fiber Communication Conference*. Optical Society of America, 2003, p. WP3.

[50] N. Liu, W.-D. Zhong, Y. J. Wen, C. Lu, L. Cheng, and Y. Wang, "PMD and chirp effects suppression in RF tone-based chromatic dispersion monitoring," *IEEE photonics technology letters*, vol. 18, no. 5-8, pp. 673–675, 2006.

[51] S. Jun, H. Kim, P. K. Park, J. Lee, and Y. Chung, "Pilot-tone-based WDM monitoring technique for DPSK systems," *Photonics Technology Letters, IEEE*, vol. 18, no. 20, pp. 2171–2173, 2006.

[52] N. Liu, W.-D. Zhong, Y. J. Wen, and Z. Li, "New transmitter configuration for subcarrier multiplexed DPSK systems and its applications to chromatic dispersion monitoring," *Optics express*, vol. 15, no. 3, pp. 839–844, 2007.

[53] Z. Pan, Y. Xie, S. Havstad, Q. Yu, A. Willner, V. Grubsky, D. Starodubov, and J. Feinberg, "Real-time group-velocity dispersion monitoring and automated compensation without modifications of the transmitter," *Optics communications*, vol. 230, no. 1, pp. 145–149, 2004.

[54] J. Zhao, C. Lu, Z. Li, H. Tam, and P. Wai, "Optical signal monitoring of DPSK signals using RF power detection," in *Opto-Electron. Commun. Conf.(OECC)*, 2008.

[55] K. T. Tsai and W. I. Way, "Chromatic-dispersion monitoring using an optical delay-and-add filter," *Lightwave Technology, Journal of*, vol. 23, no. 11, pp. 3737–3747, 2005.

[56] P. Vorreau, D. C. Kilper, and J. Leuthold, "Optical noise and dispersion monitoring with SOA-based optical 2R regenerator," *Photonics Technology Letters, IEEE*, vol. 17, no. 1, pp. 244–246, 2005.

[57] S. Li and D. V. Kuksenkov, "A novel dispersion monitoring technique based on four-wave mixing in optical fiber," *Photonics Technology Letters, IEEE*, vol. 16, no. 3, pp. 942–944, 2004.

[58] J.-Y. Yang, L. Zhang, X. Wu, O. Yilmaz, B. Zhang, and A. Willner, "All-optical chromatic dispersion monitoring for phase-modulated signals utilizing cross-phase modulation in a highly nonlinear fiber," *Photonics Technology Letters, IEEE*, vol. 20, no. 19, pp. 1642–1644, 2008.

[59] T. Luo, C. Yu, Z. Pan, Y. Wang, J. McGeehan, M. Adler, and A. Willner, "All-optical chromatic dispersion monitoring of a 40-Gb/s RZ signal by measuring the XPM-generated optical tone power in a highly nonlinear fiber," *Photonics Technology Letters, IEEE*, vol. 18, no. 2, pp. 430–432, 2006.

[60] S. Ohteru and N. Takachio, "Optical signal quality monitor using direct Q-factor measurement," *Photonics Technology Letters, IEEE*, vol. 11, no. 10, pp. 1307–1309, 1999.

[61] I. Shake, H. Takara, and S. Kawanishi, "Simple Q factor monitoring for BER estimation using opened eye diagrams captured by high-speed asynchronous electrooptical sampling," *Photonics Technology Letters, IEEE*, vol. 15, no. 4, pp. 620–622, 2003.

[62] I. Shake and H. Takara, "Averaged Q-factor method using amplitude histogram evaluation for transparent monitoring of optical signal-to-noise ratio degradation in optical transmission system," *Journal of lightwave technology*, vol. 20, no. 8, pp. 1367–1373, 2002.

[63] N. Hanik, A. Gladisch, C. Caspar, and B. Strebel, "Application of amplitude histograms to monitor performance of optical channels," *Electronics Letters*, vol. 35, no. 5, pp. 403–404, 1999.

[64] I. Shake, H. Takara, and S. Kawanishi, "Simple measurement of eye diagram and BER using high-speed asynchronous sampling," *Journal of lightwave technology*, vol. 22, no. 5, pp. 1296–1302, 2004.

[65] R. Luis, P. Andre, A. Teixeira, and P. Monteiro, "Performance monitoring in optical networks using asynchronously acquired samples with nonideal sampling systems and intersymbol interference," *Journal of lightwave technology*, vol. 22, no. 11, pp. 2452–2459, 2004.

[66] R. S. Luís, A. Teixeira, and P. Monteiro, "Optical signal-to-noise ratio estimation using reference asynchronous histograms," *Journal of Lightwave Technology*, vol. 27, no. 6, pp. 731–743, 2009.

[67] Z. Li, C. Lu, Y. Wang, and G. Li, "In-service signal quality monitoring and multi-impairment discrimination based on asynchronous amplitude histogram evaluation for NRZ-DPSK systems," *Photonics Technology Letters, IEEE*, vol. 17, no. 9, pp. 1998–2000, 2005.

[68] T. S. R. Shen, A. P. T. Lau, and G. N. Liu, "OSNR monitoring for higher order modulation formats using asynchronous amplitude histogram," *Photonics Technology Letters, IEEE*, vol. 22, no. 22, pp. 1632–1634, 2010.

[69] Z. Li and G. Li, "In-line performance monitoring for RZ-DPSK signals using asynchronous amplitude histogram evaluation," *IEEE photonics technology letters*, vol. 18, no. 1-4, pp. 472–474, 2006.

[70] Z. Li and G. Li, "Chromatic dispersion and polarization-mode dispersion monitoring for RZ-DPSK signals based on asynchronous amplitude-histogram evaluation," *Journal of lightwave technology*, vol. 24, no. 7, pp. 2859–2866, 2006.

[71] I. Shake and H. Takara, "Chromatic dispersion dependence of asynchronous amplitude histogram evaluation of NRZ signal," *Journal of lightwave technology*, vol. 21, no. 10, pp. 2154–2161, 2003.

[72] S. D. Dods and T. B. Anderson, "Optical performance monitoring technique using delay tap asynchronous waveform sampling," in *Optical Fiber Communication Conference*. Optical Society of America, 2006, p. OThP5.

[73] T. B. Anderson, A. Kowalczyk, K. Clarke, S. D. Dods, D. Hewitt, and J. C. Li, "Multi impairment monitoring for optical networks," *Lightwave Technology, Journal of*, vol. 27, no. 16, pp. 3729–3736, 2009.

[74] T. J. Morgan, Y. R. Zhou, A. Lord, and T. Anderson, "Non-intrusive simultaneous measurement of OSNR, CD and PMD on live WDM system," in *National Fiber Optic Engineers Conference*. Optical Society of America, 2012, pp. NTu2E–4.

[75] F. Khan, A. P. T. Lau, Z. Li, C. Lu, and P. Wai, "Statistical analysis of optical signal-to-noise ratio monitoring using delay-tap sampling," *Photonics Technology Letters, IEEE*, vol. 22, no. 3, pp. 149–151, 2010.

[76] F. Khan, A. P. T. Lau, Z. Li, C. Lu, and P. Wai, "OSNR monitoring for RZ-DQPSK systems using half-symbol delay-tap sampling technique," *Photonics Technology Letters, IEEE*, vol. 22, no. 11, pp. 823–825, 2010.

[77] B. Kozicki, A. Maruta, and K. Kitayama, "Experimental investigation of delay-tap sampling technique for online monitoring of RZ-DQPSK signals," *Photonics Technology Letters, IEEE*, vol. 21, no. 3, pp. 179–181, 2009.

[78] B. Kozicki, A. Maruta, and K. Kitayama, "Transparent performance monitoring of RZ-DQPSK systems employing delay-tap sampling," *Journal of Optical Networking*, vol. 6, no. 11, pp. 1257–1269, 2007.

[79] B. Kozicki, A. Maruta, and K. Kitayama, "Experimental demonstration of optical performance monitoring for RZ-DPSK signals using delay-tap sampling method," *Optics express*, vol. 16, no. 6, pp. 3566–3576, 2008.

[80] J. Zhao, Z. Li, D. Liu, L. Cheng, C. Lu, and H. Tam, "NRZ-DPSK and RZ-DPSK signals signed chromatic dispersion monitoring using asynchronous delay-tap sampling," *Journal of Lightwave Technology*, vol. 27, no. 23, pp. 5295–5301, 2009.

[81] Z. Li, Z. Jian, L. Cheng, Y. Yang, C. Lu, A. P. T. Lau, C. Yu, H. Tam, and P. Wai, "Signed chromatic dispersion monitoring of 100Gbit/s CS-RZ DQPSK signal by evaluating the asymmetry ratio of delay tap sampling," *Optics express*, vol. 18, no. 3, pp. 3149–3157, 2010.

[82] J. Yang, M. He, H. Lu, C. Yu, and Z. Li, "Chromatic dispersion monitoring of DQPSK and D8PSK signals based on delay-tap sampling technique," in *Communication Systems (ICCS), 2010 IEEE International Conference on*. IEEE, 2010, pp. 184–188.

[83] A. P. T. Lau, Z. Li, F. Khan, C. Lu, and P. Wai, "Analysis of signed chromatic dispersion monitoring by waveform asymmetry for differentially-coherent phase-modulated systems," *Optics express*, vol. 19, no. 5, pp. 4147–4156, 2011.

[84] G.-W. Lu, Y.-C. Ku, L.-K. Chen, and C.-K. Chan, "A novel technique for pulse-carver and data alignment monitoring in RZ-DPSK systems using off-center optical filtering," *Photonics Technology Letters, IEEE*, vol. 17, no. 3, pp. 711–713, 2005.

[85] K. T. Tsai, G.-W. Lu, L.-K. Chen, and W. I. Way, "Alignment monitoring technique for pulse carver and data modulator in RZ-DPSK systems using an optical frequency discriminator," *IEEE photonics technology letters*, vol. 18, no. 9/12, pp. 1119–1121, 2006.

[86] X. Wu, L. Christen, B. Zhang, W.-R. Peng, J.-Y. Yang, L. Zhang, S. R. Nuccio, L. Paraschis, J. A. Jargon, and A. Willner, "Synchronization monitoring of I/Q data and pulse carving misalignment for a parallel-type RZ-DQPSK transmitter by measuring RF clock tone/low frequency power," *Photonics Technology Letters, IEEE*, vol. 20, no. 24, pp. 2138–2140, 2008.

[87] Y.-C. Ku and C.-K. Chan, "High-speed data and pulse-carver alignment in RZ-OOK systems using delay tap asynchronous waveform sampling," in *Proc. ECOC*, 2006.

[88] G. Charlet, J. Renaudier, P. Brindel, P. Tran, H. Mardoyan, O. Bertran-Pardo, M. Salsi, and S. Bigo, "Performance comparison of dpsk, P-DPSK, RZ-DQPSK and coherent PDM-QPSK at 40gb/s over a terrestrial link," in *Optical Fiber Communication Conference*. Optical Society of America, 2009, p. JWA40.

[89] A. Gnauck, G. Charlet, P. Tran, P. Winzer, C. Doerr, J. Centanni, E. Burrows, T. Kawanishi, T. Sakamoto, and K. Higuma, "25.6-Tb/s WDM transmission of polarization-multiplexed RZ-DQPSK signals," *Journal of Lightwave Technology*, vol. 26, no. 1, pp. 79–84, 2008.

[90] W. Shieh, H. Bao, and Y. Tang, "Coherent optical OFDM: theory and design," *Optics Express*, vol. 16, no. 2, pp. 841–859, 2008.

[91] S. K. Korotky, "Lithium niobate integrated optics: selected contemporary devices and system applications," *Optical Fiber Telecommunications IIIB*, vol. 3, p. 377, 1997.

[92] I. Kaminow, T. Li, and A. E. Willner, *Optical Fiber Telecommunications VB: Systems and Networks*. Elsevier, 2010.

[93] K.-P. Ho, *Phase-modulated optical communication systems*. Springer, 2005, vol. 42.

[94] R. Griffin, R. Johnstone, R. Walker, J. Hall, S. Wadsworth, K. Berry, A. Carter, M. Wale, J. Hughes, P. Jerram *et al.*, "10 Gb/s optical differential quadrature phase shift key (DQPSK) transmission using GaAs/AlGaAs integration," in *Optical Fiber Communication Conference*. Optical Society of America, 2002, p. FD6.

[95] X. Zhou and J. Yu, "Multi-level, multi-dimensional coding for high-speed and high-spectral-efficiency optical transmission," *Lightwave Technology, Journal of*, vol. 27, no. 16, pp. 3641–3653, 2009.

[96] N. Froberg, G. Raybon, U. Koren, B. Miller, M. Young, M. Chien, G. Harvey, A. Gnauck, and A. Johnson, "Generation of 2.5 Gbit/s soliton data stream with an integrated laser-modulator transmitter," *Electronics Letters*, vol. 30, no. 22, pp. 1880–1881, 1994.

[97] M. Suzuki, H. Tanaka, K. Utaka, N. Edagawa, and Y. Matsushima, "Transform-limited 14ps optical pulse generation with 15GHz repetition rate by InGaAsP electroabsorption modulator," *Electronics Letters*, vol. 28, no. 11, pp. 1007–1008, 1992.

[98] M. Nazarathy and E. Simony, "Multichip differential phase encoded optical transmission," *Photonics Technology Letters, IEEE*, vol. 17, no. 5, pp. 1133–1135, 2005.

[99] H. Kim and P. J. Winzer, "Robustness to laser frequency offset in direct-detection DPSK and DQPSK systems," *Lightwave Technology, Journal of*, vol. 21, no. 9, pp. 1887–1891, 2003.

[100] P. J. Winzer, S. Chandrasekhar, and H. Kim, "Impact of filtering on RZ-DPSK reception," *Photonics Technology Letters, IEEE*, vol. 15, no. 6, pp. 840–842, 2003.

[101] J. Horner, *Optical signal processing*. Elsevier, 2012.

[102] J. G. Proakis, *Digital signal processing: principles algorithms and applications*. Pearson Education India, 2001.

[103] W. Chen, R. Tucker, X. Yi, W. Shieh, and J. S. Evans, "Optical signal-to-noise ratio monitoring using uncorrelated beat noise," *Photonics Technology Letters, IEEE*, vol. 17, no. 11, pp. 2484–2486, 2005.

[104] H. Choi, Y. Takushima, and Y. C. Chung, "Phasor monitoring of DxPSK signals using software-based synchronization technique," *Optics express*, vol. 18, no. 21, pp. 21 511–21 518, 2010.

[105] H. Choi, J. Chang, and Y. Chung, "OSNR monitoring technique based on software-based synchronous amplitude histogram analysis," in *OptoElectronics and Communications Conference and Photonics in Switching*. Optical Society of America, 2013, p. TuR2_5.

[106] X. Wu, L. Christen, S. Nuccio, O. F. Yilmaz, L. Paraschis, Y. K. Lize, and A. E. Willner, "Experimental synchronization monitoring of I/Q data and pulse-carving temporal misalignment for a serial-type 80-Gbit/s RZ-DQPSK transmitter," in *Optical Fiber Communication Conference*. Optical Society of America, 2008, p. OTuG2.

[107] J. Yang, C. Yu, L. Cheng, Z. Li, C. Lu, A. P. T. Lau, H.-y. Tam, and P. Wai, "CD-insensitive PMD monitoring based on RF power measurement," *Optics express*, vol. 19, no. 2, pp. 1354–1359, 2011.

# List of Publications

## Journal Papers

1. *Yi Yu*, Banghong Zhang, and Changyuan Yu, "Optical signal to noise ratio monitoring using single channel sampling technique," *Optics Express*, vol. 22, no. 6, pp. 6874–6880, 2014.

2. *Yi Yu* and Changyuan Yu, "Dispersion insensitive optical signal to noise ratio monitoring of PDM signal by using uncorrelated signal power," *Optics Express*, vol. 22, no. 11, pp. 12823–12828, 2014.

3. *Yi Yu* and Changyuan Yu, "Optical signal to noise ratio monitoring by using software synchronized sampling technique," to be submitted.

4. *Yi Yu* and Changyuan Yu, "Pulse carver and I/Q mis-alignment monitoring in RZ-QPSK system by using electrical sampling technique," to be submitted.

## Conference Papers

1. *Yi Yu* and Changyuan Yu, "Pulse carver alignment monitoring for RZ-DPSK and DQPSK signals based on delay-tap sampling technique," in *Proc. 9th International Symposium on Communication Systems Networks and Digital Signal Processing (CSNDSP) 2014*, pp. 1-4, 2014.

2. Changyuan Yu and *Yi Yu*, "Optical performance monitoring in fiber transmission systems based on electrical sampling technique," in *Proc. International Conference on Transparent Optical Networks (ICTON) 2014*, pp.1-4, 2014.

3. *Yi Yu* and Changyuan Yu, "OSNR monitoring by using single sampling channel generated 2-D phase portrait," in *Proc. OFC/NFOEC 2014*, Paper Th2A.49, 2014.

4. Changyuan Yu and *Yi Yu*, "OSNR monitoring in optical fiber communication systems," in *Proc. International Conference on Lasers, Optics and Photonics (OPTICS) 2013*, pp.1, 2013, (invited).

5. *Yi Yu*, Chung Fatt Loh, Zhuoran Xu, and Changyuan Yu, "OSNR Monitoring for PDM RZ-DQPSK system by low bandwidth sampling technique," in *Proc. Asia-Pacific Conference on Communications (APCC) 2013* 2013, Paper V-2.1, pp. 1-2, 2013.

6. *Yi Yu* and Changyuan Yu, "Simultaneous OSNR and CD monitoring for NRZ-DPSK and DQPSK signals by single-channel sampling technique," in *Proc. Asia-Pacific Conference on Communications (APCC) 2013* 2013, Paper VII-3.1, pp. 1-2, 2013.

7. Changyuan Yu and *Yi Yu*, "Optical performance monitoring in high-speed fiber communication systems based on low-bandwidth delay-tap sampling," in *Proc. 8th International Conference on Communications and Networking in China (ChinaCom) 2013*, pp. 1-4, 2013, (invited).

8. Changyuan Yu and *Yi Yu*, "Optical performance monitoring based on filtering in high-speed optical fiber communication systems," in *Proc. Signal Processing in Photonics Communications Conference, OSA Advanced Photonics Congress (SPPCom) 2013*, Paper SP4D.4, pp. 1-3, 2013, (invited).

9. *Yi Yu*, Jing Yang, and Changyuan Yu, "Optical signal to noise ratio monitoring using a novel optical notch filtering scheme," in *Proc. IEEE Photonics Global Conference (PGC) 2012* Paper 2-2G-4, pp. 1-4, 2012.

10. Changyuan Yu, Jing Yang, and *Yi Yu*, "Dispersion and OSNR monitoring in high-speed optical fiber communication system," in *Proc. 11th International Conference on Optical Communications and Networks (ICOCN) 2012*, Paper FRI-18, pp. 1-4,2012, (invited).

11. *Yi Yu*, Jing Yang, and Changyuan Yu, "Low cost and CD insensitive optical signal to noise ratio monitoring method using beat noise," in *Proc. International Conference on Communications Systems (ICCS) 2012* Paper MC7-2, pp. 1-4, 2012.